ROLE OF GLACIAL INFLUX AND WIND IN SHAPING CIRCULATION AND PRODUCTIVITY IN AN ANTARCTIC GLACIAL BAY

ROLA DOPŁYWU WÓD LODOWCOWYCH I WIATRU W KSZTAŁTOWANIU CYRKULACJI I PRODUKTYWNOŚCI W ANTARKTYCZNEJ ZATOCE LODOWCOWEJ

PhD dissertation by

Maria Osińska

written under supervision of :

Agnieszka Herman, PhD, DSc, prof. of IO PAS

and

Robert Józef Bialik, PhD, DSc, prof. of IBB PAS

Gdynia, 2025

Table of Contents

Abstract

My PhD dissertation investigates the hydrodynamics of Antarctic glacial bays, using Admiralty Bay (AB), King George Island, as a representative example of other glacial bays in the West Antarctic Peninsula (WAP) region. The research aims to address existing knowledge gaps regarding the roles of glacial meltwater influx and wind forcing in shaping coastal water circulation and primary productivity.

My dissertation comprises three publications (two published, one after first round of reviews) that collectively address six research goals. These were achieved using a combination of high-resolution *in situ* measurements and 3D numerical modeling to provide a holistic understanding of the investigated system. A comprehensive dataset of AB's water properties measurements was collected from December 2018 to March 2023, reflecting seasonal variability in physical, chemical, and biological water properties. Numerical modeling, using Delft3D, was employed to simulate AB's hydrodynamics under various glacial influx and wind scenarios. A Lagrangian particle model was coupled to the hydrodynamic model to track the transport of suspected primary sources of iron, a productivity-limiting factor in AB, and the penetration of open ocean waters into AB.

The research identified a general circulation pattern in AB, characterized by a strong inflow current along the western boundary and an outflow current in the east, transporting glacially modified waters out of the bay. Two cyclonic circulation cells regulate water exchange between AB and the ocean. The results showed that ocean forcing consistently acts as the primary driver of AB’s circulation. However, significant glacial influx can induce a shift in circulation within the smaller inlets.

This study provides the first high-resolution estimate of seasonal variability in glacial water input to an Antarctic bay. The AB contribution to freshwater input to the Southern Ocean ranges from 0.434 to 0.632 Gt/year, with peak values during late summer and minimal input in winter and spring.

The most common winds in AB are westerly, the strongest storms tend to originate from the east; both directions are perpendicular to the main axis of the bay. This research highlights the role of these cross-bay winds in shaping AB hydrodynamics. While increased wind magnitude elevates energy levels and reduces water column stratification, wind direction was found to have a previously underappreciated significance. Westerly winds promote water mass retention within AB, generating submesoscale eddies that concentrate particles suspected to be primary sources of iron, creating areas conducive to biological hotspot formation. Conversely, easterly winds rapidly flush all tracked water types from the bay, likely limiting primary production. While measurement data and satellite-derived chlorophyll-a estimates offer supporting evidence, the influence of cross-bay winds on primary production remain incompletely validated due to observational constraints. However, the results indicate that cross-bay winds can either enhance or inhibit biological productivity in broad glacial bays, depending on their orientation relative to the bay's main axis.

The results of my PhD dissertation have significant implications for understanding the dynamics of Antarctic glacial bays and their response to climate change. As the volumes of glacial meltwater increase and wind regimes shift, the insights gained from AB can inform predictions of future changes in WAP coastal waters and their capacity to sustain productive ecosystems. The study also underscores the importance of considering local geomorphology and wind forcing when assessing glacial bay hydrodynamics. The developed approach that combined an observational dataset, a hydrodynamic model, and a detailed bathymetry provide valuable tools for future research in this critical region.

Streszczenie (abstract in Polish)

Niniejsza rozprawa doktorska koncentruje się na badaniu hydrodynamiki antarktycznych zatok lodowcowych. Obszarem badawczym jest Zatoka Admiralicji (Admiralty Bay; AB) na Wyspie Króla Jerzego, stanowiąca reprezentatywny przykład zatoki lodowcowej w regionie Zachodniego Półwyspu Antarktycznego (West Antarctic Peninula, WAP). Celem pracy jest określenie roli dopływu wód lodowcowych i wiatru w kształtowaniu cyrkulacji i produktywności biologicznej tych akwenów.

Rozprawa doktorska obejmuje trzy publikacje (dwie opublikowane, jedną po pierwszej rundzie recenzji), w których zrealizowano sześć celów badawczych. Osiągnięcie tych celów było możliwe dzięki połączeniu analizy danych obserwacyjnych z trójwymiarowym modelowaniem numerycznym. W okresie od grudnia 2018 roku do marca 2023 roku zgromadzono obszerny zbiór danych pomiarowych, szczegółowo opisujący właściwości wód w AB. Dane te dokumentują sezonową zmienność parametrów fizycznych, chemicznych i biologicznych. Do symulacji hydrodynamiki zatoki, uwzględniającej dopływ wód lodowcowych oraz oddziaływanie wiatru, zastosowano model Delft3D. Dodatkowo, sprzężony z nim model Lagrange'a posłużył do śledzenia transportu potencjalnych źródeł żelaza, jak również penetracji wód oceanicznych. Monitorowanie przepływu cząstek zawierających żelazo jest szczególnie istotne, ponieważ stanowi ono czynnik ograniczający produkcję pierwotną w Oceanie Południowym.

Ogólny wzorzec cyrkulacji w AB obejmuje intensywny prąd wpływający do zatoki wzdłuż jej zachodniego brzegu oraz prąd wypływający na wschodzie, który eksportuje wody pochodzenia lodowcowego. Wymianę wód pomiędzy zatoką a oceanem modulują dwie cyklonalne komórki cyrkulacyjne. Oddziaływanie oceaniczne odgrywa kluczową rolę w kształtowaniu cyrkulacji w AB. Należy jednak zaznaczyć, że znaczący wzrost dopływu wód lodowcowych może modyfikować cyrkulację w mniejszych, wewnętrznych zatokach AB.

Praca zawiera również ilościową ocenę zmienności sezonowej dopływu wód lodowcowych do antarktycznej zatoki lodowcowej. Szacowany wkład lodowców z AB w ogólny dopływ słodkiej wody do Oceanu Południowego mieści się w zakresie od 0.434 do 0.632 Gt/rok, przy czym wartości maksymalne obserwowane są pod koniec lata, a minimalne w okresie zimy i wiosny.

Badania wskazują, że w AB dominują wiatry zachodnie, choć najsilniejsze sztormy wykazują tendencję do występowania z kierunków wschodnich. Oba te kierunki wiatru są prostopadłe do głównej osi zatoki. Niniejsza praca bada wpływ tych prostopadłych kierunków wiatru na kształtowanie hydrodynamiki AB. Zwiększona prędkość wiatru podnosi energię kinetyczną i redukuje stratyfikację w kolumnie wody, a kierunek wiatru odgrywa istotną, choć dotychczas niedocenianą rolę. Wiatry zachodnie sprzyjają retencji wód wewnątrz AB, generując wiry submezoskalowe, które akumulują masy wodne wraz z cząstkami bogatymi w żelazo. Ta akumulacja może sprzyjać tworzeniu lokalnych stref podwyższonej produktywności pierwotnej. Z kolei wiatry wschodnie powodują szybki eksport mas wodnych z zatoki, co prawdopodobnie wpływa negatywnie na produkcję pierwotną w AB. Wnioski dotyczące wpływu lokalnych wiatrów na produkcję pierwotną w AB znajdują potwierdzenie w danych pomiarowych oraz satelitarnych. Jednakże, ze względu na ograniczenia tych źródeł danych, dalsze obserwacje są niezbędne dla pełnego potwierdzenia tej hipotezy. Niemniej jednak, wyniki wskazują, że wiatry prostopadłe względem osi zatoki, w zależności od ich zwrotu, mogą stymulować lub hamować produktywność biologiczną w szerokich zatokach lodowcowych.

Wyniki niniejszej rozprawy doktorskiej poszerzają naszą wiedzę na temat hydrodynamiki antarktycznych zatok lodowcowych oraz zmian w nich zachodzących w odpowiedzi na zmiany klimatyczne. W obliczu prognozowanego wzrostu dopływu wód roztopowych z lodowców oraz zmian w reżimach wiatrowych, wnioski płynące z tych badań mogą być wykorzystane do prognozowania przyszłych zmian w regionie WAP. Wyniki podkreślają kluczowe znaczenie uwzględniania lokalnej geomorfologii oraz realistycznego modelowania oddziaływania wiatru w badaniach hydrodynamiki zatok lodowcowych. Co więcej, opracowana metodologia obejmująca zbiór danych obserwacyjnych, model hydrodynamiczny i szczegółową batymetrię stanowi cenne narzędzie dla przyszłych badań w tym kluczowym obszarze.

Introduction

Research background and significance

Due to climate change, the West Antarctic Peninsula region (WAP) is among the most quickly evolving glacial systems on the planet. As a result, it has been recognized as a "model system" that can demonstrate the effects of global warming in polar regions (Henley et al., 2019). The increased glacial melting, reduction in sea ice extent, and intensification of the circumpolar westerly winds are three features of this continuous transformation (National Snow and Ice Data Center & CIRES, 2023; Swart & Fyfe, 2012). Analyzing the implications of these processes in the coastal WAP waters is crucial, given the area's unique significance to the Southern Ocean (SO). WAP coastal waters serve as a pathway through which glacial waters are introduced into the ocean, with far-reaching impacts on its physical, chemical, and biological properties. Additionally, this region exhibits increased primary production, supporting populations of zooplankton and higher trophic level feeders important for the whole SO ecosystem (Ducklow et al., 2007). Therefore, understanding both the current state of the coastal WAP and its future changes is crucial for advancing polar marine science.

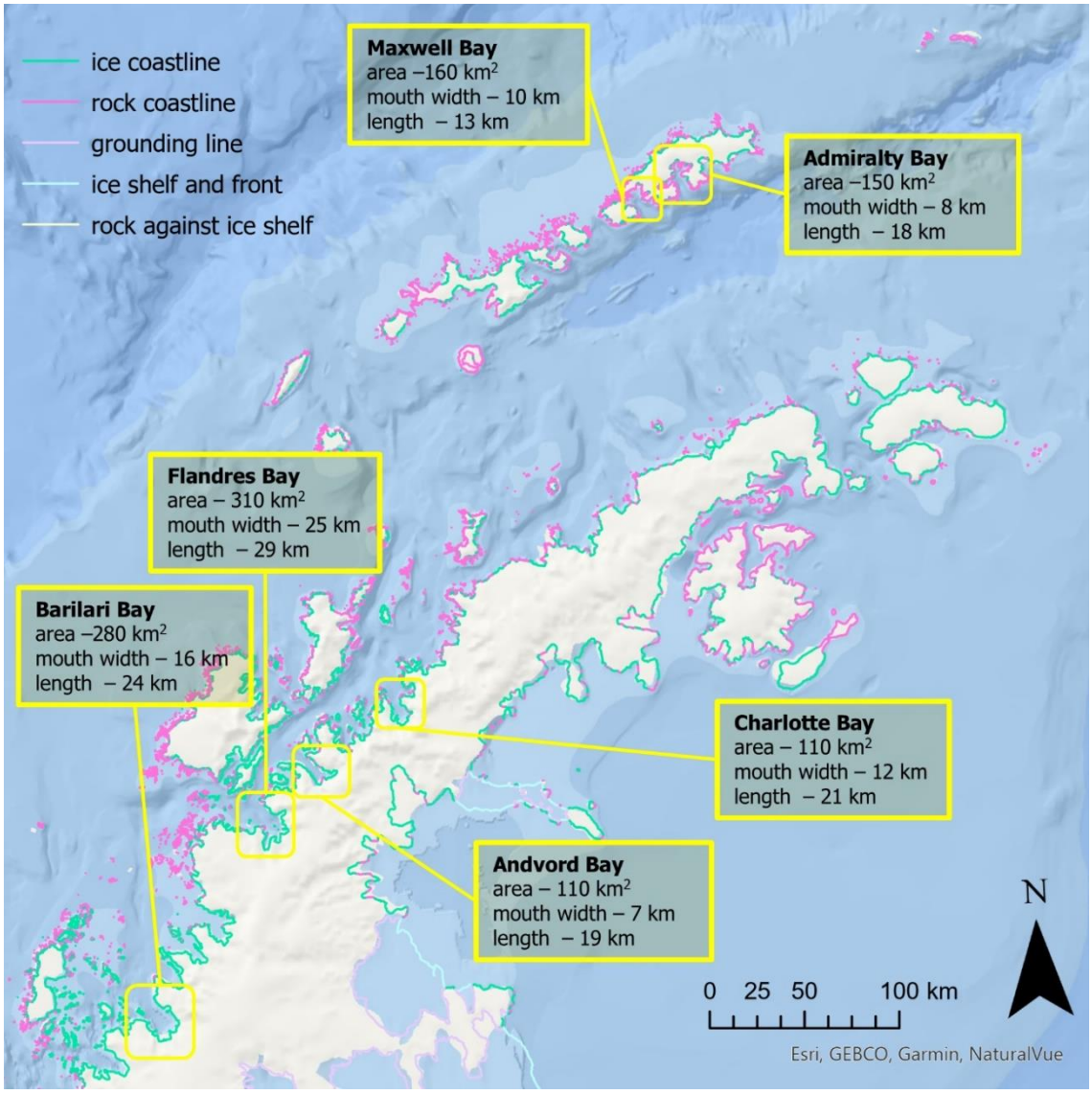

Figure 1. Example bays of the WAP region. Basemap: ArcGisPro; coastline based on Gerrish et al. (2021).

Floating ice shelves constitute the majority of the Antarctic coastline (Gerrish et al., 2021). However, in the Antarctic Peninsula there are over 800 marine-terminating glaciers, most of which are adjacent to glacial bays (see Figure 1; Davison et al., 2024). In the past, most research exploring glacial bay systems focused on fjords of the Northern Hemisphere, in Greenland, Alaska, and Spitsbergen. These fjords are typically long, narrow, and deep, characterized by a relatively large Rossby radius of deformation, which results in minimal cross-fjord circulation (Cottier et al., 2010). Moreover, most previous studies concentrated on bays bordering a single large glacier (e.g., Cowton et al., 2015; Kimura et al., 2014; Motyka et al., 2003). In contrast, the Antarctic glacial bays of the WAP region—generally broader than northern fjords and surrounded by multiple glaciers—remain relatively understudied. Recent efforts have begun to address these knowledge gaps by examining the influence of Circumpolar Deep Water intrusions, katabatic wind events, and heat fluxes on bay hydrodynamics (Cape et al., 2019; Hahn-Woernle et al., 2020; Lundesgaard et al., 2019). Nonetheless, our overall understanding of Antarctic glacial bay systems remains limited, and the significance of the various factors influencing them is not yet fully understood.

My PhD dissertation aims to further our understanding of the hydrodynamics and biogeochemical processes within Antarctic glacial bays by using Admiralty Bay (AB) in King George Island as a representative example of other glacial bays in the WAP region.

Glacial water influx is a defining feature of polar bays, exerting significant influence on local thermodynamics, geochemistry, and biological productivity (Fransson et al., 2015; Hahn-Woernle et al., 2020; Pan et al., 2019). When introduced into the marine environment, glacial water mixes with ocean water, creating glacially modified water (GMW) – a buoyant, relatively fresh water mass that influences water column stratification and circulation within the bay (Etherington et al., 2007). However, the impact of varying quantities of GMW on circulation and its significance as a factor influencing hydrodynamics of Antarctic glacial bays remains unknown.

Estimating the volume of GMW in AB and tracing its pathways are crucial for understanding its spatial and temporal influence. Previous estimates of glacial water influx into Antarctic bays had coarse temporal resolution and were primarily based on observations during the austral summer months (Cape et al., 2019; Hahn-Woernle et al., 2020; Wessem & Laffin, 2020). Such rough and seasonally limited data are insufficient for a comprehensive understanding of GMW forcing. Therefore, it is essential to accurately quantify glacial water influx volume, determine its seasonal variability, and reveal its transport pathways. As glaciers continue to retreat and sea ice extent diminishes (National Snow and Ice Data Center & CIRES, 2023; Naughten et al., 2023), the volume and impacts of GMW are expected to increase. Another pressing question, therefore, is how rising GMW volumes will influence the physical, chemical, and biological processes within the bay.

Winds can play a fundamental role in shaping the dynamics of coastal waters. However, most previous studies focusing on wind impact in glacial bays described effects brought on by along-fjord (upward/down-fjord) winds (Lundesgaard et al., 2019; Spall et al., 2017). In contrast, the influence of cross-bay wind has received comparatively little attention, despite its potential significance in broad bays like AB. In AB, the most common wind direction is from the west, while the strongest storms originate from the east (Powers et al., 2003; Turner et al., 2009). Additionally, with the climatologically induced strengthening of westerly winds around Antarctica, the influence of westerly winds in this region could become even more dominant (Swart & Fyfe, 2012). Consequently, both the most frequent and the strongest wind events act upon the water in directions perpendicular to the main axis of the bay. Therefore, one of the key objectives of this study is to understand how such cross-bay winds affect the overall circulation of broad glacial bays.

SO is recognized as the largest High-Nutrient, Low-Chlorophyll (HNLC) area of the world, which is attributed to the low availability of iron for phytoplankton growth (Martin et al., 1990). Therefore, the coastal waters of the WAP hold particular importance for the entire SO ecosystem, as they are located where two primary sources of iron are most prevalent: GMW and upwelled iron-rich bottom waters (Annett et al., 2015). Moreover, this system is currently undergoing transformation as recent observations reveal changes in local phytoplankton populations, linked to global warming (Ferreira et al., 2024). In highly dynamic bays like AB, which lack a distinct sill and are almost constantly influenced by winds, conditions rarely support the extensive phytoplankton blooms common in more sheltered environments (Schloss et al., 2014; Wasiłowska et al., 2022). Nonetheless, recurrent biologically rich areas that attract grazing whales and penguins have been repeatedly observed in specific locations within the AB. This study aims to explain the hydrodynamical conditions that can support the formation of these hotspots under the dynamic and windy conditions prevalent in the WAP.

Overall, this research is motivated by the persistent gaps in our understanding of Antarctic glacial bay hydrodynamics and their susceptibility to change under various forcing mechanisms. The study begins with providing a comprehensive description of water properties and circulation patterns in Antarctic glacial bays. Building on this, it explores the significant roles of GMW, local wind impacts, and primary productivity within AB—elements that are not only fundamental components of the bay system but are also expected to be heavily influenced by the ongoing climate change. Investigating these interactions offers vital insights into the present and future of Antarctic coastal waters and their capacity to sustain productive and resilient ecosystems.

Research goals

My PhD dissertation aimed to achieve the following goals:

- **Research Goal 1:** To develop a comprehensive dataset of measured water properties (physical, chemical, and biological) in AB, capturing their variability across seasons and different conditions, thereby providing a foundation for various studies, including hydrodynamic model setup and validation.

- **Research Goal 2:** To identify the general circulation pattern within AB.

- **Research Goal 3:** To evaluate how changes in glacial water influx volume affect the circulation dynamics of AB.

- **Research Goal 4:** To assess the seasonal variability of glacial water influx and to analyze its transport pathways following initial release.

- **Research Goal 5**: To understand the influence of cross-bay wind forcing on the hydrodynamics of AB.

- **Research Goal 6:** To investigate the role of cross-bay winds as a factor impacting primary production within AB.

Peer-reviewed publications

I have written three articles that make up my PhD dissertation:

- **Publication 1:** Osińska, M., Wójcik-Długoborska, K. A., & Bialik, R. J. (2023). Annual hydrographic variability in Antarctic coastal waters infused with glacial inflow. *Earth System Science Data*, *15*(2), 607–616. https://doi.org/10.5194/essd-15-607-2023;
  IF: 11.6; MNiSW: 200 pt.

- **Publication 2:** Osińska, M., & Herman, A. (2024). Influence of glacial influx on the hydrodynamics of Admiralty Bay, Antarctica – study based on combined hydrographic measurements and numerical modeling. *Frontiers in Marine Science*, *11*, 1365157. https://doi.org/10.3389/FMARS.2024.1365157;
  IF: 3.0; MNiSW: 100 pt.

- **Publication 3:** Osińska, M., & Herman, A. (n.d.). Hydrodynamic response of an Antarctic glacial bay to cross-bay winds and its potential impact on primary production. *Scientific Reports*, after the first round of peer review.
  IF: 3.9; MNiSW: 140 pt.

Choosing appropriate means and methods for research goals

Study Area: Admiralty Bay — an example or f other West Antarctic Peninsula glacial bays

For this research, Admiralty Bay (AB) on King George Island in the South Shetland Islands was chosen as the study site. This selection was motivated by th bay's proximity to the Arctowski Polish Antarctic Station, which allows for year-round, high-resolution observational data collection—something often unachievable in many other Antarctic glacial bays due to logistical and environmental challenges. Unlike studies based on ship-based measurements, which are typically limited to a few sampling campaigns during the warmer months (e.g., Cape et al., 2019; Forsch et al., 2021; Grange & Smith, 2013; Lundesgaard et al., 2019), continuous observations in AB provide an unprecedented opportunity to analyze the bay's physical, chemical, and biological dynamics throughout the entire year. This makes AB an ideal natural laboratory for investigating coastal processes in the remote southern polar regions. It is essential to emphasize that the primary aim of this study is not only to enhance the understanding of hydrodynamics in AB but also to provide insights into the broader WAP region. Therefore, it was important to determine whether the selected location was appropriate for that purpose.

Geomorphologically, AB exhibits characteristics typical of other glacial bays in the WAP region, which set them apart from the more extensively studied fjords of the Northern Hemisphere. Figure 1 illustrates the location, shapes, and dimensions of six WAP glacial bays that have been examined in previous research cited in this study. Considering the observed mouth widths, ranging from 7 to 25 km, and comparing them with the low Rossby radius of deformation values in Antarctic coastal waters—estimated to be as small as 1–5 km (Mack et al., 2019)—it becomes evident that cross-bay circulation plays a crucial role in their hydrodynamics. Consequently, all these bays can be classified as 'broad bays' (Cottier et al., 2010).

The shape of AB features a main body of the bay extending along a deep fault with a maximum depth exceeding 500 m, and a network of shallower inner inlets branching out from the main bay in various directions. A similar configuration is observed in the other bays illustrated in Figure 1. A significant part of the WAP coastline continues to consist of marine-terminating glaciers; however, as general glacial retreat appears imminent (Naughten et al., 2023), the coastline will become even more intricate. The newly published Bedmap3, the most detailed map to date of the Antarctic seabed and surface elevation without ice cover (Pritchard et al., 2025), depicts the projected coastline position should the glaciers retreat entirely onto land. In all of the WAP bays shown there (including those highlighted in Figure 1), the inner inlets are expected to expand and extend further inland, increasingly resembling the current shape of AB.

A key feature shared by most WAP bays—including AB—is the absence of a well-defined sill at their mouths. Such sills are central in regulating water exchange between the bay and the open ocean, impacting heat transfer, water retention, and mixing processes (Arneborg et al., 2004; Bao & Moffat, 2024; Hager et al., 2022; Kawase & Bang, 2013; Mortensen et al., 2013; Nilsson et al., 2023). Bays without a distinct sill, like AB, are characterized by more vigorous circulation and higher exchange rates with the open ocean, driven by winds and internal waves.

Despite the discussed similarities, key differences distinguish AB from other WAP bays. About 25% of the AB coastline is occupied by marine-terminating glaciers, contrasting with some other bays where glaciers make up a much larger proportion of the shore (see Figure 1 and different colored lines indicating ice and rock coastlines). Consequently, the waters in AB are less dominated by persistent glacial calving and meltwater input. Additionally, as a result of climate change, the AB waters are no longer within the area of a persistent sea ice extent that continues

to cover the nearby coastal WAP waters for several months each year (National Snow and Ice Data Center & CIRES, 2023). The enduring sea ice cover of glacial bay waters limits the energy exchange between the hydrosphere and atmosphere, can restrict glacial calving, and significantly impacts the hydrodynamics and biological productivity of the entire basin (Mortensen et al., 2013; Wasiłowska et al., 2022). Meteorologically, King George Island is subject to less precipitation and weaker katabatic winds than the Antarctic Peninsula (Cape et al., 2019; Lundesgaard et al., 2019; Plenzler et al., 2019)—factors that can also heavily influence local circulation.

The ongoing climate warming accelerates glacier retreat, reduces the extent and duration of sea ice, and modifies wind regimes across the WAP. Although these changes are complex, it is evident that current conditions in AB exemplify many of the transformations expected throughout the region. Consequently, studying AB not only deepens our understanding of its unique processes but also provides valuable insights into the potential future evolution of similar bays in the WAP.

In summary, the geomorphology and environmental conditions of AB establish it as a valuable natural laboratory representative of other bays in the WAP region. Given its geomorphological, hydrodynamic, and meteorological features, AB is likely to be an early indicator of how the glacial bay system responds to ongoing regional changes. Consequently, the study of AB is a crucial step in predicting future transformations within this dynamic Antarctic coastal system.

Observation and modeling used in tandem for holistic understanding of the glacial bay system

One of the key strengths of my dissertation is its comprehensive methodology. Selecting AB as the study site enabled collection of an unusually large and detailed dataset—likely the most comprehensive description of Antarctic glacial bay properties compiled to date. Nevertheless, given the limitations of observational data in fully capturing the complex hydrodynamics and environmental variability of AB, a rigorous numerical modeling framework utilizing both Eulerian and Lagrangian approaches was implemented. These two methods, observations and modelling, working synergistically, enabled me to develop a detailed and verifiable understanding of the bay's physical system.

An observational campaign, conducted from December 2018 to February 2023, provided vital information on physical, chemical, and biological water parameters in AB, forming the foundation of this study. High-precision CTD sondes (YSI EXO1 and EXO2) were used to measure temperature, salinity, pH, turbidity, and oxygen content throughout all seasons. From March 2021, these measurements were supplemented with biological parameters, including chlorophyll-a, phycoerythrin, and fluorescent dissolved organic matter content. This dataset is described in detail in **Publication 1** and is publicly available through PANGAEA and Zenodo (Bialik & Osińska, 2023; Osińska et al., 2022). During my PhD, I was directly involved in all stages of this measurement campaign, from planning and initial equipment setup to participating in numerous measurement days during three stays at the Arctowski Polish Antarctic Station. As curator of the marine monitoring program in AB, I collaborated with four successive marine monitoring crews to ensure data consistency and continuity. My responsibilities included data acquisition, curation, and quality control. Furthermore, I served as the primary point of contact for new team members, providing support and troubleshooting assistance to ensure the smooth continuation of the monitoring program.

The 3D numerical modeling was performed using Delft3D software, an open-source model developed by Deltares (Deltares, 2020). Delft3D was specifically designed for complex coastal and estuarine environments, offering the flexibility required to create a highly detailed mesh grid. The AB hydrodynamical model grid includes over 30,000 points, capturing essential features of

Antarctic bays, such as small skerries, islands, and intricate inlets, that are frequently neglected in simpler model domains.

One of the goals of the **Publication 2** was to understand the general hydrodynamics of AB and its susceptibility to change with different amounts of glacial water added to the system. This investigation was based on 14 different model scenarios in the Eulerian setup using Delft3D-Flow. In **Publication 3,** an effect of cross-bay winds on the AB circulation was investigated, and particle tracking of suspected iron-rich particles was performed, showing the effect of these winds on the creation of accumulation areas that could promote biological hotspot formation. This required an additional 7 model scenarios in Delft3D-Flow and further calculations of particle tracking model DWAQ (Deltares, 2024).

However, before these model scenarios could be calculated, both models' setups involved extensive testing. Multiple grid resolutions, layering schemes, turbulence models, diffusion coefficients, open boundary conditions, time steps, bottom roughness coefficients, and smoothing parameters were tested. The entire process of setup, calibration, and testing comprised over a hundred different model runs. A full simulation of two months of Delft3D FM model output required approximately 9 days of continuous computation, plus an additional day for DWAQ model runs. The final results from all calculations took up over 10 TB of data space and took nearly 1.5 years from the initial model compilation to the first results publication.

A critical aspect of the modeling process was how to represent the interaction between glacial fronts and the ocean. Initially, a coupled glacial-sea model based on Buoyant Plume Theory (BPT, Jenkins, 1999) was considered, following the approach developed by Cowton et al. (2015). This theory outlines a system where subglacial discharge is introduced into the model at the grounding line of the glacier. The glacial water, due to its greater buoyancy, is then lifted upward, creating a glacial water plume that extends far from the glacial front. Additionally, the upward movement of water stimulates the submarine melt of the glacial front. However, this approach proved infeasible for our system. There are twenty separate marine-terminating glaciers in AB that would have to be coupled individually, posing significant computational demand. More importantly, data required for establishing realistic Buoyant Plume Models for AB is unavailable. There is no information on the specific locations of subglacial discharges, as they can either be spread out along the front or concentrated in channelized outlets (Chauché et al., 2014). There are no records on the initial velocity of the influxes and the relationship between subglacial discharge and submarine melt rates. This information is essential for BPT-based modelling, considering that this relationship has been shown to exhibit significant variability depending on the location of the study (Kimura et al., 2014; Xu et al., 2012). Finally, there is no reliable information regarding the detailed bathymetry near the glacial fronts, as available data comes from either dated observations (Battke, 1990) or from large-resolution reanalysis (Pritchard et al., 2025).

Given that the AB glaciers are grounded at relatively shallow depths (maximum 150-200 m) compared to the overall depth of AB (~500 m), the potential impact of BPT on the bay's overall hydrodynamics was investigated (details of this analysis in **Publication 2**). Consequently, four extreme scenarios were modeled to assess the potential impact of BPT on the AB model. These scenarios included two extreme configurations of initial glacial water influx velocities (a minimum of 0 m/s and an exaggerated 2 m/s) and two extreme configurations of the relationship between subglacial discharge and submarine melt rates (one with solely subglacial discharge and no submarine melt, and another with glacial water influx distributed uniformly across the entire ice front, representing an extreme case of maximal subglacial discharge influence on submarine melt rates). This analysis demonstrated that, from a bay-wide perspective, the influence of specific details of glacier-ocean interactions is negligible. This suggests that the prevalent paradigm of BPT as a key aspect in modeling glacial bays, primarily derived from research on deeply grounded,

single-glacier fjords in the Northern Hemisphere (e.g., Cowton et al., 2015; Kimura et al., 2017; Motyka et al., 2003), may not be universally applicable. In fact, for many Antarctic glacial bays and other broad bays with multiple, shallower glacier-water boundaries, detailed plume modeling may not significantly influence bay-scale circulation and transport. In light of these conclusions, for all following calculations I employed a simplified setup with glacial water influx distributed uniformly across the glacier-water fronts at 0 m/s velocity. It is important to acknowledge that, due to this decision, my study focuses on the AB system as a whole and does not fully resolve the complexities of smaller-scale processes.

Realistic results were reached by a strategy that combined observational and modeling methods. This technique resulted in the development of a novel method for analyzing glacial influx volume that used freshwater thickness (FWT) as its measure (details in **Publication 2**). This approach enabled a quantification of glacial water influx volume into AB and its seasonal variability.

Personal experience played a vital role in this research. I visited AB three times, witnessing feeding hotspots and other phenomena firsthand. These field observations provided crucial context that complemented and validated modeling results, emphasizing that, if possible, modelers should also physically explore their study regions to gain a deeper understanding of the systems they are investigating.

Analyzed model scenarios

Publication 2 is a study examining the effect of glacial influx on the hydrodynamics of AB. In pursuit of this goal, calculations were conducted for 14 model scenarios featuring varying volumes of glacial influx. The values used were: 0, 0.15, 0.3, 0.6, 0.9, 1.7, 3.0, 4.5, 6.0, 8.0, 11.0, 14.0, 28.0, and 60.0 m^3/s of freshwater volume discharged per approximately 1 km of glacial front. These values serve as identifiers for specific model runs.

Publication 3 concentrated on the influence of cross-bay winds on the AB hydrodynamics and its consequences for local primary production. Since the most common winds in AB are westerly and the strongest storms are easterly, these two wind directions were considered. The analyzed model scenarios included a model run without wind forcing and three scenarios with west and east winds of three magnitudes each (7.5, 10 and 14 m/s), which are the 50^{th}, 70^{th}, and 90^{th} percentiles of all wind magnitudes in AB (Powers et al., 2003).

Also, in **Publication 3** particle tracking was performed on three water types:

- Open boundary waters (OB) are the waters that enter AB with the inflowing current from Bransfield Strait, and their pathway variability describes the penetration of AB by the ocean waters.
- Two presumed primary sources of iron, given its established role as a limiting factor for primary production in AB and the broader WAP region:
    - glacially modified waters (GMW),
    - iron-rich bottom waters (BW).

Results summary

Publication 1 provides a description of the observational data collected during the measurement campaign in AB. The data presents repeated measurement results from 31 sites in AB, located in various regions of the bay and at differing distances from glacial fronts. The data encompasses all seasons of the year, with an average of 98.2 measurements taken at each site, totaling 3045 individual measurements collected on 142 days. The key result from this study is the detailed description of AB water properties that can be utilized by various researchers in investigating physical, chemical, geological, and biological processes in the Antarctic glacial bay (**Research goal 1**).

The observational results from **Publication 1** offered two crucial pieces of information for enhancing our understanding of the AB system, as well as for establishing the hydrodynamical model, thereby facilitating the achievement of the project's further goals. An analysis of the variations in water salinity, temperature, and turbidity revealed that the GMW is consistently the most buoyant water mass and therefore is invariably elevated to the surface. Only the surface layer of AB waters has been found to exhibit distinct properties, which is attributed to the presence of GMW or the effect of atmospheric forcing. The remainder of the water column of AB across all seasons was found to be generally uniform. This indicates that AB is a dynamic system with strong mixing that minimizes the stratification of the water column. This, in turn, lowers the first baroclinic Rossby radius of deformation and increases the significance of rotation (Chelton et al., 1998). Additionally, the homogeneity of the water column indicates that, except for GMW, no distinct water masses have been identified during the measurements. There were no external inflows of waters with distinct properties that might interact with AB glacial fronts or alter local flow patterns. This is important because, for instance, the presence of warm and saline Circumpolar Deep Water in other glacial bays of the WAP region has been shown to stimulate glacial melt and impact the local ecosystem (Cape et al., 2019). A similar factor s also the warm Atlantic Water found in the fjords of Svalbard and Greenland (Cottier et al., 2017; Jackson et al., 2014). The conclusions drawn from **Publication 1** were utilized in the establishment of the hydrodynamical model of AB, which was subsequently used in **Publications 2 and 3**. The measured temperature and salinity values have also been utilized to determine the initial conditions for the model.

The investigation described in **Publication 2** aimed to achieve three research goals. Using the Delft3D hydrodynamical model, a general circulation pattern in AB was identified (**Research goal 2**). It is characterized by a strong inflow current along AB's western boundary and an outflow current in the east that transports GMW waters out of the bay. There are two cyclonic circulation cells that regulate the water exchange between the open ocean and the bay. The most powerful currents tend to follow the isobaths, around 50–100 meters deep, and do not fully penetrate the inner inlets of the bay. This pattern has been demonstrated to persist throughout all seasons of the year, even in the presence of strong glacial water inflow **(Publication 2)** and wind forcing **(Publication 3).**

The second major objective of **Publication 2** focused on assessing the vulnerability of the AB system to GMW impact (**Research goal 3**). This was explored through the analysis of results from 14 model scenarios that implemented different volumes of glacial water fluxes into the model domain. This analysis has proven that ocean forcing consistently acts as the main factor shaping the circulation within the bay. The PCA analysis of water level changes across the studied scenarios shows that this feature remains largely unaffected, even in scenarios with unrealistically large amounts of GMW in AB. However, in high glacial influx scenarios, a change in circulation occurred

within the smaller inlets of the bay. In them the predominantly horizontal circulation is converted into a vertical pattern, with oceanic waters entering inner bay waters in the deeper layers and GMW being transported out of the inlets at the surface.

Finally, **Publication 2** has addressed **Research Goal 4** and produced an assessment of the seasonal variability of quantities of glacial water released into AB. GMW transport pathways have been identified, illustrating the spreading of its impact. The estimate of glacial water volume was obtained by comparing FWT values from 14 model scenarios with those derived from observations (dataset described in **Publication 1**). The estimated AB contribution to freshwater input to SO ranges from 0.434 to 0.632 Gt/year, with monthly values of 0.104 to 0.128 Gt during summer, 0.039 to 0.055 Gt in autumn, 0.001 to 0.016 Gt in winter, and 0.000 to 0.010 Gt in spring. This represents, to my knowledge, the first high-resolution estimate of seasonal glacial influx volume to an Antarctic glacial bay. The GMW presence is observed primarily during the warm months of the year, with peak values noted at the end of austral summer. In contrast to Greenland glacial bays, where glacial water is present year-round, glacial water is virtually absent from AB during the winter and spring (Mortensen et al., 2013; Straneo et al., 2011). The cyclonic circulation in AB creates a pathway for the export of GMW along the eastern boundary of the bay's main body, moving out fresher waters in the surface layer into the ocean. The validation of this result was additionally supported by the measured salinity differences between the eastern and western edges of the main body of AB.

The subsequent thesis objective was to reveal the influence of cross-bay wind forcing on the AB hydrodynamics (**Research goal 5**). This investigation was based on modeling results from 7 model scenarios with varying magnitudes of westerly and easterly winds, as detailed in **Publication 3.** While increased wind magnitude elevates energy levels in AB and reduces water column stratification, it was determined that wind direction plays a crucial role in shaping the effects of wind on AB circulation. The prevailing westerly winds facilitate Ekman transport directed northward, thereby limiting the outflow from the bay. Moreover, it produces heightened vorticity at the entrances of the inner inlets, which leads to the development of persistent submesoscale eddies. The easterly winds induce southward Ekman transport, increasing the velocities and magnitude of the cyclonic circulation cell within the main body of AB and significantly enhancing the transport out of the bay. The outflowing current is further intensified by upwelling in the eastern section of the main body of AB, which is produced by strong easterly winds creating a pressure gradient from east to west.

Publication 3 presents an investigation into the effects of cross-bay winds on primary production in AB (**Research Goal 6**). Previous studies suggest that high productivity in AB is achievable only during calm periods, which sustain strong water column stratification and support phytoplankton growth (Schloss et al., 2014; Wasiłowska et al., 2022). However, direct observations by researchers, including myself, at the Arctowski Polish Antarctic Station indicate that feeding hotspots for whales and penguins—indicative of heightened biological productivity—form at the mouth of Ezcurra Inlet, an inner AB inlet to the west of the main bay, even after strong wind events. This research aimed to understand the hydrodynamic drivers of this apparent paradox.

To achieve **Research Goal 6** (**Publication 3),** a Lagrangian particle tracking model was developed and integrated with the results from the AB hydrodynamical model across various wind scenarios. Three water mass types were monitored: two suspected primary sources of iron, GMW and BW, and open boundary waters (OB). Consistent with the hydrodynamic model's conclusions, easterly winds were shown to rapidly flush all tracked water types from the bay, potentially limiting primary production by exporting nutrient-rich waters before phytoplankton blooms could develop. Conversely, westerly winds produced the opposite effect. Eddies generated by westerly winds were observed to concentrate GMW and BW particles, for periods exceeding a month. These

accumulation zones have the potential to trap not only suspected iron-rich particles but also phytoplankton and zooplankton, providing a food source for higher trophic levels. Consequently, areas at the mouth of the inner AB inlets—where submesoscale eddies form in response to westerly winds—were determined to be particularly favorable for the formation of localized biological blooms.

These findings align with observations of aforementioned feeding frenzies near the Ezcurra Inlet mouth and are supported by direct measurements of chlorophyll-a content in AB (described in **Publication 1**) and chlorophyll-a estimates acquired from satellite-derived Copernicus Globcolour product (E.U. Copernicus Marine Service Information). However, it is important to acknowledge that these observational datasets were insufficient to fully validate the hypothesis regarding the influential role of cross-bay winds on primary productivity in AB. Easterly winds, though infrequent, tend to be strong when they occur, often precluding measurements from Zodiac boats. Consequently, the observational dataset described in **Publication 1** does not fully represent all wind conditions in AB, which means **Research Goal 1** was not fully achieved. Additional measurements under easterly wind conditions would be valuable to have a validation of model results. Overall, **Publication 3** demonstrates that wind direction exerts a significant influence on AB hydrodynamics and likely plays a role in regulating primary production in this region.

Publications 2 and **3** highlight the essential influence of local geomorphology on glacial bay hydrodynamics, GMW distribution, and the development of biological hotspots. The findings emphasize that exploring these processes could not be accomplished through modeling using a simplified grid. Nevertheless, general conclusions can be translated to other bays in the WAP region that share similar shapes. In examining both wind and GMW effects on local hydrodynamics, it is necessary to emphasize the particular significance of the bay's inner inlets. Here a substantial volume of GMW can alter water circulation patterns, and westerly winds can increase water vorticity, consequently supporting the creation of biological hotspots.

Publications 2 and **3** indicate the existence of specific threshold values in glacial influx volume and wind forcing that can alter the general circulation pattern in AB. Such a threshold level for glacial influx is suspected to be between 14 and 28 m^3/s per 1 kilometer of glacial front. With an influx of such volume, there is a significant restriction of water exchange between the AB and the ocean (at this level, transport through the AB boundary drops by an order of magnitude from $\sim 10^5$ m^3/s to $\sim 10^4$ m^3/s). Such glacial influx volumes are not currently present in AB (conclusion from glacial influx estimates from **Publication 2**); however, they might be reached in the future. Furthermore, strong easterly winds of 14 m/s yield qualitatively distinct results compared to other analyzed wind patterns. It results in the highest energy levels, showing a 352% increase in kinetic energy compared to the scenario without wind forcing, while all other tested wind scenarios exhibit changes ranging from 25% to 127%. This scenario also facilitates the fastest export of GMW and BW particles, as demonstrated by the flushing-out time, which is defined as the duration required to decrease the initial quantity of particles by a fraction of $1-\exp^{-1} \approx 0.63$. With 14 m/s easterly winds, the mean flushing-out time for GMW particles is 10 days, and for BW particles it is 5 days. In contrast, all other scenario flushing times range from 20 to over 33 days for GMW particles and 7 to 13 days for BW particles. Given that the most powerful storms in AB originate from the east, it is a valid conclusion that such intense easterly wind events can rapidly reduce primary productivity in the bay, hence affecting all higher trophic level feeders.

A noteworthy result of my research is the creation of the most comprehensive bathymetric map of AB to date, as detailed in **Publication 2**. This map integrates data from (Battke, 1990; Magrani et al., 2015; Majdański et al., 2008) alongside direct ADCP measurements, uncovering previously uncharted features of the AB seabed.

Key outcomes, conclusions, and outlook for the future

The coastal waters of the WAP are of particular importance to the broader SO for two reasons: they serve as conduits for glacial meltwater entering the ocean and represent biologically rich regions that support entire SO ecosystems. In my PhD dissertation, I have investigated the hydrodynamics of Antarctic glacial bays, focusing on these two distinctive features. Therefore, it is important to note that this work does not aim to provide a comprehensive overview of all processes shaping Antarctic glacial bay systems but rather focuses on a select set of factors that are both important and insufficiently understood.

To this end, a wide dataset describing AB's water properties was procured, and its general circulation pattern was described. The subsequent phases of the investigation concentrated on analyzing the impact of glacial meltwater input and cross-bay winds as significant factors affecting local circulation. In addressing primary production, particular attention was given to the formation of biological hotspots that emerge under common high-energy conditions, predominantly shaped by cross-bay winds—an intriguing phenomenon not previously explored in Antarctic glacial bays.

My findings indicate that, under current conditions, glacial meltwater exerts a limited influence on overall bay-scale hydrodynamics. However, with predicted future rise in glacial meltwater input, especially in the AB's inner inlets, this influence could become transformative. The presence of glacial water remains significant, as it has numerous effects on the ocean waters, among others stimulating phytoplankton growth. Consequently, estimating the seasonal variability of glacial freshwater flux emerges as a key result of this study, with potential applications in refining the SO freshwater budget—a critical but currently uncertain element in regional climate models (Swart et al., 2023).

The direction of cross-bay winds, rather than their magnitude, was found to be an influential factor in shaping AB hydrodynamics, with likely consequences for biological hotspot creation. This finding is particularly significant given that AB is recognized as a key ecological area and an important feeding ground for marine mammals and seabirds. Due to this richness, it is currently protected as both an Antarctic Specially Managed Area (ASMA) and, in part, as an Antarctic Specially Protected Area (ASPA). The locally observed high biological activity was previously difficult to reconcile with the bay's high energy levels and relatively low average chlorophyll-a concentrations. The hypothesis that prevailing westerly winds support formation of localized biological blooms provides a potential mechanism to explain this discrepancy.

Beyond the scientific conclusions, this study provides a valuable framework for future research. The observational dataset described in **Publication 1** offers a rich foundation for a wide range of follow-up studies. It was already utilized in studies researching marine phytoplankton communities by Medina Marcos et al. (2024) and dissolved organic content by Zhang et al. (2025) A new high-resolution bathymetric map of AB has both scientific and practical applications. Furthermore, a 3D hydrodynamic model of AB was developed and validated, representing one of the first efforts to model circulation in a bay adjacent to multiple marine-terminating glaciers. This model allows further investigation into other features of the AB system. For example, it is currently being used as a tool in a study focusing on the spread of nutrient-rich, guano-infused waters from bird colonies.

The findings of my PhD dissertation offer valuable insights that can be applied to other Antarctic glacial bays. For instance, emerging remote sensing technologies may soon allow for the detection of submesoscale eddies. Since earlier efforts into evaluating phytoplankton presence in WAP waters using teledetection relied primarily on ocean color imagery, their effectiveness was often limited by the persistent cloud cover characteristic of the region. However, recent advancements, including high-resolution satellite-based LIDAR and NASA's Surface Water and Ocean Topography (SWOT) mission, may enable the identification of eddies through subtle variations in surface roughness and elevation. These developments could open new avenues for investigating how changing wind regimes influence biological productivity across the WAP coastal waters.

In conclusion, this study advances our understanding of the physical and biological dynamics within AB, offering insights applicable to other glacial bays along the WAP. As climate change continues to alter both glacial melt and atmospheric circulation in the region, these findings may help us anticipate and interpret the impacts of these changes on SO system.

References

- Annett, A. L., Skiba, M., Henley, S. F., Venables, H. J., Meredith, M. P., Statham, P. J., & Ganeshram, R. S. (2015). Comparative roles of upwelling and glacial iron sources in Ryder Bay, coastal western Antarctic Peninsula. Marine Chemistry, 176. https://doi.org/10.1016/j.marchem.2015.06.017
- Arneborg, L., Erlandsson, C. P., Liljebladh, B., & Stigebrandt, A. (2004). The rate of inflow and mixing during deep-water renewal in a sill fjord. In Limnol. Oceanogr (Vol. 49, Issue 3).
- Bao, W., & Moffat, C. (2024). Impact of shallow sills on circulation regimes and submarine melting in glacial fjords. The Cryosphere, 18(1), 187–203. https://doi.org/10.5194/tc-18-187-2024
- Battke, Z. (1990). Admiralty Bay, King George Island 1:50.000 map. Insitute of Ecology PAS.
- Bialik, R. J., & Osińska, M. (2023). CTD+ hydrographic measurement results from Admiralty Bay, Antarctica from February 2022 to February 2023 [Data set]. In Zenodo.
- Cape, M. R., Vernet, M., Pettit, E. C., Wellner, J., Truffer, M., Akie, G., Domack, E., Leventer, A., Smith, C. R., & Huber, B. A. (2019). Circumpolar deep water impacts glacial meltwater export and coastal biogeochemical cycling along the west Antarctic Peninsula. Frontiers in Marine Science, 6(MAR), 144. https://doi.org/10.3389/FMARS.2019.00144/BIBTEX
- Chauché, N., Hubbard, A., Gascard, J. C., Box, J. E., Bates, R., Koppes, M., Sole, A., Christoffersen, P., & Patton, H. (2014). Ice-ocean interaction and calving front morphology at two west Greenland tidewater outlet glaciers. Cryosphere, 8(4), 1457–1468. https://doi.org/10.5194/tc-8-1457-2014
- Chelton, D. B., Deszoeke, R. A., Schlax, M. G., El Naggar, K., & Siwertz, N. (1998). Geographical variability of the first baroclinic Rossby radius of deformation. Journal of Physical Oceanography, 28(3). https://doi.org/10.1175/1520-0485(1998)028<0433:GVOTFB>2.0.CO;2
- Cottier, F., Nilsen, F., Asplin, L., Gerland, S., & Torsvik, T. (2017). Effects of glacier runoff and wind on surface layer dynamics and Atlantic Water exchange in Kongsfjorden, Svalbard; a model study. Estuarine, Coastal and Shelf Science, 187. https://doi.org/10.1016/j.ecss.2017.01.015
- Cottier, F. R., Nilsen, F., Skogseth, R., Tverberg, V., Skardhamar, J., & Svendsen, H. (2010). Arctic fjords: A review of the oceanographic environment and dominant physical

processes. Geological Society Special Publication, 344, 35–50. https://doi.org/10.1144/SP344.4

- Cowton, T., Slater, D., Sole, A., Goldberg, D., & Nienow, P. (2015). Modeling the impact of glacial runoff on fjord circulation and submarine melt rate using a new subgrid-scale parameterization for glacial plumes. Journal of Geophysical Research: Oceans, 120(2), 796–812. https://doi.org/10.1002/2014JC010324
- Davison, B. J., Hogg, A. E., Moffat, C., Meredith, M. P., & Wallis, B. J. (2024). Widespread increase in discharge from west Antarctic Peninsula glaciers since 2018. The Cryosphere, 18(7), 3237–3251. https://doi.org/10.5194/tc-18-3237-2024
- Deltares. (2020). Delft3D 3D/2D modelling suite for integral water solutions Hydro-Morphodynamics. In User Manual. Deltares.
- Deltares. (2024). D-WAQ PART - User Manual.
- Ducklow, H. W., Baker, K., Martinson, D. G., Quetin, L. B., Ross, R. M., Smith, R. C., Stammerjohn, S. E., Vernet, M., & Fraser, W. (2007). Marine pelagic ecosystems: The West Antarctic Peninsula. Philosophical Transactions of the Royal Society B: Biological Sciences, 362(1477), 67–94. https://doi.org/10.1098/rstb.2006.1955
- E.U. Copernicus Marine Service Information (CMEMS). Global Ocean Colour (Copernicus-GlobColour), Bio-Geo-Chemical, L4 (monthly and interpolated) from Satellite Observations (1997-ongoing). In *Marine Data Store (MDS)*. https://doi.org/https://doi.org/10.48670/moi-00281
- Ferreira, A., Mendes, C. R. B., Costa, R. R., Brotas, V., Tavano, V. M., Guerreiro, C. V., Secchi, E. R., & Brito, A. C. (2024). Climate change is associated with higher phytoplankton biomass and longer blooms in the West Antarctic Peninsula. Nature Communications 2024 15:1, 15(1), 1–11. https://doi.org/10.1038/s41467-024-50381-2
- Forsch, K. O., Hahn-Woernle, L., Sherrell, R. M., Roccanova, V. J., Bu, K., Burdige, D., Vernet, M., & Barbeau, K. A. (2021). Seasonal dispersal of fjord meltwaters as an important source of iron and manganese to coastal Antarctic phytoplankton. Biogeosciences, 18(23), 6349–6375. https://doi.org/10.5194/BG-18-6349-2021
- Fransson, A., Chierici, M., Nomura, D., Granskog, M. A., Kristiansen, S., Martma, T., & Nehrke, G. (2015). Effect of glacial drainage water on the CO2 system and ocean acidification state in an Arctic tidewater-glacier fjord during two contrasting years. Journal of Geophysical Research: Oceans, 120(4), 2413–2429. https://doi.org/10.1002/2014JC010320
- Gerrish, L., Fretwell, P., & Cooper, P. (2021). High resolution vector polylines of the Antarctic coastline (7.4) [Data set]. https://doi.org/https://doi.org/10.5285/e46be5bc-ef8e-4fd5-967b-92863fbe2835
- Grange, L. J., & Smith, C. R. (2013). Megafaunal Communities in Rapidly Warming Fjords along the West Antarctic Peninsula: Hotspots of Abundance and Beta Diversity. PLoS ONE, 8(11), 77917. https://doi.org/10.1371/journal.pone.0077917
- Hager, A. O., Sutherland, D. A., Amundson, J. M., Jackson, R. H., Kienholz, C., Motyka, R. J., & Nash, J. D. (2022). Subglacial Discharge Reflux and Buoyancy Forcing Drive Seasonality in a Silled Glacial Fjord. Journal of Geophysical Research: Oceans, 127(5), e2021JC018355. https://doi.org/10.1029/2021JC018355
- Hahn-Woernle, L., Powell, B., Lundesgaard, Ø., & van Wessem, M. (2020). Sensitivity of the summer upper ocean heat content in a Western Antarctic Peninsula fjord. Progress in Oceanography, 183, 102287. https://doi.org/10.1016/J.POCEAN.2020.102287
- Henley, S. F., Schofield, O. M., Hendry, K. R., Schloss, I. R., Steinberg, D. K., Moffat, C., Peck, L. S., Costa, D. P., Bakker, D. C. E., Hughes, C., Rozema, P. D., Ducklow, H. W., Abele, D., Stefels, J., Van Leeuwe, M. A., Brussaard, C. P. D., Buma, A. G. J., Kohut, J., Sahade, R., … Meredith, M. P. (2019). Variability and change in the west Antarctic Peninsula marine system: Research

priorities and opportunities. Progress in Oceanography, 173. https://doi.org/10.1016/j.pocean.2019.03.003

- Jackson, R. H., Straneo, F., & Sutherland, D. A. (2014). Externally forced fluctuations in ocean temperature at Greenland glaciers in non-summer months. Nature Geoscience 2014 7:7, 7(7), 503–508. https://doi.org/10.1038/ngeo2186
- Jenkins, A. (1999). The Impact of Melting Ice on Ocean Waters. Journal of Physical Oceanography, 29(9), 2370–2381. https://doi.org/10.1175/1520-0485(1999)029<2370:TIOMIO>2.0.CO;2
- Kawase, M., & Bang, B. (2013). Seasonal variability of salinity and circulation in a silled estuarine fjord: A numerical model study. Continental Shelf Research, 71. https://doi.org/10.1016/j.csr.2013.10.005
- Kimura, S., Holland, P. R., Jenkins, A., & Piggott, M. (2014). The Effect of Meltwater Plumes on the Melting of a Vertical Glacier Face. Journal of Physical Oceanography, 44(12), 3099–3117. https://doi.org/10.1175/JPO-D-13-0219.1
- Kimura, S., Jenkins, A., Regan, H., Holland, P. R., Assmann, K. M., Whitt, D. B., Van Wessem, M., van de Berg, W. J., Reijmer, C. H., & Dutrieux, P. (2017). Oceanographic Controls on the Variability of Ice-Shelf Basal Melting and Circulation of Glacial Meltwater in the Amundsen Sea Embayment, Antarctica. Journal of Geophysical Research: Oceans, 122(12), 10131–10155. https://doi.org/10.1002/2017JC012926
- Lundesgaard, Ø., Powell, B., Merrifield, M., Hahn-Woernle, L., & Winsor, P. (2019). Response of an Antarctic Peninsula Fjord to Summer Katabatic Wind Events. Journal of Physical Oceanography, 49(6), 1485–1502. https://doi.org/10.1175/JPO-D-18-0119.1
- Mack, S. L., Dinniman, M. S., Klinck, J. M., McGillicuddy, D. J., & Padman, L. (2019). Modeling Ocean Eddies on Antarctica's Cold Water Continental Shelves and Their Effects on Ice Shelf Basal Melting. Journal of Geophysical Research: Oceans, 124(7), 5067–5084. https://doi.org/10.1029/2018JC014688
- Magrani, F., Neto, A. A., & Vieira, R. (2015). Glaciomarine sedimentation and submarine geomorphology in Admiralty Bay, South Shetland Islands, Antarctica. 2015 IEEE/OES Acoustics in Underwater Geosciences Symposium (RIO Acoustics), 1–6. https://doi.org/10.1109/RIOAcoustics.2015.7473614
- Majdański, M., Środa, P., Malinowski, M., Czuba, W., Grad, M., Guterch, A., & Hegedűs, E. (2008). 3D seismic model of the uppermost crust of the Admiralty Bay area, King George Island, West Antarctica. Polar Res, 29(4), 303–318.
- Martin, J. H., Gordon, R. M., & Fitzwater, S. E. (1990). Iron in Antarctic waters. Nature, 345(6271). https://doi.org/10.1038/345156a0
- Medina Marcos, K., Loarte, E., Rodriguez-Venturo, S., Baylón Coritoma, M., Tapia, P. M., Medina-Marcos, K., Loarte, E., Rodriguez-Venturo, S., Baylón-Coritoma, M., & Tapia, P. M. (2024). Influencia glaciar en la composición y diversidad de la comunidad del fitoplancton marino en la Bahía Almirantazgo, Isla Rey Jorge, Antártida. Ciencias Marinas, 50. https://doi.org/10.7773/cm.y2024.3423
- Mortensen, J., Bendtsen, J., Motyka, R. J., Lennert, K., Truffer, M., Fahnestock, M., & Rysgaard, S. (2013). On the seasonal freshwater stratification in the proximity of fast-flowing tidewater outlet glaciers in a sub-Arctic sill fjord. Journal of Geophysical Research: Oceans, 118(3), 1382–1395. https://doi.org/10.1002/jgrc.20134
- Motyka, R. J., Hunter, L., Echelmeyer, K. A., & Connor, C. (2003). Submarine melting at the terminus of a temperate tidewater glacier, LeConte Glacier, Alaska, U.S.A. Annals of Glaciology, 36, 57–65. https://doi.org/10.3189/172756403781816374
- National Snow and Ice Data Center, & CIRES. (2023). Sea Ice Index. Https://Nsidc.Org/Data/Seaice_index. https://nsidc.org/data/seaice_index

- Naughten, K. A., Holland, P. R., & De Rydt, J. (2023). Unavoidable future increase in West Antarctic ice-shelf melting over the twenty-first century. Nature Climate Change, 13(11), 1222–1228. https://doi.org/10.1038/s41558-023-01818-x
- Nilsson, J., Van Dongen, E., Jakobsson, M., O'Regan, M., & Stranne, C. (2023). Hydraulic suppression of basal glacier melt in sill fjords. Cryosphere, 17(6). https://doi.org/10.5194/tc-17-2455-2023
- Osińska, M., Wójcik-Długoborska, K. A., & Bialik, R. J. (2022). Water conductivity, salinity, temperature, turbidity, pH, fluorescent dissolved organic matter (fDOM), optical dissolved oxygen (ODO), chlorophyll a and phycoerythrin measurements in Admiralty Bay, King George Island, from Dec 2018 to Jan 2022. PANGAEA. https://doi.org/https://doi.org/10.1594/PANGAEA.947909
- Pan, B. J., Vernet, M., Reynolds, R. A., & Mitchell, B. G. (2019). The optical and biological properties of glacial meltwater in an Antarctic fjord. PLOS ONE, 14(2), e0211107. https://doi.org/10.1371/journal.pone.0211107
- Plenzler, J., Budzik, T., Puczko, D., & Bialik, R. J. (2019). Climatic conditions at Arctowski Station (King George Island, West Antarctica) in 2013-2017 against the background of regional changes. Polish Polar Research, 40(1), 1–27. https://doi.org/10.24425/PPR.2019.126345
- Powers, J. G., Monaghan, A. J., Cayette, A. M., Bromwich, D. H., Kuo, Y. H., & Manning, K. W. (2003). Real-time mesoscale modeling over Antarctica: The Antarctic mesoscale prediction system. Bulletin of the American Meteorological Society, 84(11). https://doi.org/10.1175/BAMS-84-11-1533
- Pritchard, H. D., Fretwell, P. T., Fremand, A. C., Bodart, J. A., Kirkham, J. D., Aitken, A., Bamber, J., Bell, R., Bianchi, C., Bingham, R. G., Blankenship, D. D., Casassa, G., Christianson, K., Conway, H., Corr, H. F. J., Cui, X., Damaske, D., Damm, V., Dorschel, B., … Zirizzotti, A. (2025). Bedmap3 updated ice bed, surface and thickness gridded datasets for Antarctica. Scientific Data, 12(1), 414. https://doi.org/10.1038/s41597-025-04672-y
- Schloss, I. R., Wasilowska, A., Dumont, D., Almandoz, G. O., Hernando, M. P., Michaud-Tremblay, C. A., Saravia, L., Rzepecki, M., Monien, P., Monien, D., Kopczyńska, E. E., Bers, A. V., & Ferreyra, G. A. (2014). On the phytoplankton bloom in coastal waters of southern King George Island (Antarctica) in January 2010: An exceptional feature? Limnology and Oceanography, 59(1), 195–210. https://doi.org/10.4319/lo.2014.59.1.0195
- Spall, M. A., Jackson, R. H., & Straneo, F. (2017). Katabatic Wind-Driven Exchange in Fjords. Journal of Geophysical Research: Oceans, 122(10), 8246–8262. https://doi.org/10.1002/2017JC013026
- Straneo, F., Curry, R., Sutherland, D., Hamilton, G., Cenedese, C., Vaage, K., & Stearns, L. (2011). Impact of ocean stratification on submarine melting of a major Greenland outlet glacier. Nature Precedings. https://doi.org/10.1038/npre.2011.5670.1
- Swart, N. C., & Fyfe, J. C. (2012). Observed and simulated changes in the Southern Hemisphere surface westerly wind-stress. Geophysical Research Letters, 39(16). https://doi.org/10.1029/2012GL052810
- Swart, N. C., Martin, T., Beadling, R., Chen, J. J., Danek, C., England, M. H., Farneti, R., Griffies, S. M., Hattermann, T., Hauck, J., Haumann, F. A., Jüling, A., Li, Q., Marshall, J., Muilwijk, M., Pauling, A. G., Purich, A., Smith, I. J., & Thomas, M. (2023). The Southern Ocean Freshwater Input from Antarctica (SOFIA) Initiative: scientific objectives and experimental design. Geoscientific Model Development, 16(24). https://doi.org/10.5194/gmd-16-7289-2023
- Turner, J., Chenoli, S. N., Abu Samah, A., Marshall, G., Phillips, T., & Orr, A. (2009). Strong wind events in the Antarctic. Journal of Geophysical Research Atmospheres, 114(18). https://doi.org/10.1029/2008JD011642

- Wasiłowska, A., Tatur, A., & Rzepecki, M. (2022). Massive diatom bloom initiated by high winter sea ice in Admiralty Bay (King George Island, South Shetlands) in relation to nutrient concentrations in the water column during the 2009/2010 summer. Journal of Marine Systems, 226, 103667. https://doi.org/10.1016/j.jmarsys.2021.103667
- Wessem, J. M. V., & Laffin, M. K. (2020). Regional Atmospheric Climate Model 2 (RACMO2), version 2.3p2. https://doi.org/10.5281/zenodo.3677641
- Xu, Y., Rignot, E., Menemenlis, D., & Koppes, M. (2012). Numerical experiments on subaqueous melting of Greenland tidewater glaciers in response to ocean warming and enhanced subglacial discharge. Annals of Glaciology, 53(60), 229–234. https://doi.org/10.3189/2012AoG60A139
- Zhang, R., Deng, R., Ying, J., Li, J., Guo, Y., Yang, J., & Lei, C. (2025). Remote sensing monitoring of fluorescent dissolved organic matter in Admiralty Bay: fusion of multi-source signal removal and machine learning. Science of Remote Sensing, 100260. https://doi.org/10.1016/J.SRS.2025.100260

Gdynia, 14 września 2025 r.

OŚWIADCZENIE O WSPÓŁAUTORSTWIE W PUBLIKACJACH

Oświadczam, że mój udział w publikacji:

- Osińska, M., Wójcik-Długoborska, K. A., & Bialik, R. J. (2023). Annual hydrographic variability in Antarctic coastal waters infused with glacial inflow. *Earth System Science Data*, *15*(2), 607–616. https://doi.org/10.5194/essd-15-607-2023

obejmował branie udziału w kampanii pomiarowej, opracowanie koncepcji i metodologii badań, zarządzanie danymi pomiarowymi, formalną analizę, walidację wyników, Mój udział w tej publikacji oceniam na 80%.

Mój udział w publikacji:

- Osińska, M., & Herman, A. (2024). Influence of glacial influx on the hydrodynamics of Admiralty Bay, Antarctica – study based on combined hydrographic measurements and numerical modeling. Frontiers in Marine Science, 11, 1365157. https://doi.org/10.3389/FMARS.2024.1365157;

obejmowała opracowanie koncepcji i metodologii badań, kompilację i ustawienie modelu hydrodynamicznego, przeprowadzenie obliczeń, analizę oraz walidację wyników oraz napisanie i edycję manuskryptu. Mój udział w tej publikacji oceniam na 90%.

Mój udział w publikacji:

- Osińska, M., & Herman, A. (n.d.). Hydrodynamic response of an Antarctic glacial bay to cross-bay winds and its potential impact on primary production. *Scientific Reports*, after peer review.

obejmowała opracowanie koncepcji i metodologii badań, przeprowadzenie modelowania numerycznego, analizę oraz walidację wyników oraz napisanie i edycję manuskryptu. Mój udział w tej publikacji oceniam na 90%.

Maria Osińska

Warszawa, 22 sierpnia 2025 r.

OŚWIADCZENIE O WSPÓŁAUTORSTWIE W PUBLIKACJI

Oświadczam, że mój udział w publikacji:

- Osińska, M., Wójcik-Długoborska, K. A., & Bialik, R. J. (2023). Annual hydrographic variability in Antarctic coastal waters infused with glacial inflow. *Earth System Science Data*, *15*(2), 607–616. https://doi.org/10.5194/essd-15-607-2023

obejmował branie udziału w kampanii pomiarowej, opracowanie metodologii oraz sprawdzenie i edycję manuskryptu. Mój udział w tej publikacji oceniam na 10%.

Kornelia Wójcik-Długoborska

Kornelia Wójcik-Długoborska

INSTYTUT BIOCHEMII I BIOFIZYKI
POLSKIEJ AKADEMII NAUK

Warszawa, 30.08.2025 r.

Oświadczenie o współautorstwie w publikacji

Oświadczam, że mój udział w przygotowanie publikacji:

Osińska, M., Wójcik-Długoborska, K.A., Bialik R.J. (2023). Annual hydrographic variability in Antarctic coastal waters infused with glacial inflow. *Earth System Science Data* 15(2): 607-616

obejmował współprowadzenie i nadzór merytoryczny nad pracami terenowymi, zorganizowanie i dostarczenie środków (w tym sprzętu badawczego i zaplecza terenowego), bez których badania nie mogłyby być prowadzone, a także udział w redakcji manuskryptu. Ponadto, praca powstała w ramach realizacji projektu finansowanego przez Narodowe Centrum Nauki nr UMO-2017/25/B/ST10/02092, którego byłem pomysłodawcą i kierownikiem.

Szacuję swój wkład w powstanie publikacji na około 10%.

Robert J. Bialik

Bialik

Sopot, 22 września 2025 r.

dr hab. Agnieszka Herman, prof. IO PAN
Instytut Oceanologii Polskiej Akademii Nauk
Powstańców Warszawy 55, 81-712 Sopot
e-mail: agaherman@iopan.pl

OŚWIADCZENIE O WSPÓŁAUTORSTWIE W PUBLIKACJACH

Oświadczam, że mój udział w następujących publikacjach:

1. Osińska, M., Herman, A., 2024. Influence of glacial influx on the hydrodynamics of Admiralty Bay, Antarctica – study based on combined hydrographic measurements and numerical modeling, *Frontiers in Marine Science*, 11, doi: 10.3389/fmars.2024.1365157
2. Osińska, M., Herman, A., 2025. Hydrodynamic response of an Antarctic glacial bay to cross-bay winds and its potential impact on primary production, under review in *Scientific Reports*

obejmował opiekę merytoryczną nad całością prac (koncepcja badań, metodologia dotycząca modelowania hydrodynamicznego oraz analizy danych, dyskusja i interpretacja wyników), a także pomoc w redagowaniu i korekcie manuskryptów.

Mój udział w każdej z tych publikacji oceniam na nie więcej niż 10 %.

Agnieszka Herman

Dokument podpisany przez Agnieszka Herman
Data: 2025.09.22 21:05:08 CEST

Agnieszka Herman

Earth Syst. Sci. Data, 15, 607–616, 2023
https://doi.org/10.5194/essd-15-607-2023

Open Access Earth System Science Data

Annual hydrographic variability in Antarctic coastal waters infused with glacial inflow

Maria Osińska[1], Kornelia A. Wójcik-Długoborska[2], and Robert J. Bialik[2]

[1]Institute of Oceanography, University of Gdańsk, Piłsudskiego 46, 81-378 Gdynia, Poland
[2]Institute of Biochemistry and Biophysics, Polish Academy of Sciences,
Pawińskiego 5a, 02-106 Warsaw, Poland

Correspondence: Robert J. Bialik (rbialik@ibb.waw.pl)

Received: 16 September 2022 – Discussion started: 4 October 2022
Revised: 14 December 2022 – Accepted: 10 January 2023 – Published: 7 February 2023

Abstract. During the 38 months between December 2018 and January 2022, multiparameter hydrographic measurements were taken at 31 sites within Admiralty Bay, King George Island, Antarctica. These records consisted of water column measurements (down to 100 m) of temperature, conductivity, turbidity, and pH as well as the dissolved oxygen, dissolved organic matter, chlorophyll-*a* and phycoerythrin contents. The sites were chosen due to their variable distances from glacial fronts and open ocean waters. Fifteen sites were localized within smaller glacial coves, with waters highly impacted by glacial infusions; seven sites were located in the open waters of the main body of Admiralty Bay; and nine sites were located in the intermediate conditions of the Ezcurra Inlet. The final dataset consists of measurements carried out over 142 separate days, with an average of 3.74 measurements per month. However, data were not collected regularly throughout the year and were collected less frequently during winter, although data were gathered for all but 2 winter months. On average, each site was investigated 98.2 times. Due to calibration issues, absolute values of optically measured properties occasionally show unrealistic negative values, but the relative distributions of these values remain valid. Variabilities in the measured properties each season and throughout the whole duration of the project reveal regular oscillations as well as possible long-term trends. The described dataset is freely available at PANGAEA: https://doi.org/10.1594/PANGAEA.947909 (Osińska et al., 2022).

1 Introduction

When freshwater from glaciers is introduced to marine environments, it mixes with ambient ocean water masses, leading to the formation of new glacially modified water (GMW; Straneo, 2012). In this way, freshwater export has been shown to influence properties of the coastal ocean, with impacts on the hydrodynamics and thermodynamics (Bendtsen et al., 2015; Chauché et al., 2014). Therefore, there are significant justifications to investigate water quality properties in glacial bays and fjords and to track their variability in order to potentially predict future changes.

While the majority of studies examining the influence of glacial meltwater on the marine ecosystem have been performed in the Northern Hemisphere, the importance of the effect of glacial meltwater for the functioning of coastal Antarctic waters has long been hypothesized. Nevertheless, widely available data that describe water quality in glacial bays beyond seasonal timescales at high sampling resolutions and that examine multiple variables remain nonexistent. In fact, such datasets are scarce for the Arctic and Alaska as well.

To address this deficiency, an intricate investigation campaign was designed with the intention of comprehensively observing the seasonal oscillations and long-term trends in water quality variability in Admiralty Bay (AB), King George Island, Western Antarctica. The goal of this project was to widen the scope of previously gathered observations by expanding the overall duration of monitoring, increasing

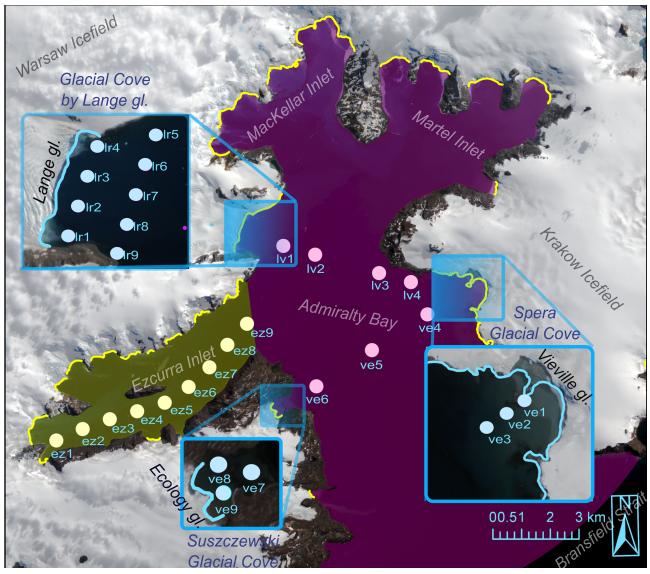

Figure 1. Map of Admiralty Bay showing the measurement points in the following three distinct zones: the main body of Admiralty Bay (pink), glacial coves (blue inset boxes) and the Ezcurra Inlet (yellow lines based upon Gerrish et al., 2021). Bright yellow denotes the current position of the ice–water coastline, and the bright blue insets show the position of the coastline on 10 March 2018. (Sourced from Sentinel imagery, 29 December 2021.)

the frequency and number of measured parameters, and to acquire data across all seasons of the year.

2 Research area

AB is a 177.04 km^2 cove southeast of King George Island, the largest island of the South Shetland Islands in Western Antarctica. In its interior, AB is subdivided into three distinct areas: the Ezcurra, Mackellar and Martel inlets, which all blend together approximately 11 km from the open ocean waters of the Bransfield Strait, forming the main body of AB (Fig. 1). Its coastline has a length of 150 km: 102 km consists of rocky coastline, and the remaining 38 km consists of ice–water boundaries (Fig. 1, yellow lines; Gerrish et al., 2021). The tidewater glaciers that form these frontiers are the outer regions of two large icefields, the Warsaw and Kraków icefields. Both icefields are reportedly experiencing unprecedented transformation due to the effects of climate warming (Rückamp et al., 2010; Dziembowski and Bialik, 2022) and are draining into AB through numerous glacial creeks.

The dataset as a whole was split into three different zones within the AB, identified based on distinct seawater properties and proximity to both glacial fronts and the mouth of the bay (i.e. proximity to open ocean source waters). These include the following:

- *Glacial coves*, comprising distinct smaller bays formed near tidewater glaciers in which marine waters are under the direct influence of glacial meltwater input. Here, three glacial coves were analysed in depth, namely the cove near Lange Glacier (1.50 km^2 in area with a 2.81 km long ice–water frontline), Spera Cove (2.45 km^2 in area with a 4.33 km long ice–water frontline) near Vieville (Viéville) Glacier and Suszczewski Cove near Ecology Glacier (0.69 km^2 in area with a 0.36 km long ice–water frontline). All three of these basins are undergoing long-term transformation caused by continuously moving and developing glacial fronts. This is visualized in Fig. 1, where the light blue line on the glacial cove insets represents the ice–water boundary in 2018 (based on a Sentinel satellite image from 10 March 2018), which is different from the frontline shown in the satellite picture presented in Fig. 1 taken in December of 2021 (Sentinel, 29 December 2021). The change is especially noticeable in Spera Cove near Vieville Glacier, where the ice front has retreated 500 m within 3 years in some locations.

- *The main body of Admiralty Bay*, comprising open bay waters in the main body of the cove, most directly influenced by the open ocean waters of the Bransfield Strait with which it is connected by a 13.45 km wide outlet. Nevertheless, this location is also affected by glacial input, especially in its northern parts.

- *Ezcurra Inlet*, comprising an intermediate area (of 21.32 km^2) separated from Admiralty Bay waters by a relatively narrow passage (2.40 km wide) and influenced by the surrounding ice coastline (9.58 km of the 32.67 km long coastline).

These areas are shown in Fig. 1 and are used as separate, although deeply interrelated, regions for further study. To that end, measurement points were chosen, and their locations are marked on the map in Fig. 1; their details (location, depth, number of measurements performed at a given point, and, in the case of glacial cove points, distance from the water–ice boundary) are summarized in Table 1.

Measurements in the glacial coves and Admiralty Bay were taken from December 2018 until January 2022, whereas measurements in Ezcurra Inlet took place from October 2019 until January 2022.

Due to the proximity to glaciers and the harsh Antarctic weather, sampling in this region was especially strenuous. Each measurement campaign lasted only a few hours and was performed from the decks of small Zodiac boats (Fig. 2) that provided little comfort to the crew. Moreover, getting to the assigned sites often involved manoeuvring through moving ice packs and bits of icebergs coming from calving glaciers. Sampling during the winter months required working in the dark, in extremely cold temperatures and with continuous contact to freezing water.

Table 1. Details of the measurement sites. The depth measurements are based on the YSI EXO sonde depth sensor; depths > 100 at a given site indicate that the sonde was lowered to the cable limits (100 m) and did not reach the ocean bottom. Distances from glacial fronts were measured only for sites within smaller glacial coves adjacent to individual glaciers, as sites in Admiralty Bay and Ezcurra Inlet were influenced by a number of glaciers in their vicinity.

Site name and zone	Latitude	Longitude	Depth (m)	Distance from glacial front (m) (2018–2021)
Glacial coves				
lr1	−62.1227	−58.4892	19	315–322
lr2	−62.1195	−58.4868	> 100	266−330
lr3	−62.1163	−58.4845	> 100	275–332
lr4	−62.1131	−58.4821	23	260–343
lr5	−62.1120	−58.4687	8	940–1018
lr6	−62.1152	−58.4711	66	880–951
lr7	−62.1184	−58.4734	> 100	902–952
lr8	−62.1216	−58.4758	> 100	868–912
lr9	−62.1247	−58.4782	3	929–932
ve1	−62.1361	−58.3380	2	71–481
ve2	−62.1375	−58.3429	8	359–780
ve3	−62.1391	−58.3483	29	686–1118
ve7	−62.1716	−58.4613	4	455–469
ve8	−62.1709	−58.4677	2	210–232
ve9	−62.1734	−58.4668	3	113–128
Admiralty Bay				
lv1	−62.1221	−58.4624	> 100	
lv2	−62.1251	−58.4412	> 100	
lv3	−62.1313	−58.3989	71	
lv4	−62.1343	−58.3777	17	
ve4	−62.1445	−58.3671	58	
ve5	−62.1553	−58.4047	> 100	
ve6	−62.1662	−58.4424	55	
Ezcurra Inlet				
ez1	−62.1812	−58.6172	56	
ez2	−62.1778	−58.5994	67	
ez3	−62.1750	−58.5811	51	
ez4	−62.1727	−58.5626	61	
ez5	−62.1702	−58.5441	68	
ez6	−62.1655	−58.5279	84	
ez7	−62.1595	−58.5136	> 100	
ez8	−62.1526	−58.5012	> 100	
ez9	−62.1462	−58.4878	> 100	

3 Methodology

3.1 Measured water properties

Measurements were performed with two professional YSI multiparameter EXO sondes (EXO1 and EXO2); these instruments have been designed for simultaneous investigation of multiple water quality properties and have also been used and tested by researchers worldwide (Snazelle, 2015). EXO1 consists of five sensor ports, and EXO2 contains seven ports; therefore, the water properties measured varied between the particular campaigns. Of the 3045 measurements collected, 2069 were acquired using the EXO1 sonde, and the remaining 976 were acquired with EXO2 and its larger sensor capacity (details seen in Fig. 2).

The list of the sensors and the properties investigated by each are summarized in Table 2. Some hydrographic properties are derived from direct sensor measurements (e.g. turbidity from light scatter). In these cases, the sondes automatically calculated the additional related values based on universally accepted formulas (Table 2).

Table 2. List of sensors and measured water properties (based upon YSI Inc, 2017).

		Sensor	Measured property	Unit	Accuracy/linearity	Direct measurement (D) or calculated from other measurement (C)
EXO2	EXO1	Conductivity/ Temperature	Conductivity	µS cm^{-1}	0–100 mS cm^{-1}: ±0.5 % of reading or 0.001 mS cm^{-1}, whichever is greater; 100–200 mS cm^{-1}: ±1 % of reading	D
			Specific conductivity	µS cm^{-1}		C – conductivity adjusted to temperature
			nLF conductivity	µS cm^{-1}		C – with temperature compensation
			Salinity	PSU		C – based on temperature and conductivity using APHA (1989)
			Temperature	°C	±0.01°	D
		Depth and level	Pressure	PSI	±0.04 m	D
			Depth	m		C – based on water and atmospheric pressure
		Dissolved oxygen	Dissolved oxygen	mg L^{-1}	±1 % of reading or ±0.01 mg L^{-1}	C – using Stern–Volmer equation from luminescence measurement corrected with temperature and atmospheric pressure
			Dissolved oxygen saturation	%		
			Dissolved oxygen local saturation	%		
		pH	pH	–, mV	±0.01	C – from electric potential difference
		Turbidity	Turbidity	FNU	0.3 FNU or ±2 % of reading, whichever is greater	C – from light scatter
	Not measured by EXO1	fDOM	Dissolved organic matter	QSU, RFU	$R^2 > 0.999$ for serial dilution of 300 ppb quinine sulfate solution	C – from fluorescence
		Total algae (Chl and BGA)	Chlorophyll *a*	µg L^{-1}, RFU	$R^2 > 0.999$ for serial dilution of rhodamine WT solution from 0 to 400 µg L^{-1} Chl equivalents	C – from fluorescence
			BGA PE (phycoerythrin)	µg L^{-1}, RFU	$R^2 > 0.999$ for serial dilution of rhodamine WT solution from 0 to 280 µg L^{-1} PE equivalents	C – from fluorescence

The abbreviations used in the table are as follows: nLF – non-linear function, PSU – practical salinity units, fDOM – fluorescent dissolved organic matter, FNU – formazin nephelometric units, QSU – quinine sulfate units, RFU – relative fluorescence units, Chl – chlorophyll, BGA – blue-green algae and PE – phycoerythrin.

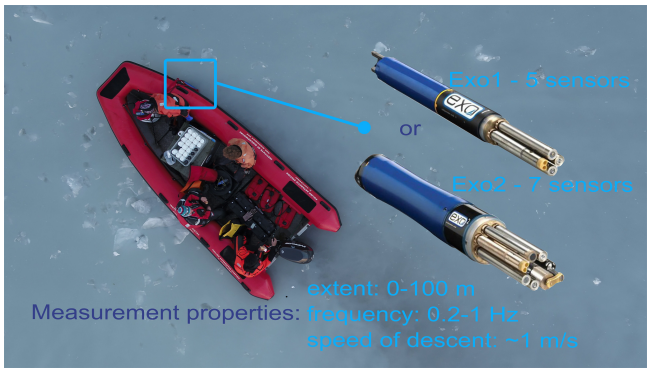

Figure 2. The images in the foreground (sourced from https://observator.com/products/ysi-exo-series-multiparameter-sonde/, last access: 3 September 2022) present the sondes used to make the measurements, and the text at the bottom of the panel outlines the measurement properties. The background image shows scientists in a Zodiac boat during measurements of water properties; the water is visibly infused with turbid GMW.

3.2 Measurement and data handling procedure: causes of possible data errors and missing values

Measurements were conducted from the deck of a Zodiac boat (Fig. 2). When the boat was at the designated point, the sonde was lowered by the cable from the reel to a maximum depth of 100 m. At sites with depth of less than 100 m (see Table 1 for information on sites' depths), the measurements were performed throughout the whole water column (until sea bottom was reached). At sites where the depth surpassed 100 m, data were only collected from the top 100 m; this is a limitation of this study, as data were not obtained from bottom portions of the water column. The sampling rate of the sondes was initially 0.2 Hz until 30 December 2019; after 30 December 2019, the sampling frequency increased to 1 Hz.

The intended descent rate of the instrument was $1\,m\,s^{-1}$; however, as this was manually controlled by the research personnel, the descent rate of the sonde varied significantly. Furthermore, the fact that the measurements were acquired by different crews may cause some discrepancy in the acquired data. The sensitivity of particular sensors varied. Therefore, if the probe was lowered too quickly, the measurements taken by some sondes may incorrectly correlate with the depth attributed to those measurements.

Other obstacles were caused by challenging weather and sea conditions. Waves and surface currents often considerably influenced the position of the boat, making it impossible to remain stationed at the assigned site location for the duration the cast. This can be seen from the position data recorded via handheld GPS during sensor deployment and included within the data file. Currents below the surface moved the sonde and cable horizontally from the initial cast position by an unknown extent.

On numerous occasions, ice prevented scientists from reaching specific sites. This was frequently the case in areas close to glacial fronts, most notably when the water surface froze during the winter months and when glacial calving increased in the summer.

All of the sensors were calibrated in accordance with guidelines found in the YSI EXO manual (YSI Inc, 2017), and they were replaced after the appropriate time or when malfunctions occurred that could not be otherwise resolved. The depth and level sensor was calibrated at the start of every survey day.

Measured data were initially recorded in the YSI proprietary format in software embedded into all of the sensors. At this stage, data went through real-time data filtering using a basic rolling filter as well as adaptive filtering and outlier rejection with the default manufacturer settings (for details, see YSI Inc, 2017). Gathered data were later downloaded using KorEXO software and exported to MATLAB where some outliers and extreme values were extracted due to one of the following reasons:

- notes from the measurement crew that indicated malfunctions or some other issues;
- the sonde showed unrealistic values from all of the sensors after reaching the bottom (caused by the contact with seafloor) at sites with depths of less than 100 m;
- the presence of other extreme values and outliers, which were scrutinized individually, such as continuous abnormal values from a particular sensor during a measurement day (indicating sensor malfunction or decalibration) or incidental extreme values recorded within otherwise reasonable datasets (indicating momentary disturbances).

Despite this series of steps, the whole dataset did not go through any formalized quality assessment/quality check procedure.

Optical sensors for total algae and fluorescent dissolved organic matter (fDOM) showed unrealistic negative values (77.82 % of chlorophyll *a*, 70.87 % of phycoerythrin and 60.45 % of fDOM readings). This was most probably caused by the chosen calibration method that employed a one-point procedure based on deionized water as a proxy for the zero fluorescence standard. This methodology was outlined by the sensor manufacturer (YSI Inc, 2017) but has proven insufficient in this environment; this suggests the necessity for a more robust method of calibration for future measurements. Nevertheless, these negative values have been retained in the data file because they represent the correct variability in the properties; however, their absolute values should be considered carefully, and more attention should be given to the relative units (RFU) for chlorophyll *a*, phycoerythrin and fDOM.

The turbidity sensor also showed negative values (19.56 % of the readings), but it was calibrated using a two-point procedure with an appropriate standard, and its FNU values

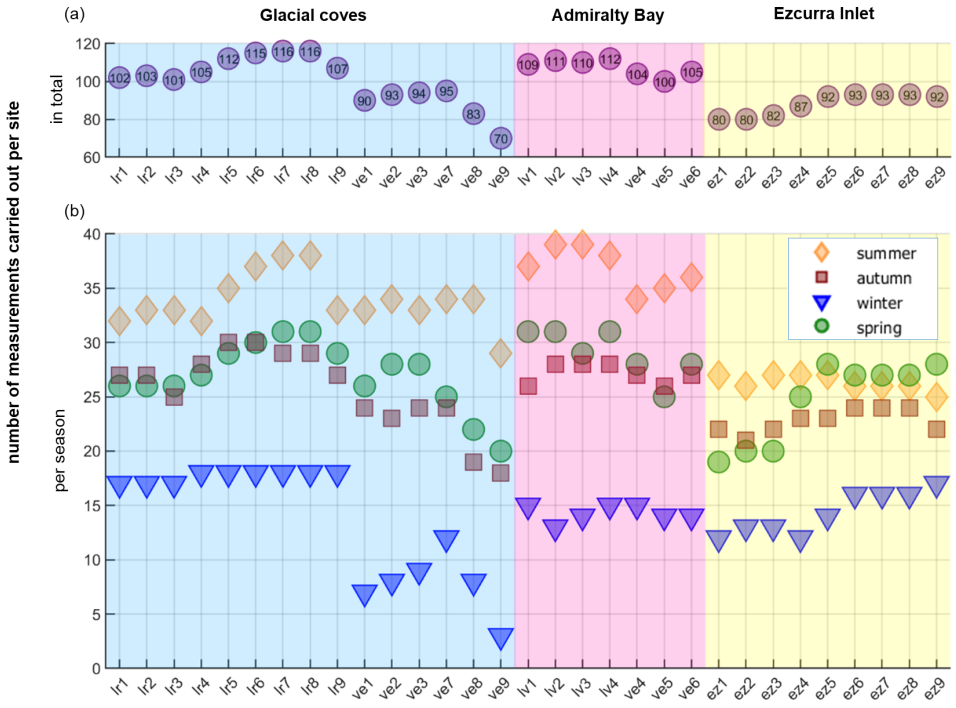

Figure 3. Number of measurements taken at the designated sites **(a)** in total and **(b)** by season (calendar) in the period from December 2018 to January 2022.

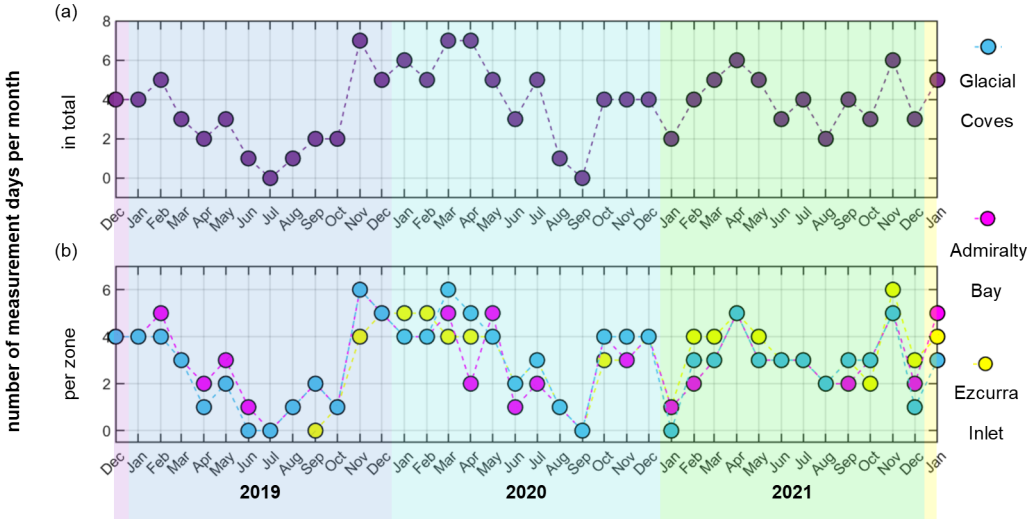

Figure 4. Number of measurement days per month **(a)** in total and **(b)** per zone (counted days on which measurements have been performed at at least half of zone's sites).

have been confirmed in Admiralty Bay waters via the laboratory procedure explained in detail by Wojcik-Długoborska et al. (2022).

4 Results

The results of the measurement campaign discussed above consist of a large and complex dataset describing the variability in the physical, chemical and biological properties in glacially influenced bays. Figure 3 presents a summary of the total number of investigations performed. This shows that, even at the sites sampled the least, it was possible to gather data during all seasons. However, most studies were performed during summer across all zones, while the fewest measurements were collected in winter. Interestingly, despite the unpredictable conditions in the glacial coves, the number

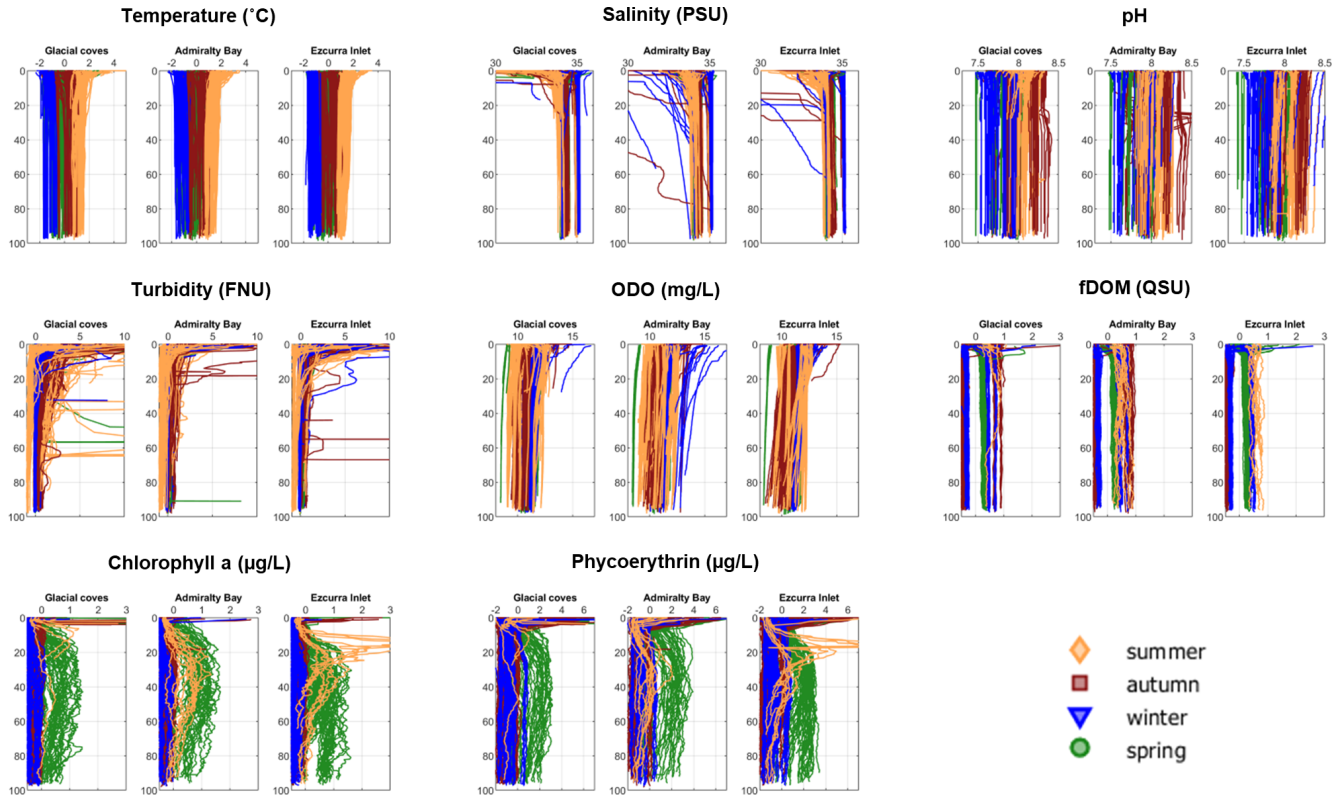

Figure 5. Vertical variability in measured properties divided by zone and season.

of surveys at each site fluctuates at around 100 per location (average of 98.2 measurements per site), which is promising for future statistical analysis.

Considering the complete duration of the projects (see Fig. 4), it is noticeable that the number of measurement days fluctuated, with increases during the warmer seasons when there was a maximum of 7 measurement days per month. In Fig. 4b, we observe that the same tendencies apply to all of the zones, and none of them have been more frequently investigated to any degree of significance. The average number of measurements per month was 3.74 in the glacial coves and 2.91 in Admiralty Bay, with the same number of successful measurement days (111) throughout the whole duration of the project, and 2.42 for Ezcurra Inlet over 92 measurement days.

The division of sites into three zones shows how proximity to glacial fronts and open ocean waters alters particular water quality properties. This effect is also notably correlated with seasonal shifts (Figs. 5, 6). In Fig. 5, the vertical distribution of all of the gathered data is presented. It is apparent that temperature, pH, optical dissolved oxygen (ODO), fDOM and phytoplankton pigment values are especially prone to change due to seasonal shifts, whereas salinity and turbidity values remain similar throughout the year. However, Fig. 6 provides a detailed illustration of how different properties vary in surface layers in contrast with the whole water column (limited to 100 m depth), most notably with respect to salinity and turbidity values, although it applies to all measured properties except for pH. This shows the impact of both atmospheric forcing and glacial outflow, which, based on buoyant plume model theory (Kimura et al., 2014; Mankoff et al., 2016; Jenkins, 2011) and observations (Chauché et al., 2014; Osińska et al., 2021), is mainly contained in the top layer of the ocean. Therefore, the results provide information on seasonal changes in water properties and glacier–ocean interactions and can be used for the validation of previously formulated methods of GMW tracking.

The 38-month-long duration of the project allowed for the tracking of seasonal variability across all measured hydrographic properties and showed consistency in all cases (Fig. 7). Moreover, this duration permits cautious predictions regarding long-term shifts in water column properties and reveals the impact of climate change or other influential conditions in this region. Using more sophisticated techniques, it is possible to more precisely determine the nature of this variability. The quantities of chlorophyll *a*, phycoerythrin and fDOM are not presented in Fig. 6, as their measurement was significantly less frequent.

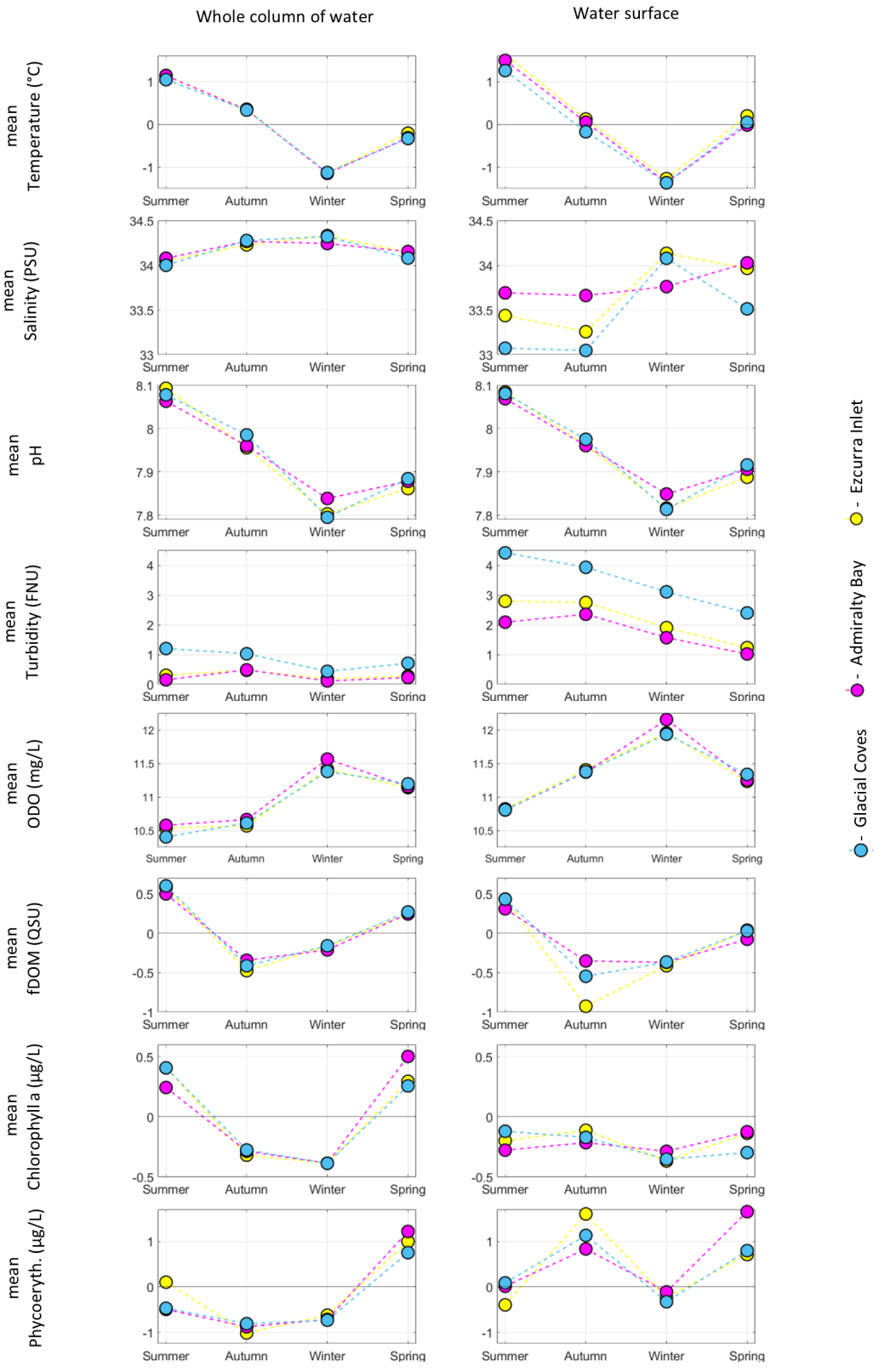

Figure 6. Mean values of measured properties dependent on season for the whole water column and the top 5 m of surface water.

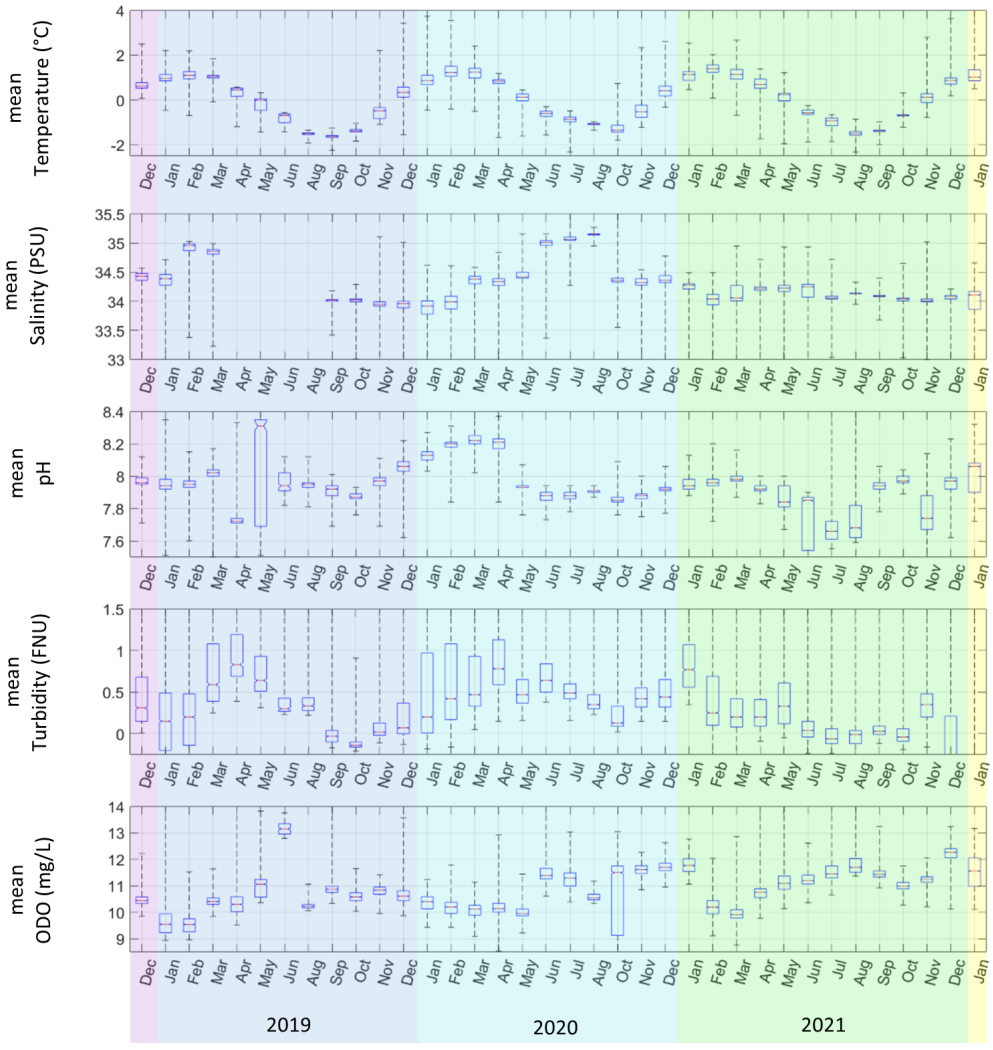

Figure 7. Box plot of monthly properties' mean values (excluding properties measured solely by EXO2 sonde devices due to their significantly shorter time series).

5 Data availability

The described dataset is freely accessible at the PANGAEA repository: https://doi.org/10.1594/PANGAEA.947909 (Osińska et al., 2022), under a non-restrictive CC BY 4.0 licence.

6 Conclusions

The assembled dataset shared here presents an opportunity to develop a better understanding of Admiralty Bay water characteristics over the 38-month survey period and can be used in further studies exploring the nature of and changes in glacially influenced regions in general. The sheer magnitude of this investigation, with 3045 separate measurements acquired on 142 different days, validates its importance and inspires optimism regarding future work and the application of these data.

The scope of the measured parameters (thermodynamic, physical, chemical and biological) paints a wide and precise picture of AB hydrographic variability during all months of the year and may allow for a multidisciplinary analysis of the complex processes that take place at this location. The varied settings of study sites allow for the tracking and identification of GMW and other water masses (Straneo et al., 2011; Chauché et al., 2014). Additionally, this sizable dataset can be used as a tool for better understanding the general hydrodynamics and thermodynamics of glacial bays and fjords and may be employed for the validation of coupled glacier–ocean modelling (Cowton et al., 2015; De Andrés et al., 2021; Bertino and Holland, 2017).

Author contributions. MO conceptualized the study; curated the data; undertook the formal analysis, investigation and validation; developed the methodology; created figures; and prepared the orig-

inal draft of the paper. KAW was responsible for carrying out the investigation, developing the methodology, and reviewing and editing the manuscript. RJB acquired funding, carried out the investigation, was responsible for project administration, acquired resources, supervised the study, and reviewed and edited the manuscript.

Competing interests. The contact author has declared that none of the authors has any competing interests.

Disclaimer. Publisher's note: Copernicus Publications remains neutral with regard to jurisdictional claims in published maps and institutional affiliations.

Acknowledgements. Calculations were made possible by software provided by CI TASK (Centrum Informatyczne TASK) in Gdańsk. The authors also wish to acknowledge the invincible members of the so-called "MorMon" team, part of Polish Antarctic Station's crew, who throughout the whole period of the project, often in trying and almost always in uncomfortable conditions, carried out the measurements presented in this work.

Financial support. This work was supported by the National Science Centre, Poland (grant no. UMO-2017/25/B/ST10/02092; Quantitative assessment of sediment transport from glaciers of South Shetland Islands on the basis of selected remote sensing methods).

Review statement. This paper was edited by Salvatore Marullo and reviewed by Mattias Cape, Luca Fiorani, and one anonymous referee.

References

APHA: Standard Methods for Examination of Water and Wastewater, 17th Edn., Washington D.C., ISBN 9780875531618, 1989.

Bendtsen, J., Mortensen, J., Lennert, K., and Rysgaard, S.: Heat sources for glacial ice melt in a west Greenland tidewater outlet glacier fjord: The role of subglacial freshwater discharge, Geophys. Res. Lett., 42, 4089–4095, https://doi.org/10.1002/2015GL063846, 2015.

Bertino, L. and Holland, M. M.: Coupled ice-ocean modeling and predictions, J. Mar. Res., 75, 839–875, https://doi.org/10.1357/002224017823524017, 2017.

Chauché, N., Hubbard, A., Gascard, J.-C., Box, J. E., Bates, R., Koppes, M., Sole, A., Christoffersen, P., and Patton, H.: Ice–ocean interaction and calving front morphology at two west Greenland tidewater outlet glaciers, The Cryosphere, 8, 1457–1468, https://doi.org/10.5194/tc-8-1457-2014, 2014.

Cowton, T., Slater, D., Sole, A., Goldberg, D., and Nienow, P.: Modeling the impact of glacial runoff on fjord circulation and submarine melt rate using a new subgrid-scale parameterization for glacial plumes, J. Geophys. Res.-Oceans, 120, 796–812, https://doi.org/10.1002/2014JC010324, 2015.

De Andrés, E., Otero, J., Navarro, F. J., and Walczowski, W.: Glacier-plume or glacier-fjord circulation models? A 2-D comparison for Hansbreen-Hansbukta system, Svalbard, J. Glaciol., 67, 797–810, https://doi.org/10.1017/jog.2021.27, 2021.

Dziembowski, M. and Bialik, R. J.: The Remotely and Directly Obtained Results of Glaciological Studies on King George Island: A Review, Remote Sens. Basel, 14, 2736, https://doi.org/10.3390/RS14122736, 2022.

Gerrish, L., Fretwell, P., and Cooper, P.: High resolution vector polylines of the Antarctic coastline (7.4), ADD – Antarctic Digital Database [data set], https://doi.org/10.5285/e46be5bc-ef8e-4fd5-967b-92863fbe2835, 2021.

Jenkins, A.: Convection-Driven Melting near the Grounding Lines of Ice Shelves and Tidewater Glaciers, J. Phys. Oceanogr., 41, 2279–2294, https://doi.org/10.1175/JPO-D-11-03.1, 2011.

Kimura, S., Holland, P. R., Jenkins, A., and Piggott, M.: The Effect of Meltwater Plumes on the Melting of a Vertical Glacier Face, J. Phys. Oceanogr., 44, 3099–3117, https://doi.org/10.1175/JPO-D-13-0219.1, 2014.

Mankoff, K. D., Straneo, F., Cenedese, C., Das, S. B., Richards, C. G., and Singh, H.: Structure and dynamics of a subglacial discharge plume in a Greenlandic fjord, J. Geophys. Res.-Oceans, 121, 8670–8688, https://doi.org/10.1002/2016JC011764, 2016.

Osińska, M., Bialik, R. J., and Wójcik-Długoborska, K. A.: Interrelation of quality parameters of surface waters in five tidewater glacier coves of King George Island, Antarctica, Sci. Total Environ., 771, 144780, https://doi.org/10.1016/j.scitotenv.2020.144780, 2021.

Osińska, M., Wójcik-Długoborska, K. A., and Bialik, R. J.: Water conductivity, salinity, temperature, turbidity, pH, fluorescent dissolved organic matter (fDOM), optical dissolved oxygen (ODO), chlorophyll a and phycoerythrin measurements in Admiralty Bay, King George Island, from Dec 2018 to Jan 2022, PANGAEA [data set], https://doi.org/10.1594/PANGAEA.947909, 2022.

Rückamp, M., Blindow, N., Suckro, S., Braun, M., and Humbert, A.: Dynamics of the ice cap on King George Island, antarctica: Field measurements and numerical simulations, Ann. Glaciol., 51, 80–90, https://doi.org/10.3189/172756410791392817, 2010.

Snazelle, T. T.: Evaluation of Xylem EXO water-quality sondes and sensors, U.S. Geological Survey Open-File Report 2015-1063, https://doi.org/10.3133/OFR20151063, 2015.

Straneo, F.: Impact of the large scale ocean circulation on Greenland's outlet glaciers, Quaternary Int., 279–280, 472, https://doi.org/10.1016/j.quaint.2012.08.1584, 2012.

Straneo, F., Curry, R. G., Sutherland, D. A., Hamilton, G. S., Cenedese, C., Våge, K., and Stearns, L. A.: Impact of fjord dynamics and glacial runoff on the circulation near Helheim Glacier, Nat. Geosci., 4, 322–327, https://doi.org/10.1038/ngeo1109, 2011.

Wójcik-Długoborska, K. A., Osińska, M., and Bialik, R. J.: The impact of glacial suspension color on the relationship between its properties and marine water spectral reflectance, IEEE J. Sel. Top. Appl., 15, 3258–3268, https://doi.org/10.1109/JSTARS.2022.3166398, 2022.

YSI Inc: Exo User Manual, Yellow Springs, 1–154 pp., 2017.

frontiers | Frontiers in Marine Science

TYPE Original Research
PUBLISHED 11 April 2024
DOI 10.3389/fmars.2024.1365157

OPEN ACCESS

EDITED BY
Luigi Jovane,
University of São Paulo, Brazil

REVIEWED BY
Craig Stevens,
National Institute of Water and Atmospheric Research (NIWA), New Zealand
Andrew Klein,
Texas A and M University, United States
Ronald Buss de Souza,
National Institute of Space Research (INPE), Brazil

*CORRESPONDENCE
Maria Osińska
maria.osinska@phdstud.ug.edu.pl

RECEIVED 03 January 2024
ACCEPTED 26 March 2024
PUBLISHED 11 April 2024

CITATION
Osińska M and Herman A (2024) Influence of glacial influx on the hydrodynamics of Admiralty Bay, Antarctica - study based on combined hydrographic measurements and numerical modeling.
Front. Mar. Sci. 11:1365157.
doi: 10.3389/fmars.2024.1365157

Influence of glacial influx on the hydrodynamics of Admiralty Bay, Antarctica - study based on combined hydrographic measurements and numerical modeling

Maria Osińska[1]* and Agnieszka Herman[2]

[1]University of Gdańsk, Faculty of Oceanography and Geography, Gdańsk, Poland, [2]Institute of Oceanology, Polish Academy of Sciences, Sopot, Poland

This study investigates the impact of glacial water discharges on the hydrodynamics of a glacial bay in Antarctica, comparing it to well-studied northern hemisphere fjords. The research was carried out in Admiralty Bay (AB) in the South Shetland Islands, a wide bay adjacent to twenty marine-terminating glaciers. From December 2018 until February 2023, AB water properties were measured on 136 days. This dataset showed that a maximally two-layered stratification occurs in AB and that glacial water is always the most buoyant water mass. Using the Delft3D Flow, a three-dimensional hydrodynamical model of AB was developed. During tests, the vertical position and initial velocity of glacial discharges have been shown to be insignificant for the overall bay circulation. Fourteen model scenarios have been calculated with an increasing glacial influx added. The AB general circulation pattern consists of two cyclonic cells. Even in scenarios with significant glacial input, water level shifts and circulation are predominantly controlled by the ocean. Glacial freshwater is carried out of AB along its eastern boundary in a surface layer. Freshwater thickness in this outflow current is maximally 0.27-0.35 m. Within the inner AB inlets, significant glacial influx produces buoyancy-driven vertical circulation. Using an approach combining hydrographic and modeling data, a four-year timeseries of glacial influx volumes into AB has been produced. On average, glacial influx in summer is 10 times greater than in spring and winter and 3 times higher than in autumn. The annual glacial influx into AB was estimated at 0.434-0.632 Gt. Overall, the study demonstrated the unique characteristics of the topography and forcings that influence the hydrodynamics of an Antarctic glacial bay.

KEYWORDS

Admiralty Bay, South Shetland Islands, West Antarctic Peninsula (WAP), numerical modeling, glacial discharge, coastal hydrodynamics, glacial fjord

1 Introduction

Antarctic coastal areas play a crucial role within the broader Southern Ocean system. In the West Antarctic Peninsula (WAP) region more than 650 marine terminating glaciers drain into the ocean, mostly through glacial bays (Cook et al., 2016). Glaciers are significant contributors to global sea level rise due to their high accumulation and ablation rates (Gregory et al., 2013). The glacial water inflow to the ocean influences a wide range of climate-sensitive processes, including shifts in the carbon cycle, ocean acidification, and reorganization of water column stratification (IPCC, 2022). With it, additional carbon, iron, and manganese are transported into the ocean, stimulating phytoplankton blooms and impacting local food chains (Schloss et al., 2012; Forsch et al., 2021). To comprehend the impact of glacial water on the Southern Ocean, it is imperative to understand the hydrodynamics of glacial bays. In particular, it is crucial to understand how bay dynamics respond to variations in the volume of glacial water influx in an era of unavoidable acceleration of the West Antarctic ice sheet melt rates (Naughten et al., 2023). This is because it is expected that unprecedentedly large amounts of freshwater will be introduced into Antarctic coastal waters in the near future, which could have complex and unanticipated consequences for regional hydrodynamics.

Freshwater from glaciers, both from subglacial discharges and submarine melting, mixes with ambient water, forming Glacially Modified Water (GMW; Straneo and Cenedese, 2015). To date, the majority of studies into GMW transport and its influence on coastal hydrodynamics have concentrated on fjords in the northern hemisphere, which differ geomorphologically from Antarctic glacial bays (Cottier et al., 2010). Fjords in Greenland, Alaska, and Spitsbergen are typically long, narrow, and deep. In these basins, described by a large Rossby internal radius (Cottier et al., 2010; Valle-Levinson, 2022), the role of cross-fjord circulation is often minimal, allowing for simplified analysis and modeling in only two dimensions (Motyka et al., 2003; Mortensen et al., 2013; Sciascia et al., 2013).

Motyka et al. (2003) demonstrated that circulation in narrow fjords may be reduced to a single vertical cell with GMW flowing away from the glacial front in the surface layer and ocean waters flowing in towards the front beneath it, upwelling along the glacier, entrained by rising subglacial discharge. This basic model, however, is inadequate in larger Greenlandic fjords, since glacial waters do not always reach the surface due to a larger scale and complex water column stratification (Straneo et al., 2011; Sciascia et al., 2013).

"Unmixing GMW" methods based on hydrographic data are the most widely used techniques for quantifying and tracking pathways of glacial water in the ocean (Jenkins, 1999; Jenkins and Jacobs, 2008; Straneo et al., 2011; Bartholomaus et al., 2013; Mortensen et al., 2013). When GMW spreads in a narrow fjord from a singular glacial front, this analysis can provide almost the entire story of GMW transport since it shows the spatial variability of freshwater content as a function of depth and distance from the outlet. However, in wide bays with complex bathymetry and several marine terminating glaciers, freshwater, after its initial injection, can circulate within the bay, mixing with ambient waters and impacting other ice–water fronts. Three-dimensional (3D) modeling is required to characterize such circulation, and it has been applied successfully in multiple studies. However, the setup used most commonly describes long, deep, and narrow fjords with a single glacial front (e.g., Xu et al., 2012; Sciascia et al., 2013; Cowton et al., 2015; Slater et al., 2018).

Our study area, Admiralty Bay (AB, 62°10′S, 58°25′W), is located in the South Shetland Islands, adjacent to the northern WAP region. AB has the distinctive traits of Antarctic bays rarely seen in the northern hemisphere: it is wide, has a complex coastline, and is adjacent to twenty marine terminating glaciers.

Although previous studies into GMW impact have predominantly focused on the northern hemisphere, recent research has also expanded our understanding of the hydrodynamics of the glacial bays of the WAP. In Marguerite Bay (68°30′S, 68°30′W), seasonal freshwater content variations were measured, and its sources were identified (Clarke et al., 2008; Meredith et al., 2010). The waters of Marguerite Bay and Barilari Bay (65°55′S, 64°43′W) were shown to be subject to intrusions of warm Upper Circumpolar Deep Water (UCDW), which can be an additional driver of glacial melting (Clarke et al., 2008; Cape et al., 2019). The study by Cape et al. (2019) examined the impact of glacial-oceanic interactions on coastal dynamics in Barilari Bay. Specifically, the study concentrated on the formation of surface GMW plumes and its consequences for local biogeochemistry. Lundesgaard et al. (2020) conducted a thorough investigation of the physical properties of water in Andvord Bay (64°50′S, 62°39′W), where the influence of UCDW was found to be limited due to the presence of a sill at the bay's outlet. Based on these findings, Hahn-Woernle et al. (2020) demonstrated the significant role of surface water thermodynamics in the bay system. Lundesgaard et al. (2019) showed how episodic strong wind events can play a substantial role in the export of GMW from Andvord Bay. Meredith et al. (2018) investigations in Potter Cove (62°14'S, 58°41′W), King George Island (KGI), have revealed the characteristics of glacial meltwater spreading from land-terminating Fourcade Glacier, a glacial form that is more prevalent in the South Shetlands than in the southern WAP region. In conclusion, our knowledge of the Antarctic glacial bay systems has grown over the past few years; a number of hydrodynamical drivers, such as the presence of UCDW, wind, heat content of the upper ocean, and glacial termini type, have been studied. The seasonal variations and long-term increase in glacial runoff have been shown through the analysis of hydrographic and glaciological data (Meredith and King, 2005; Vaughan, 2006; Clarke et al., 2008). However, the impact of glacial influx on the hydrodynamics of Antarctic glacial bays, particularly how it affects water level oscillations, circulation patterns, water column stratification, and freshwater distribution, have not yet been thoroughly studied in this region. Moreover, there have not been many prior attempts to analyze the seasonal variations in these processes. This is the goal of this study.

The structure of this paper follows the logical reasoning underlying this project, in which numerical modeling is based on the conclusions from the analysis of observational data. The study area is described in Section 3.1, followed by the details of *in situ* measurement methodology (Section 3.2.1). Section 3.2.2 provides a

general overview of water property variations in AB. A 3D circulation model was developed based on the conclusions of Section 3.2.2 (technical details in Section 3.3.1). The problem of determining the appropriate location of glacial water injection points in the model was essential. Therefore, the Section 3.3.2 describes its theoretical background and presents the results of model test runs conducted to examine it. The model was run in fourteen scenarios with an increasing glacial influx volume. The findings revealed the character and magnitude of glacial water's impact on water level variations, circulation, freshwater thickness (FWT), and pycnocline depth in the bay (Section 4.1). This enabled identification of boundaries between regions dominated by glacially and tidally-driven circulation patterns (Spall et al., 2017). Finally, in Section 4.2, an attempt was made to estimate the glacial runoff volume into AB. This estimate was based on a novel approach in which differences between modeling results and *in situ* measurements were used to select an optimal (most probable) influx volume at a given time instance, yielding a 136-record-long timeseries of glacial influx volumes in the period from December 2018 to February 2023 (Mortensen et al., 2014; Straneo et al., 2011; Sciascia et al., 2013). The results are followed by a discussion in Section 5.

The overall objective of this research is to identify key features of Antarctic bay's hydrodynamics, and its variability in response to glacial influx. It is one of the first attempts to model a 3D circulation within a bay with multiple marine-terminating glaciers, showing relative significance of different forcing mechanisms. Additionally, by comparing measurement and model results, seasonal estimates of glacial influx volumes were obtained.

2 Materials and methods

2.1 Study area

Admiralty Bay is a large inlet of KGI, the biggest island in the South Shetlands (Figure 1), a region described as especially sensitive to climate change (Bers et al., 2013). The acceleration of glacial melting during summer (Rückamp et al., 2010) and the recent absence of sea ice during winter are the most prominent indicators of this vulnerability (Eayrs et al., 2021; National Snow and Ice Data Center, C, 2023).

KGI is covered in 90% with ice, divided into interconnected icecaps (Simões et al., 1999). Twenty-five percent of AB's 150 km

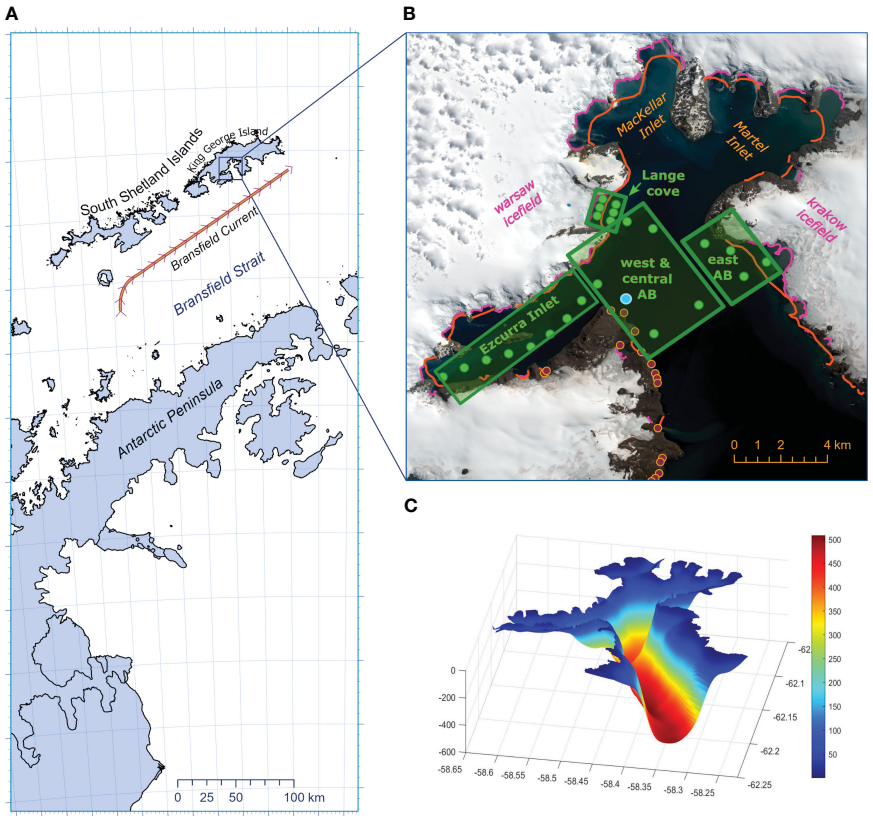

FIGURE 1
Admiralty Bay. **(A)** Regional map (Gerrish et al., 2021), Bransfield Current as per Thompson et al. (2009); **(B)** Admiralty Bay map; ocean-ice boundaries: in 2021 marked with pink lines (Gerrish et al., 2021), and in 1990 – orange lines (Battke, 1990); red points correspond to known creek outlets (Potapowicz et al., 2020 and observations); green points show *in situ* measurement sites and green boxes their groupings; blue dot indicates wavemeter mooring location (inset based on Sentinel imagery, 29.12.2021); **(C)** AB bathymetric map (m) and modeling domain.

long coastline consists of ice–water boundaries, formed by twenty maritime glaciers draining directly into the bay waters (indicated with orange lines in Figure 1A). All of them are relatively shallow (Figure 1C), with an estimated maximum grounding depth of ~150 m, and the majority of glacial fronts submerged by less than 50 m. Because of that, AB glacial fronts are considered to be nearly uniform vertically, without evidence for undercutting or floating tongues (Carroll et al., 2016). AB glaciers can be classified as intermediate forms between polar and temperate glaciers, with both geothermal and frictional heating as well as external warming inducing water discharge into the ocean (Jenkins, 2011). A comparison of a regional map from 1990 and recent satellite imagery (Battke, 1990) shows a significant retreat of local glacier fronts over the past 31 years (Figure 1B, orange lines – ice-water boundaries in 1990, pink lines – ice water boundaries in 2021).

Additional freshwater input into the bay is produced by glacial creeks, which frequently carry waters from glaciers that have recently retreated to land. Their existence and the amount of water being supplied through them vary significantly throughout the year. Consistently reoccurring summer creeks (17 separate outlets) noted by Potapowicz et al. (2020) and observed by the crew of the Arctowski Polish Antarctic Station have been marked in Figure 1B with red points. The mean annual precipitation in AB is approximatively 0.07 Gt (Plenzler et al., 2019). Considering estimated annual mean value of glacial influx of 0.434-0.632 GT (see sections 4.2 for details) the input from precipitation to the AB freshwater budget is relatively minor and was not considered in this analysis.

AB has an area of 150 km^2 and has been previously described as a wide fjord, however, geomorphologically, it is a tectonic estuary (Valle-Levinson, 2010), formed by geological faults (Majdański et al., 2008), which explains its distinction from northern hemisphere fjords. For the purposes of this study, a new, hitherto most precise bathymetric map of AB has been created, compiling data from Battke (1990), Majdański et al. (2008); Magrani et al. (2016) and self-conducted ADCP measurements (Figure 1C). It shows that AB's mean depth is 160 m, but in its central part there is a relatively narrow trough up to 600 m deep. AB is connected with Bransfield Strait through a 8 km wide opening, notably, without a well-defined sill.

Tidally controlled water level shifts oscillate between −1.5 and 1 m at the AB outlet (Padman et al., 2002). Locally, the most common wind direction is SW, present for around 25% of the time; wind events from other directions take up from 5 to 10% of the time (Plenzler et al., 2019). The occurrence frequency of long-lasting periods of along-fjord (NW or SE) katabatic winds, controlling water exchange with the ocean is, low. This is in contrast to Greenland, as noted by (Spall et al., 2017). Nevertheless episodic occurrence of this process is possible as recorded, e.g., in Andvord Bay by Lundesgaard et al. (2019).

In Bransfield Strait, Bransfield Current flows in a northeastern direction along the southern border of the South Shetlands and creates an effective barrier from outside currents (Zhou et al., 2006; Poulin et al., 2014; Moffat and Meredith, 2018); see Figure 1B). This blocking mechanism is strengthened by local bathymetry, which, close to the AB outlet, drops rapidly to over 2000 m, so that relatively shallow AB-shelf waters are only to a limited extent influenced by deep ocean hydrodynamics. Consequently, currents impacting the AB directly are forced by tides, with the Coriolis force playing a key role, which together drive water exchange with the ocean. According to Zhou et al. (2020) the full water exchange between AB and Bransfield Strait takes approximately 147 hours.

2.2 Hydrographic measurements

2.2.1 Methodology

Since December 2019, a comprehensive *in situ* measuring campaign has been conducted using YSI Exo CTD+ sondes to investigate the AB water properties. It comprised of vertical measurements of water conductivity, temperature, pH, turbidity, and dissolved oxygen, dissolved organic matter, chlorophyll A, and phycoerythrin content at 31 sites across four years. The openly accessible data up until January 2022 can be found in the PANGAEA repository (Osińska et al., 2022). Detailed information regarding the scope and methodology of data collection is described in Osińska et al. (2023). Measurements conducted using an unaltered methodology have continued up until February 2023, and their findings have been analyzed in this study. For the present analysis, 23 measurement sites with depths exceeding 10 m were chosen (Figure 1A; green points) and divided into four zones (Figure 1A; green boxes):

- *west and central AB* – west and central region of AB's main body,
- *east AB* – sites in the east part within the main body of AB,
- *Ezcurra Inlet* – within the smaller western inlet of AB,
- *Lange cove* – sites less than 1 km away from the medium-sized Lange glacier

Measurements with missing salinity records and those from the depths above 0.5 m have been excluded from the analysis (due to high uncertainty of near-surface measurements It was found that several salinity records had abnormally high mean values of >35.5, which raised suspicions. Consequently, it was decided that extracting outliers from the dataset was appropriate. A time-averaged salinity profile [$S^x(z)$] was calculated for each site from all measurements at that site $s_n^x(z)$, where z denotes depth, x denotes a specific site and n is an index of individual measurement at that site. The following records have been classified as outliers and removed from the dataset:

- 5% of profiles at each site with the largest standard deviation of differences (σ_D) from that site's mean salinity profile
- 5% of profiles at each site with the largest difference between vertically-averaged $s_n^x(z)$ and vertically-averaged $S^x(z)$

After this procedure, the remaining dataset consisted of 1830 profiles from 136 days and all seasons of the year.

Freshwater thickness (FWT) was determined for all profiles using the Holfort et al. (2008) formula:

$$\mathbf{FWT} = \int \left(\frac{S_{ref} - s_n^x(z)}{S_{ref}} \right) dz \quad (1)$$

where S_{ref} is a reference salinity value. S_{ref} was determined for each measurement day as the mean salinity value from all measurements from that day below 60 m. The decision to use records from below 60 m was based on modeling results that showed glacial water spreading maximally to this depth (details in Section 4.1.2).

2.2.2 Results analysis

Figure 2 provides a comprehensive depiction of the fluctuations in AB water properties over four years of hydrographic measurements (see also this data presented in vertical profiles of salinity in Supplementary Figure 1). Overall, the water temperature varied in a range of −2 to 2°C, while the salinity ranged from 33.3 to 34.6 (Figures 2A–H).

The surface freezing line seen in TS diagrams (Figure 3) shows that most of the time AB water properties were well above freezing conditions during all seasons of the year (details in Osińska et al., 2022). This is the reason for the absence of winter sea ice coverage in AB over the course of the measuring campaign.

The freshening of AB's surface water during austral summer (Figures 2B, D, F, H) and the corresponding peaks in FWT (Figure 4) indicate the presence of GMW. This is because marine terminating glaciers are a primary source of freshwater in the northern WAP region, as established by Powell and Domack (2002). Additionally, it has been determined that the contribution of sea ice and precipitation to AB's freshwater content is limited. No evidence of fresher water plumes in subsurface layers was detected (Figure 2H and more details in Osińska et al., 2023). Hence, the GMW continuously exhibits the highest buoyancy among the water masses in the AB region, a finding that has been corroborated by prior investigations conducted in the area (Monien et al., 2017; Meredith et al., 2018; Osińska et al., 2021).

The FWT variations exhibit a similar seasonal pattern across the entire AB. However, FWT values are lowest in the *west and central AB*, with a mean of 0.09 m and a median of 0.07 m (Figure 4). The FWT mean and median values in the *east AB* are 0.15 m and 0.14 m, respectively; in *Ezcurra Inlet*, they are 0.12 m and 0.10 m; and in *Lange cove*, they are 0.14 m and 0.12 m. This would suggest that the presence of GMW is lowest in the western regions of the main basin of AB and noticeably highest in its eastern region, even surpassing that of regions directly adjacent to glacial fronts, such as sites in the Lange cove.

TS diagrams, as shown in Figure 3, are used to differentiate between water masses inside of the AB. AB waters during the winter are generally homogenous, with temperature and salinity marginally rising as depth increases. During the spring season, a fresher and warmer layer of water is formed on the surface, overlaying waters characterized by increasing salinity and temperature with depth. Two layers in the AB water column are also present during summer and autumn. The summer surface layer experiences maximum freshening (average salinity dropping to 33.2) and warming (mean temperature ranging from 1 to 1.5°C). During the autumn, the upper layer, in comparison to the summer season, exhibits lower temperatures and higher salinity.

Observations indicate that AB contains up to two characteristic water layers throughout the course of a year. The distribution of these layers' salinity and temperature values can be largely attributed to atmospheric and glacial influences. The water mass found below the surface layer during the seasons of spring, summer, and autumn, as well as the principal water mass observed during winter, shall be referred to as ambient water (AW). This water mass

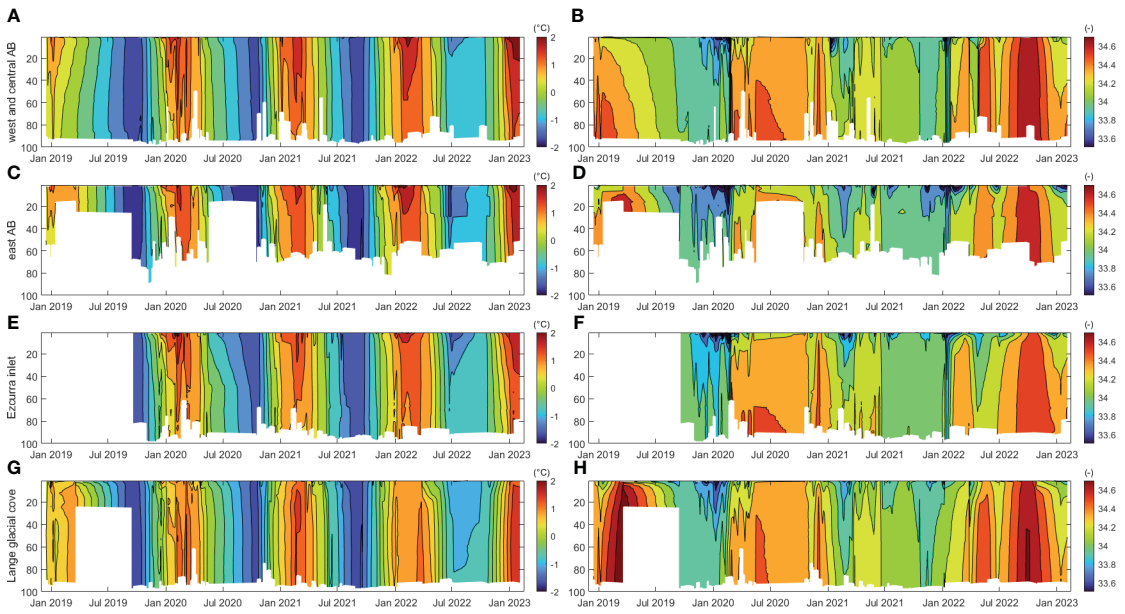

FIGURE 2
Overview of salinity and temperature records in AB. **(A, C, E, G)** mean temperature (°C) and **(B, D, F, H)** mean salinity in four zones: **(A, B)** – west and central AB, **(C, D)** east AB, **(E, F)** Ezcurra inlet, **(G, H)** Lange cove.

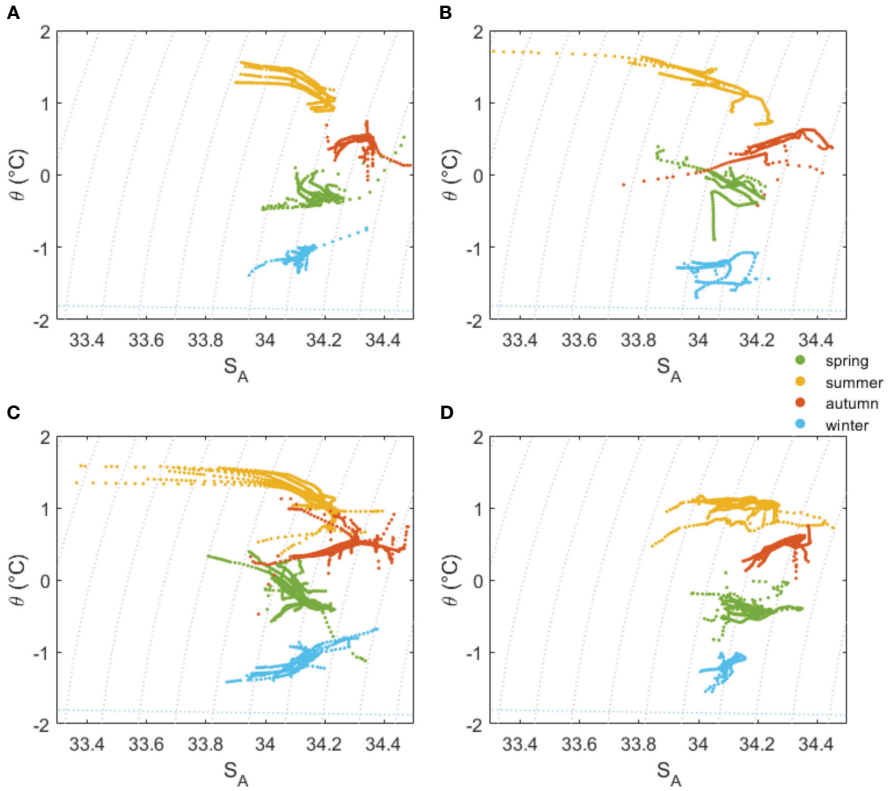

FIGURE 3
TS diagrams of mean seasonal values from each site; **(A)** – west and central AB, **(B)** east AB, **(C)** Ezcurra inlet, **(D)** Lange cove; blue dotted line – surface freezing line.

is primarily impacted by the waters of the Bransfield Strait and by atmospheric forcing. AW exhibit relatively small variability throughout the year and display typical patterns of seasonal fluctuation commonly observed in estuarian deep waters (Cottier et al., 2010). Fresh surface waters found in spring, autumn, and particularly during the summer are classified as GMW. GMW consists of a mixture of AW and glacial water that originates from subglacial discharge, submarine melting, glacial creeks, and icebergs. These waters are heated and cooled to varying extents through atmospheric forcing. The lowest summer surface temperatures were recorded in *Langel cove* since the freshly formed GMW surface layer has a limited duration of atmospheric exposure. Notably, there is a possibility of external freshwater entering AB at the surface, which may be indistinguishable from GMW using solely salinity records.

The presence of warm and highly saline Atlantic Waters in Greenland (Straneo et al., 2011; Sciascia et al., 2013; Slater et al., 2018) and CDW in the Antarctic (Moffat et al., 2009; Cape et al., 2019) has been shown to directly stimulate glacial melting and play an important role in shaping the hydrodynamics of glacial bays. The hydrographic data analyzed here does not support the existence of such warm external water masses in AB. The measurements conducted in this investigation were limited to a maximum depth of 100 m. Consequently, it is possible that distinct water masses could infiltrate deeper AB waters and remain undetected. Nevertheless, the probability of such an event and its substantial

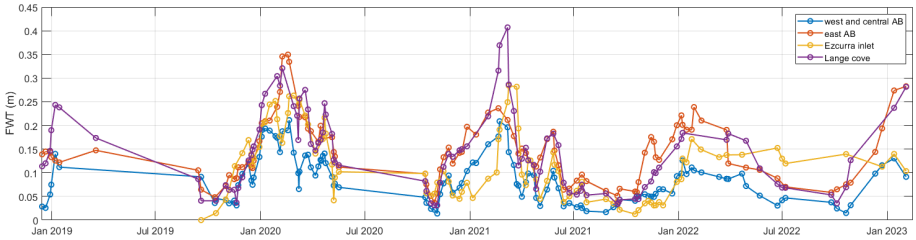

FIGURE 4
Mean freshwater thickness (m) from all sites in four zones in AB.

influence on AB's glacial-oceanic boundary is low. Because water depth near AB glaciers seldom exceeds 100 m (Figure 1C), any warmer and more saline water intrusions would be unable to reach glacial fronts unless their presence were recorded at shallower measurement sites. Additionally, earlier measurements conducted in AB over a wider vertical range also did not find any signs of the presence of such water masses (Carbotte et al., 2007). Finally, studies of regional ocean circulation concluded that CDW intrusions into AB are unlikely (Hofmann et al., 2011; Sangrà et al., 2011).

The general two-layered stratification enables the determination of the internal Rossby radius ($r_i = \frac{c_i}{f}$, where ${c_i}^2$ is the internal wave speed and f is the Coriolis parameter) which serves as a metric for evaluating the relative significance of water column stratification in comparison to rotation (Cottier et al., 2010). In the AB, depending on conditions, the internal Rossby radius varies between 0.41 and 11.86 km (its average values are 0.91 in winter, 1.00 in spring, 1.39 in autumn and 1.83 km in summer). Therefore compared to the ~8 km wide opening, it indicates that the AB can be classified as a "broad bay", where the presence of cross-bay circulation has substantial importance. This is valid for all seasons, even the period of enhanced glacial melting, when freshwater influx strengthens the water column's stratification.

2.3 Hydrodynamic modelling

2.3.1 Model setup

The presence of a two-layered stratification in AB, where the surface layer consists of the most buoyant layer of glacial meltwater (GMW), is reminiscent of the conditions outlined in the small-fjord single-cell circulation model proposed by (Motyka et al., 2003). However, due to the "broad" character of the bay, the AB model must be three-dimensional.

Modelling of AB hydrodynamics has been performed using the open-source Delft3D-Flow model, developed as part of a Delft3D suite created specifically for coastal, river, and estuarine hydrodynamics (Deltares, 2020). The calculations were performed on a high-resolution curvilinear grid of over 30,000 points, thus, an average grid cell corresponds to an area of approximately 55 m^2. Figure 1C shows the entire model domain. The analysis was conducted in 3D, with fifty layers utilizing a vertically scaled σ-coordinate system, with more densely spaced layers toward the domain's bottom and top. The bathymetric map shown in Figure 1C was used with a single smooth, ~10 km long open boundary between AB and Bransfield Strait.

The model was driven by tides, and temperature and salinity gradients. The tidal water level at the open boundary was calculated using the CATS2008 Antarctic tides model (Padman et al., 2002). Temperature and salinity data reanalysis by Dotto et al. (2021) was used to determine temperature and salinity values at the open boundary since it is the most robust data source for water properties in the northern WAP region, combining the majority of available *in situ* measurement records from 1990 to 2019. Seasonally averaged (for spring and summer) reanalysis values were extracted from a grid point closest to the model's open boundary and interpolated in time and space to create varied vertical salinity and temperature profiles. Dotto et al. (2021) results show that Bransfield waters are weakly stratified (Supplementary Figure 2) with seasonal mean temperature and salinity variations of -1.23–0.51°C and 34.22 – 34.27. The *in situ* measurement results from Osińska et al. (2023) were used to determine initial values of water salinity and temperature inside AB, which were uniformly set throughout the domain. It has been found during preliminary model testing that after less than three days of simulations, the salinity stratification in the whole bay was predominantly influenced by the open boundary input, therefore no variation in the initial conditions setting was necessary.

To capture the variability associated with the entire range of tidal patterns in this region, calculations lasted 58 days (from 1.12.2021 to 28.01.2022), consisting of 3.5 days of model warm-up followed by two full lunar cycles.

Following Deltares recommendation, bottom roughness was calculated using the 3D Chézy formula (Deltares, 2020), and assumed spatially homogenous due to lack of information on bottom roughness variations in AB. During model testing, it was discovered that unreasonably high values of kinetic energy dissipation rate (>1000 m^2/s^3) were obtained close to the open boundary after approximately two days of calculations and persisted throughout the simulation length. It was determined that this was caused by inappropriately assessed bottom roughness. Through several additional test runs it was experimentally found that uniform 3D Chézy bottom roughness coefficients of 40 $m^{1/2}/s$, in both U and V directions, is the highest coefficient value which does not result in unrealistic energy dissipation anomalies, which cause a rapid increase in flow velocities near the open boundary, and consequent model destabilization. The energy dissipation rates had a reasonable median value in the order of 10^{-8} m^2/s^3 (comparable values were found in Andvord Bay by Lundesgaard et al., 2020). Although they were greater in the bottom layer they were still within the realistic range of 10^{-6} -10^{-4} m^2/s^3 (see Supplementary Table 1, Inall and Rippeth, 2002). Therefore, it was determined that a bottom roughness coefficient of 40 $m^{1/2}/s$ was suitable and used all subsequent calculations.

Test runs were carried out to investigate the impact of boundary conditions on the model domain. In general, its impact was not significant. The only part of the model domain where the results were affected by the boundary conditions is the outermost, inflow region in the west (see Section 4.1.2). This implies that the results in this area should be interpreted with caution. The Reynolds number, which is a measure of turbulence, was in the range of 10^4–10^6 close to the open boundary and was lower than 100 close to the inner inlet heads.

Additional information regarding the model configuration can be found in Supplementary Table 2. Importantly, as indicated by the aforementioned description of the model configuration, no atmospheric forcing was considered, i.e., ocean-atmosphere momentum, heat, and moisture fluxes were set to zero. This decision is justified by the fact that, first, the salinity differences between the oceanic and glacial waters dominate the density structure and gradients in the domain of study, and second,

volume fluxes associated with tidal currents dominate those generated by wind, particularly over the time scales of several tidal cycles considered here. Such simplification is not unusual in studies at this scale (Straneo et al., 2011).

The typical density anomaly of water entering through the open boundary and that of the meltwater is σ=27.4 kg/m^3 (at S=34.1 and T=−0.2°C) and σ=0 kg/m^3 (at S=0 and T=0°C), respectively. The highest recorded value of surface water temperature observed in AB in the summer was 3.54°C (at 1.15 m depth), which was exceptionally high (Osińska et al., 2023); the corresponding density anomaly at S=32.56 is σ=26.0 kg/m^3. Therefore, the contribution of temperature to the net variability of water density in AB is minor. Accordingly, the core of the analysis and discussion in the following sections is considering factors driven by salinity fluctuations. Since seasonal salinity variations derived from Dotto et al. (2021) dataset are small (<0.1 difference between mean seasonal values) model setup accurately replicates AB open boundary conditions throughout the year.

For model validation purposes, an RBR wavemeter was moored within Admiralty Bay (location indicated with blue dot in Figure 1A) logging water level at 2 Hz frequency during the period from 6.12.2021 to 21.12.2021. The standard deviation of differences between Delft3D model data at this location and *in situ* RBR measurements is 0.08 m, the bias is 0.03 m, and their correlation coefficient is 0.99, i.e., the modeling results correspond very closely to the real water level changes in that part of AB. Analogously, CATS2008 compared with RBR measurements has a 0.08 m standard deviation of differences, a bias of 0.01 m, and correlation coefficient of 0.99.

2.3.2 Location, dispersal and volume of glacial freshwater influx

The representation of interactions between glaciers and oceans is a crucial component in establishing the framework for glacial bay hydrodynamical modelling. The description of oceanic dynamics near marine terminating glaciers often relies on the buoyant plume theory (BPT). The BPT explains how freshwater discharged from underneath the glacier upwells along the glacial front, entraining and mixing with ambient waters to form a GMW plume. This plume then induces the submarine melting of the glacier's front (Jenkins, 2011). The submarine melt rate is influenced by subglacial discharge volume and ambient water temperature; however, this relationship varies depending on the study location (Kimura et al., 2014; Xu et al., 2012; Sciascia et al., 2013). When GMW reaches its depth of neutral buoyancy, which may occur at or below the ocean surface, it forms a layer of distinct properties within the water column (Jenkins, 2011). The influence of glacial water on ocean hydrodynamics is contingent upon the distribution of subglacial discharge points, namely whether they are channelized or uniformly distributed along the glacial front, and the momentum of the discharge (Cowton et al., 2015; Slater et al., 2018).

The Buoyant Plume Model (BPM) coupled with the general circulation model (GCM) is currently considered the most sophisticated method for investigating the hydrodynamics of glacial bays (Cowton et al., 2015). However, its application may not always be necessary or practical. In an earlier investigation conducted by Chauché et al. (2014) observational data indicated that subsequent to channelized release, subglacial influx rapidly spreads laterally along the glacial front, effectively blurring the distinction between effects of localized and uniformly dispersed freshwater injection points. The study by Sciascia et al. (2013) demonstrated that the hydrodynamics of near-glacial waters is influenced to a greater extent by the volume of subglacial discharge than the momentum of its inflow. The usage of the BPM coupled with GCM for the purpose of modeling the hydrodynamics of bays with multiple ice-water boundaries is challenging. Firstly, such multiway coupling is computationally expensive. Furthermore, it requires detailed bathymetric and glaciological data, including discharge location points, volumes, and submarine melt rates (Carroll et al., 2016) which is currently unattainable in AB and, we argue, in the majority of glacial bays in Antarctica.

In light of the practical challenges involved, a question arises regarding the extent to which accurately reproduced vertical location and velocity of glacial water influx is significant for the understanding of general AB hydrodynamics. In order to address this question, several iterations of model tests were conducted, in which glacial water discharge locations and velocities were varied. The following are the identifiers and details of these test runs:

- *H0* - test run with glacial water discharged from all glaciers, homogenously through the entirety of glacial front, with zero initial velocity (treated as reference case for other scenarios)
- *H2* - test run with glacial water discharged from all glaciers, homogenously through the entirety of glacial front, with an initial velocity of 2 m/s
- *S0* - test run with glacial water discharged from all glaciers subglacially, with zero initial velocity
- *S2* - test run with glacial water discharged from all glaciers subglacially, with an initial velocity of 2 m/s

In order to emphasize the potential influence of glacial discharge velocity on AB hydrodynamics, a high value of 2 m/s was selected for testing (Xu et al., 2012; Cowton et al., 2015). The volume of the glacial discharge for all test runs was established at ~6 m^3/s per 1 km of glacial front, a value that was deemed reasonable for the AB region during the summer melt season (see section 4.2).

Three measures were employed to examine disparities between test run results: FWT (Figures 5A–D), pycnocline depth (Figures 5E–H), and depth-averaged flow velocity (Figures 5I–L). These metrics serve as the foundation for further analysis of AB hydrodynamics, making them suitable instruments for determining if the results of test scenarios exhibit substantial differences between each other. FWT was calculated using Formula (1), where S_{ref} was determined as the mean salinity from below 60 m across the entire AB. Given the stratification of model open boundary waters, the utilization of this FWT calculation method shows the presence of freshwater influx from the Bransfield Strait into AB. Hence, in order to illustrate the distribution of freshwater originating exclusively from AB glaciers, the FWT values calculated for a scenario devoid of

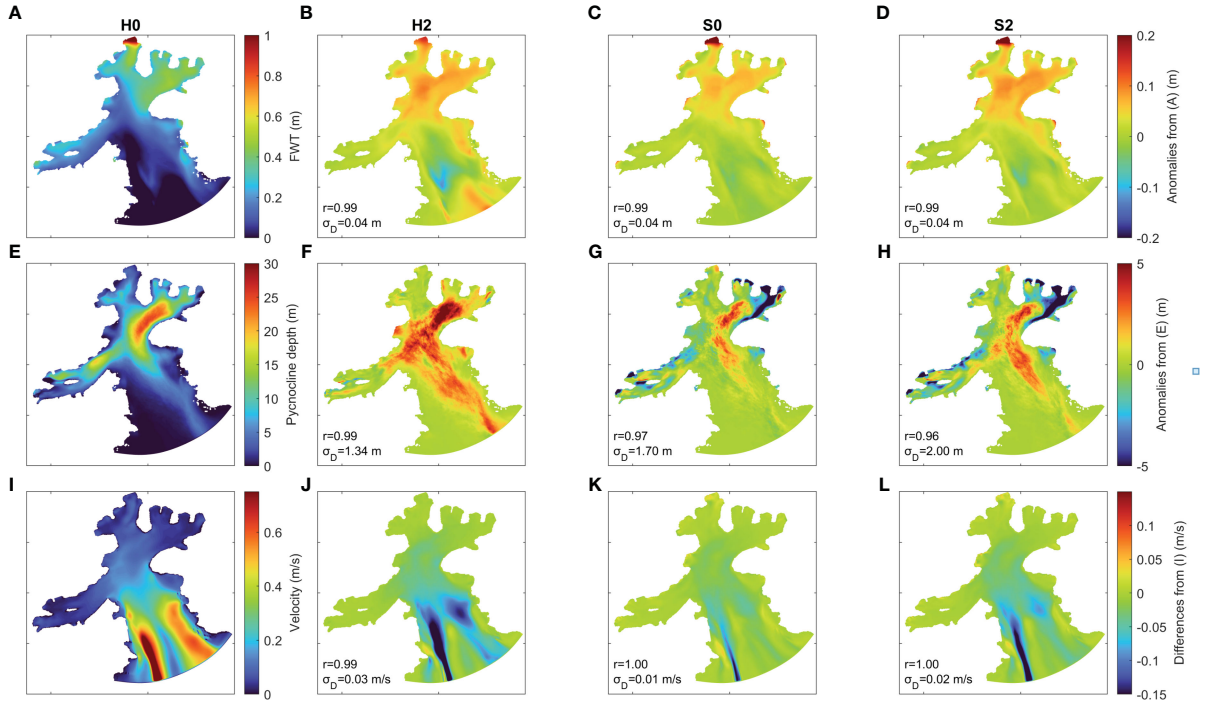

FIGURE 5
Comparison between model results with different glacial discharge locations and velocities. **(A–D)** FWT (m); **(E–H)** Pycnocline depth (m); **(I–L)** depth averaged velocities in m/s; **(A, E, I)** *H0* scenario – reference case; **(B, F, J)** *H2* scenario differences from the reference case; **(C, G, K)** *S0* scenario differences from the reference case; **(D, H, L)** *S2* scenario differences from the reference case. *r*, σ_D – correlation coefficients and standard deviation of differences between shown results and reference case respectively. All figures depict mean values from period from 1.01.2022 to 28.01.2022.

glacial water inflow (scenario *0* m^3/s) were subtracted from the FWT results of the four test runs. The pycnocline depth was calculated as the depth at which $d\sigma/dz < 0.025$ kg/m^3. The data that have been analyzed and presented in Figure 5 were averaged over a period from January 1st, 2022 to January 28th, 2022, which corresponds to a one complete lunar cycle.

All test run results show consistent patterns in the FWT, pycnocline depth, and flow velocity values distributions across the AB Supplementary Figure 3). On the other hand, discrepancies are visible when comparing maps of differences between test runs and the reference case *(H0)* results (Figure 5).

For all test scenarios the FWT values are highest in the northwest region of AB, ranging from 0.35 to 0.55 m, (Figures 5A–D). In that area the three scenarios *H2*, *S0*, and *S2* have slightly greater FWT values (<0.1 m) than the reference scenario *H0*. The overall FWT differences between scenarios range from −0.1 to 0.15 m (Figures 5B–D). In test runs with solely subglacial discharge, narrow regions of elevated FWT form along glacial fronts. The biggest differences in FWT and pycnocline depth are observed in scenario *H2* (Figures 5B, F). For instance, in an area of a maximum pycnocline depth (~25 m) for *H0*, the pycnocline depth increases by up to 4 m in *S0* and *S2*, and by over 6 m in *H2*. In *S0* and *S2* scenarios the presence of subglacial discharge and subsequent turbulent mixing prevents pycnocline formation in regions close to glacial fronts (blue areas in Figures 5G, H). Crucially, the overall flow pattern remains consistent in all examined cases, characterized by a strong influx from Bransfield Strait along the AB's western bank and an outflow in the east (see more details in section 4.1.2). The differences in flow velocities, shown in Figures 5I–L, are largest close to the AB opening. In scenarios *H2*, *S0*, and *S2*, the AB's inflow and outflow have reduced velocities compared to the reference case results. This slowing down is largest in cases in which glacial waters are discharged with 2 m/s velocity (up to a −0.25 m/s decrease in *H2* and −0.15 m/s decrease in *S2*).

The model test run results show that the freshwater content, the water column stratification, and the flow velocities in AB are locally impacted by changes in the location and momentum of glacial influx. In general, larger differences in the analyzed metrics were caused by variations in the velocity of glacial input rather than an alteration in its vertical position. Nevertheless, the overall circulation and glacial freshwater distribution patterns in AB have not changed as a result of employing any of the studied model configurations (Supplementary Figure 5). This conclusion is further strengthened by the high correlation coefficients (*r*) and low σ_D for all employed metrics across all scenarios (Figure 5). Therefore, it i justified to conclude that for examining the overall impact of glacial water on AB hydrodynamics, a simplified methodology that disregards the influence of the vertical position and velocity of glacial injections is adequate.

Consequently, further model simulations were performed with glacial water discharged homogenously through the entirety of the glacial front, from all glaciers, with zero initial velocity. A total of fourteen scenarios with increasing volumes of glacial runoff were

calculated: 0, 0.15, 0.3, 0.6, 0.9, 1.7, 3.0, 4.5, 6.0, 8.0, 11.0, 14.0, 28.0, and 60.0 m^3/s of freshwater volume discharged per ~1 km of glacial front. Henceforth, these values will be employed as identifiers for the scenarios in order to enhance the conciseness and clarity of the text. Input of freshwater from the creeks was assumed to be vertically homogenous, was of equivalent volume to runoff from ~1 km of a glacial front in a given scenario and was introduced through a single grid cell.

3 Results

3.1 Response of AB hydrodynamics' to the increase in glacial discharge

3.1.1 Water level changes

Modeling results were analyzed through Principal Component Analysis (PCA) of water levels, using results from two full tidal cycles from 4.12.2021 12:00 to 28.01.2022 00:00. Each PCA mode consists of a spatial distribution (map) of PCA coefficients (also known as loadings), a time series of PCA scores showing the relative strength of that mode through time, and the overall percentage of the total variance of the dataset explained by that mode. Through the calculation of the squared correlation coefficients (r^2) between scores of PCA modes and time series of water level in all active grid points, maps of the spatial distribution of percentages of variance explained by the first four modes have been obtained (Figures 6B–E).

Tides are a primary driver of water level fluctuations in AB. This is demonstrated in Figure 6A where a comparison of *in situ* measurements collected by RBR wavemeter moored 9.5 km away from the AB outlet (location marked in Figure 1A) with tidal data from CATS2008 at the open boundary of the Delft3D model is shown. The blue line corresponding to *in situ* measurements exhibits only small deviations from modeled data, presumably during periods of very strong winds. The yellow line represents Delft3D model results at the grid point closest to the wavemeter location. The very good agreement between the three curves shows that the water level in the whole AB reacts almost instantaneously to the open boundary forcing.

PCA analysis of water level in the *0 m^3/s* scenario further confirms almost instantaneous response of the whole AB to tidal shifts. Figures 6B–E shows maps of coefficients corresponding to the first four PCA modes and the percentage of water level variance explained by them, respectively. The first PCA mode (PCA 1), which represents homogenous changes in the water level of the whole AB, explains more than 99.8% of the variance in all studied scenarios. Accordingly, the PCA 1 score correlates almost perfectly with the time series of water level at the boundary and inside of the model domain (see time series in Figure 6A). This indicates that anomalies from this pattern are of the order of a hundredth of a percentage, even in the *60 m^3/s* scenario, in which an additional 2000 m^3 of water is pumped into AB every second. The predominance of tidal impact on water level changes is not surprising, since volume flux through the open boundary is of the order of 100,000 m^3/s.

Although explaining small percentages of variance, other PCA modes of water level shifts are showing important characteristics of water level fluctuations in AB. Modes 2-4 represent standing-wave-like water level fluctuations with respectively one, two, and three nodes (Valle-Levinson, 2022). Each of the maps in Figures 6B–E

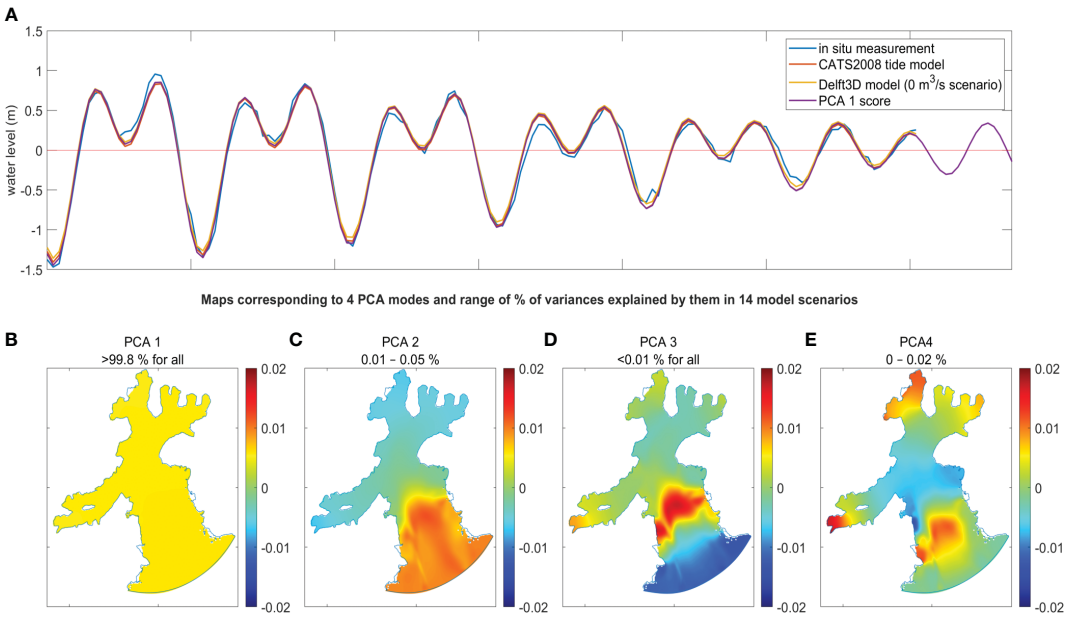

FIGURE 6
Results of PCA analysis of water level changes in 14 scenarios. **(A)** comparison of *in situ* water level measurements, CATS2008 tide model input data, Delft3D 0 m^3/s model results and normalized PCA1 score (note that score values are non-dimensional, they have been divided by its double standard deviation to fit); **(B–E)** maps corresponding to first four principal components of water level 0 m^3/s scenario (-); the percentages of water level variance explained by each mode in fourteen scenarios are shown above each map.

emphasizes a region in central AB that corresponds to the location of a smaller circulation cell in the overall AB circulation pattern (Section 4.1.2 and Figure 7).

3.1.2 Changes in circulation and freshwater distribution

The most notable feature of AB general circulation is a strong northerly flow along its western boundary (Figure 7A). It is formed by the Coriolis force acting upon Bransfield Strait waters flowing northeast along the edge of the South Shetland Islands (Zhou et al., 2002). The existence of this current was recognized by prior modeling conducted in the AB by (Robakiewicz and Rakusa-Suszczewski, 1999). Following its initial development, the AB inflow current continues in a northerly direction and subsequently undergoes bifurcation. Part of it flows to the right in the central region of the main body of the AB, approximately 7 km

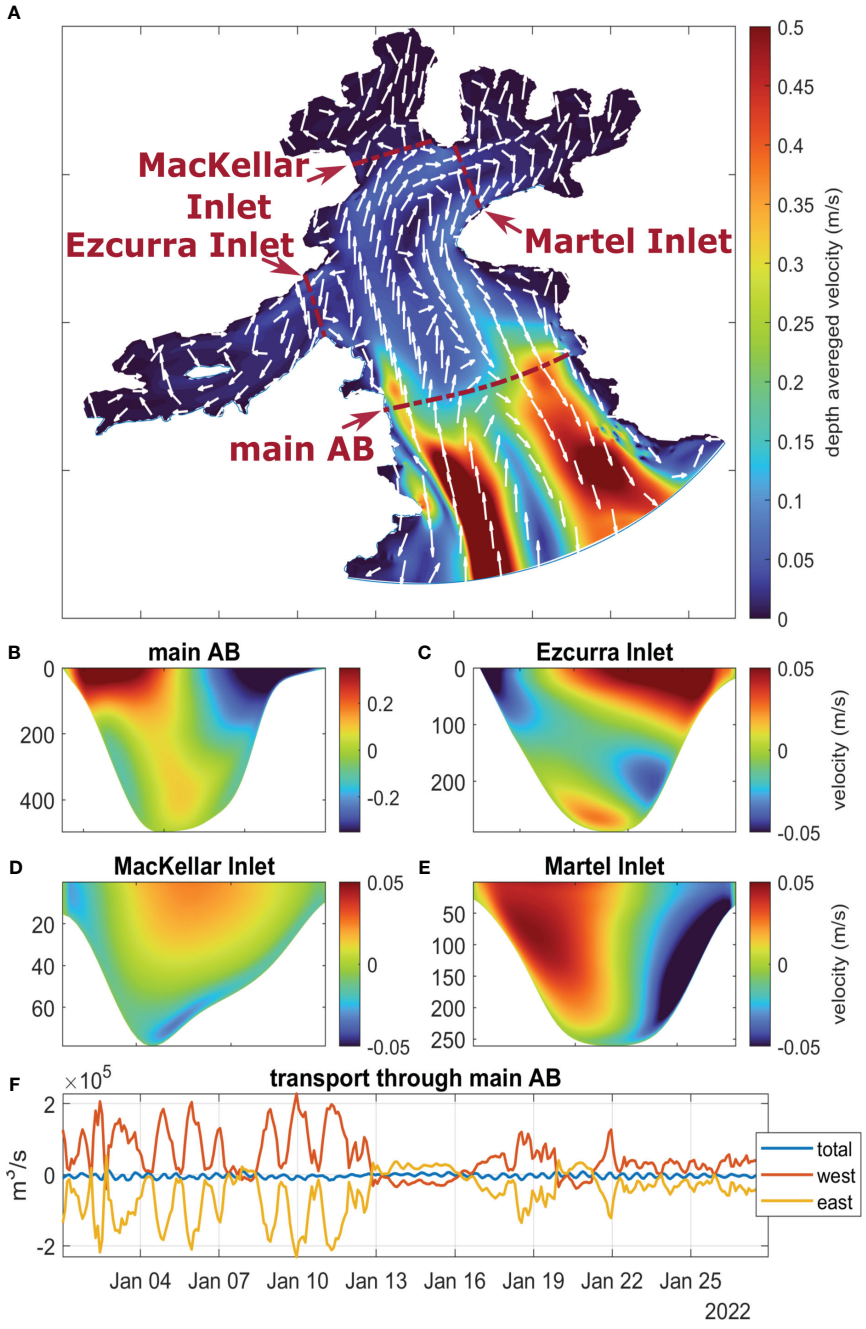

FIGURE 7
General circulation pattern of AB without glacial influx; **(A)** horizontal flow depth averaged velocities (map colors) and directions (white arrows); **(B–E)** horizontal velocities across four crossections (their location in Figure 7A, positive values correspond to inflow into inlets, negative to outflow; **(F)** transport through main AB crossection, total (blue line) and divided into western (red line) and eastern half (yellow line). Values in **(A–E)** are average for the period 1.01.2022-28.01.2022.

from the AB outlet (around the location of *main AB* cross-section), and then exits the bay in close proximity to its eastern boundary. The second limb of the current penetrates deeper before reversing its course in the main embranchment of the bay (~13.5 km from the opening) and also flows back to the bay opening along its eastern coast. The clockwise (cyclonic) circulation cells formed by these two branches are crucial elements of the water exchange mechanism between the ocean and inner bay waters. A visualization of monthly average velocities across the *main AB* cross-section (Figure 7B) reveals that this exchange has the greatest magnitude in the surface layer. In the scenario without glacial influx there exists a state of equilibrium between the amount of water flowing into AB via its western half and the amount flowing out of it through the eastern half of the *main AB* cross-section (Figure 7F). At spring tide, the volume of water transported through each of the halves reaches $2{\cdot}10^5$ m^3/s. The quantities of water penetrating the three inner inlets of AB, Ezcurra, MacKellar, and Martel Inlet are two orders of magnitude smaller, with proportionally lower velocities observed across their respective cross-sections (Figures 7C–E).

When glacial influx is introduced, AB's cyclonic circulation explains the development of distinct patterns in glacial water dispersal, illustrated by FWT and pycnocline depth maps (Figure 8). In each of the model scenarios, following an initial warm-up period, a quasi-stationary state is reached, in which the distribution of FWT remains approximately constant (Supplementary Figure 4). With rising glacial influx levels, freshwater accumulates in the northeastern region of AB, specifically in MacKellar and Martel Inlets. This freshwater is then transported to Bransfield Strait by the AB's eastern outflowing current. In the accumulation zones, the FWT values range from 0 to 0.5 m. The FWT exceeds 1 m in larger areas only in the two strongest glacial influx scenarios, *28 m^3/s* and 60 *m^3/s*. The increase of glacial input results in the expansion of the region where the pycnocline occurs, as well as in its deepening. The pycnocline

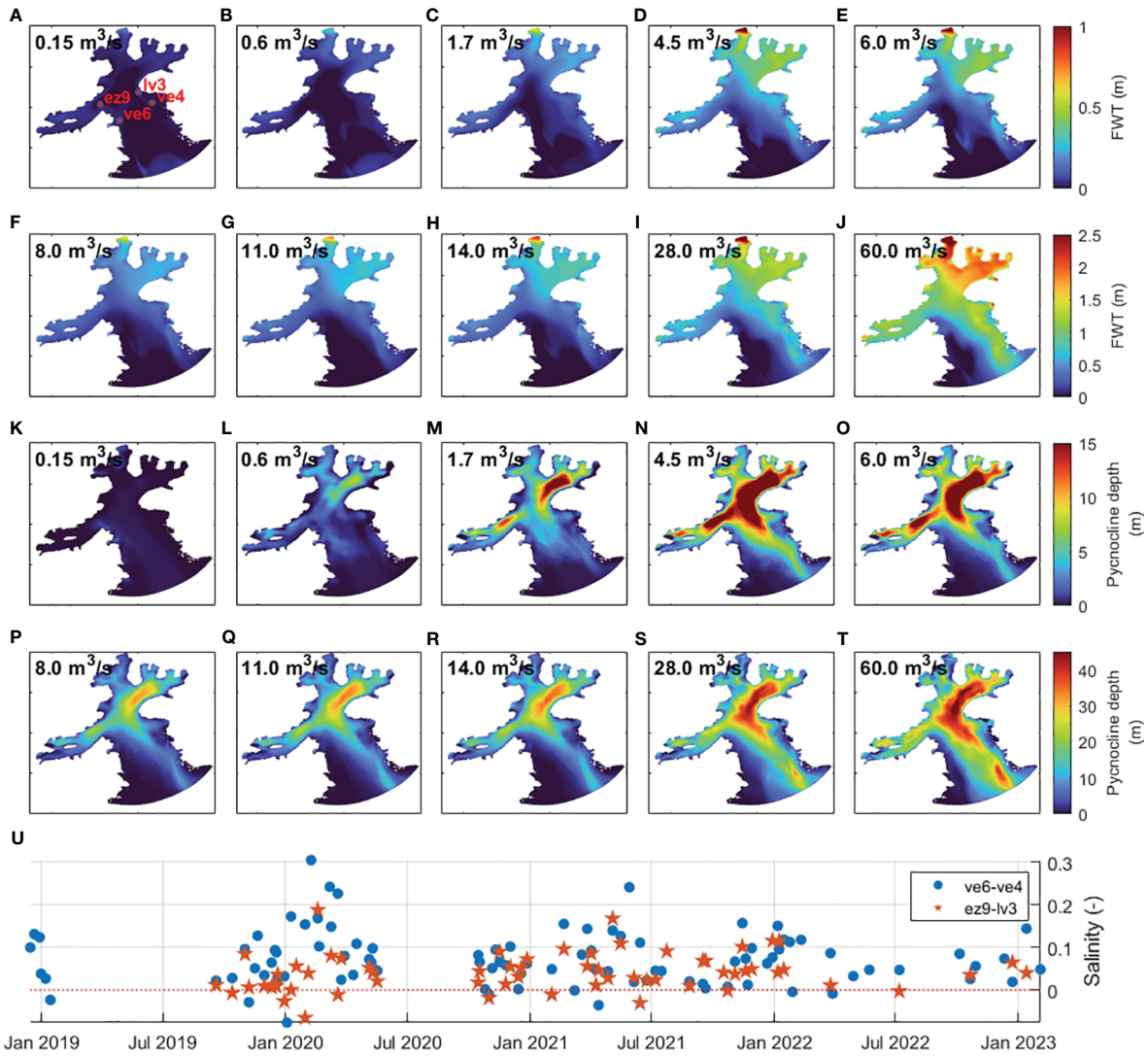

FIGURE 8
Variability of FWT and pycnocline depth with increasing glacial input; **(A–J)** FWT; **(K–T)** pycnocline depth. Note changing scales in different rows; **(U)** difference in average salinity readings from top 60 m of inflow (ve6 and ez9) and outflow (ve4 and lv3) sites [sites' locations seen in **(A)**] Values in **(A–T)** are average for the period 1.01.2022-28.01.2022.

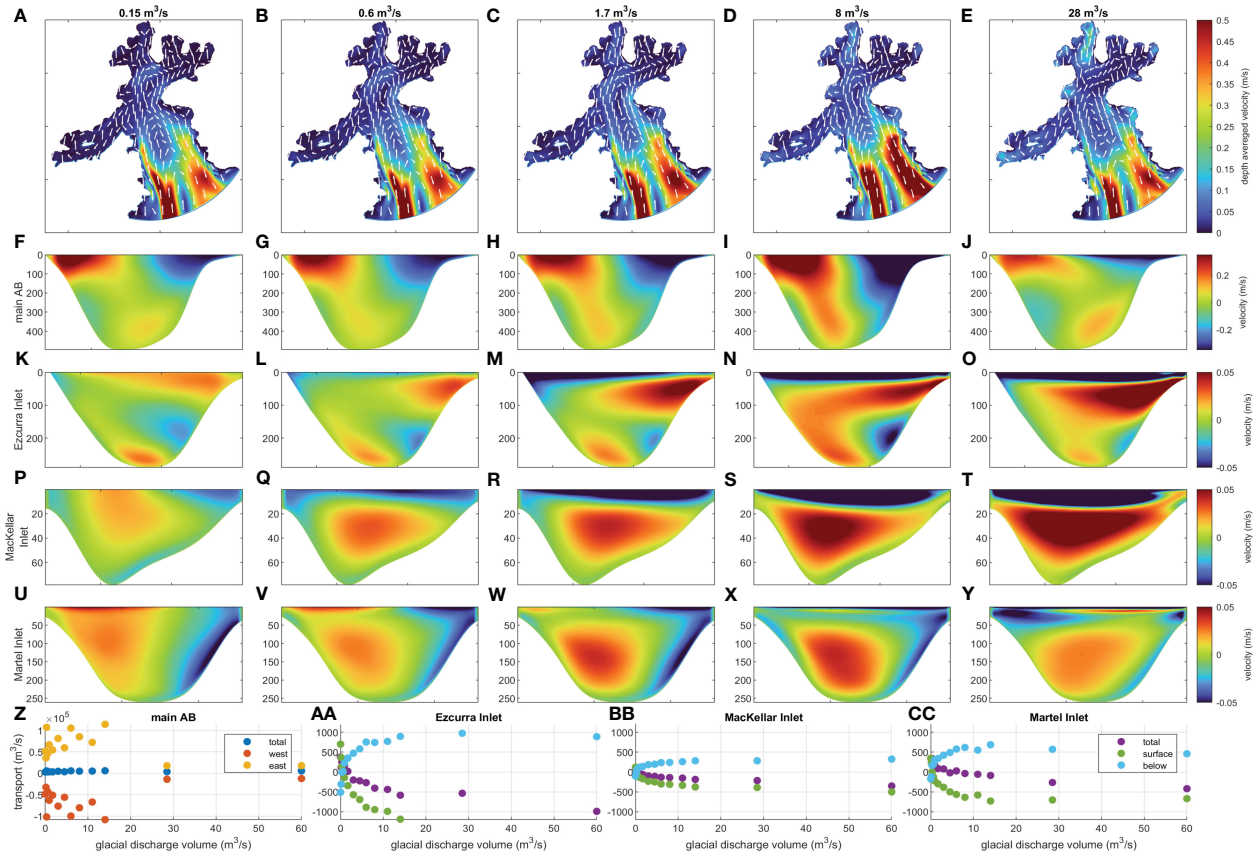

FIGURE 9
AB circulation influenced by growing glacial influx (five chosen model scenarios' results); **(A–E)** flow depth averaged horizontal velocities in whole AB; **(F–Y)** horizontal velocity throughout cross-sections (locations in Figure 7A); **(Z)** variability in mean transport through cross-section main AB in total and divided into western and eastern half; **(AA–CC)** variability in transport through AB inlets: total and divided into surface and below surface layers; for **(F–CC)** positive values =inflow, negative =outflow. All values are average for the period 1.01.2022-28.01.2022.

depth is determined by the local bathymetry, resulting in the deepest pycnocline developing in the area of the main AB embranchment. In all scenarios, the depth of the pycnocline does not exceed 60 m.

The model results demonstrate circulation and freshwater distribution patterns that are consistent with the *in situ* measurement data. The average salinity values from the top 60 m of water at two sites in the western inflow area, *ve6* and *ez9*, consistently exceed those reported at the outflow sites, *ve4* and *lv3*. Despite the close proximity and similar distance from the glacial front and bay's outlet between inflow and outflow sites, this salinity difference can reach 0.3 (Figure 8U and Figure 8A for).

In all the model scenarios, the circulation pattern of two cyclonic circulation cells is preserved in AB (Figures 9A–E). The analysis of flow velocities and transport volumes across the *main AB* cross-section reveals that in scenarios ranging from *0* to *14* m^3/s, the water exchange is consistently strongest near the surface and has a volume of ~10^5 m^3/s for both inflow and outflow (Figures 9F–J, and Figure 9Z, analogous to Figures 7B, F). However, in two highest glacial influx scenarios (*28* and *60* m^3/s), the water transport on both sides of the main AB cross-section decreases significantly to ~10^4 m^3/s (Figure 9Z). Similarly, in these scenarios, the flow velocities are reduced (see Figures 9E, J). This observation suggests that a threshold value of glacial inflow volume exists limiting water interchange between the bay and the ocean. Specifically this threshold is observed to be between *14* and *28* m^3/s ~1 km of glacial front, which adds up to 450 and 900 m^3/s of overall freshwater input into AB.

In cross-sections located at the openings of inner AB inlets, Ezcurra, MacKellar, and Martel Inlets, the impact of increasing glacial influx is visible from relatively low glacial water inflow rates below 0.6 m^3/s, (Figures 9F–Y). The surface outflow layer forms there, moving GMW out of the bay, most evidently in the Ezcurra and MacKellar Inlets (Figures 9K–T). Figures 9AA–CC shows the variability in water volume transported through the three inlet cross-sections in 14 model scenarios, in total, and split into layers above (surface layer) and below the pycnocline depth (calculated as in section 3.3.2). In AB inlets, surface outflow and deeper inflow increase with rising glacial influx, up to *14* m^3/s scenario, when their values stabilize. This demonstrates how glacial influx drives vertical circulation, similar to the 2D glacial bay circulation of (Motyka et al., 2003). The drop in total transport values in Figures 9AA–CC indicates the importance of additional freshwater input for the water budget of AB inner inlets, which is barely visible in the flow transport sum up through the *main AB* cross-section, where overall values are 100 times higher (Figure 9Z).

Maps depicting the correlation coefficients between the glacial influx volumes and horizontal flow velocities and directions have been generated (Figure 10). They show areas in which glacial bay buoyancy-driven vertical circulation can be a dominant flow pattern. The maps are shown in three versions: for the entire water column, for depths below the pycnocline, and for surface waters inside and above the pycnocline. In regions where pycnocline was not present, the entire column of water was treated as waters below the pycnocline. In order to acquire representative description of changes in waters above pycnocline (Figures 10C, F), correlations have been calculated for points in which pycnocline was present in at least six model scenarios. To reduce the possible influence of outliers and increase the robustness of the results, a bootstrap resampling of the data was performed (Trauth, 2010). The areas outlined with black borders in all of the maps in Figure 10 represent points where this analysis produced statistically significant results.

In three inner AB inlets, the whole of Ezcurra and MacKellar Inlets, and most of Martel Inlet, there is a strong correlation between horizontal flow velocity and glacial influx (Figures 10A–C). Overall, based on the evidence in Figures 9, 10, we conclude that in these areas glacial input can create vertical circulation, driving local water exchange.

In the entire water column and in the bottom layers, the distributions of correlation coefficients of flow direction changes versus glacial influx volumes do not show any discernible pattern (Figures 10D–E). However, in the surface waters, a distinct areas can be recognized where, with rising glacial input, water flow turns to the right in a broad area in the middle of AB and to the left in a smaller area in the east part of the main embranchment of AB (Figure 10F). This shows how the GMW surface layer deflects surface water following the general circulation pattern (Figure 7A), redirecting it toward the AB outlet and restricting its penetration of inner bay waters.

3.2 Assessment of seasonal variability in glacial influx volume

Ice mass balance models, such as the Regional Atmospheric Climate Model (RACMO2, Wessem and Laffin, 2020), are commonly used to predict glacial influx volumes (Xu et al., 2012; Mankoff et al., 2016). However, due to its coarse scale in both time and space, as well as considerable uncertainty in its results (Mernild et al., 2010; Cape et al., 2019), a more locally conformable method has been developed.

Estimates of glacial input volume into AB were obtained by comparing FWT values from hydrographic observations to FWT values from 14 model scenarios, at grid points nearest to measurement site locations. A best-fitting scenario was identified for each site, per measurement day, as one with the smallest FWT difference from the FWT in measurement. The results for each day were summarized in a boxplot (Figure 11), displaying a range in glacial influx volumes of best-fitting scenarios for each day across all locations.

Figure 11 shows that the range of glacial discharge volumes employed in modeling was reasonable: the maximum glacial influx scenario of *60* m^3/s never fits best to observed results, and the second greatest scenario of *28* m^3/s fits best once. Figure 11 depicts

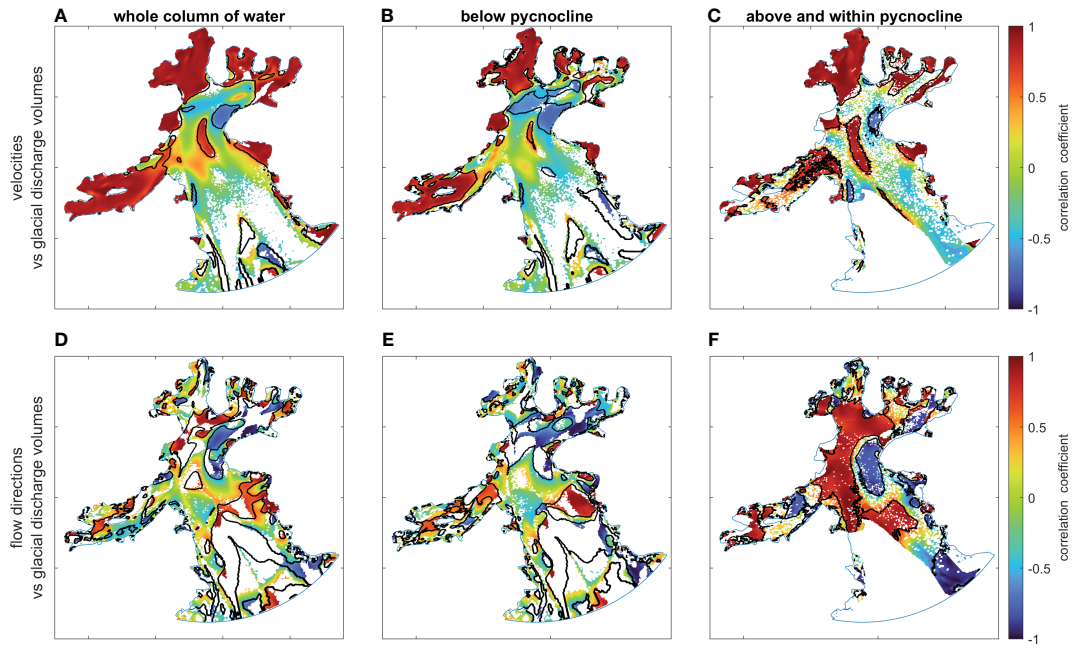

FIGURE 10
Correlation between rising glacial influx and flow horizontal velocities and directions; **(A–C)** correlation coefficients between flow velocities and glacial discharge volumes; **(D–F)** correlation coefficients between flow directions and glacial discharge volumes; positive values correspond to flow turning to the right, negative to the left; **(A, D)** average value over the water column; **(B, E)** below pycnocline; **(C, F)** above and within pycnocline. Areas within black boundaries contain statistically significant values.

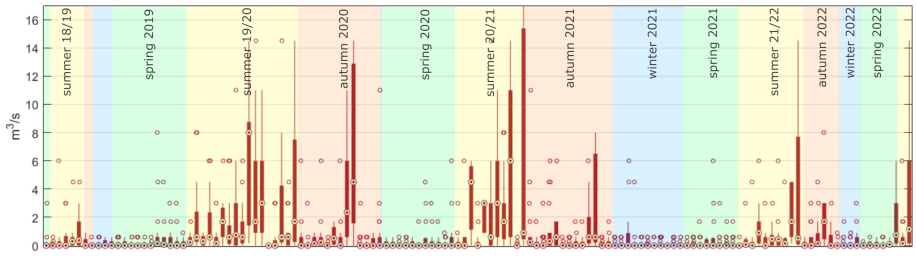

FIGURE 11
Estimation of glacial influx into AB assessed via a comparison of modeling and hydrographic measurement results; Glacial influx volume of scenarios with the smallest FWT difference from the measurement FWT (best-fitting scenario), in each boxplot information from all sites per measurement day (central mark=median, bottom and top edges of the box=25th and 75th percentiles, whiskers=extreme points, circles=outliers);.

how winter and spring glacial influx values are close to 0 m^3/s, while continuous highest discharge volumes occur in late summer and autumn, reaching a maximum daily median value of 8 m^3/s. The median value of projected glacial influx volume is comparatively low, maximally 1.06-1.30 m^3/s in the summer (Table 1). This observation implies that periods characterized by significant glacial influx are of limited duration.

Table 1 contains the seasonally averaged differences between the 75th and 25th percentiles of glacial influx estimates obtained from all sites on one measuring day. Their high values, particularly during the summer (2.32 m^3/s), imply that the model does not accurately capture details of circulation in AB. The disparities between model and measurements might be caused by the unrealistic assumption of homogeneous and constant volumes of injections from all glaciers, by not taking into account the contribution of other freshwater sources and/or effects of wind-induced circulation. Nonetheless, the low glacial influx values of the best fitting model scenarios in the winter and spring (mean daily median of 0.01 and 0.00 m^3/s, respectively) would suggest that the omission of precipitation and sea ice contribution was reasonable.

In general, the measurements confirm the overall circulation pattern of AB that was identified through modeling. This was first shown in salinity differences between west and east sites in Figure 8U. Through the course of the study period, the FWT in *east AB*, in the area of GMW outflow, was no thicker than 0.35 m (0.05-0.35 m - measurements, 0.00-0.27 m - modelling). The difference between the FWT values in *east AB* and *west and central AB* sites varied from -0.04 to 0.21 m (difference between the red and blue plot in Figure 4), which indicates the creation of a surface GMW outflow layer along the eastern boundary. Accordingly, the difference in FWT from analogous model points in a timeseries generated from the daily median of the best-fit scenarios shown in Figure 11 was in the range of 0.00–0.14 m, i.e., the model tends to underestimate the observed west-east FWT differences, but reproduces the overall pattern.

The daily estimate of glacial influx was defined as the median of the glacial influx volumes of the best-fit scenario from all sites on one day. Seasonal glacial influx values were obtained using two methods (Table 1): 1. Calculating the seasonal mean of all daily glacial influx estimates; 2. Calculating the seasonal means for each of the four zones, and then averaging these four values. The difference in results from these two methods established a range of seasonal glacial influx estimates. Based on these results glacial discharge per ~1 km of glacial front in AB is estimated to be

TABLE 1 Statistics of glacial influx estimation results.

			spring	summer	autumn	winter
median (m^3/s)	**Mean value from zones :**	west and central AB	0.09	1.54	0.64	0.15
		east AB	0.32	0.57	0.38	0.38
		Ezcurra Inlet	0.01	1.48	0.64	0.16
		Lange cove	0.02	1.62	0.58	0.00
	Mean from mean values of each zone (glacial influx estimates – method 2)		**0.11**	**1.30**	**0.56**	**0.17**
	Mean from all sites (glacial influx estimates – method 1)		**0.00**	**1.06**	**0.40**	**0.01**
mean 75th -25th percentile (m^3/s) from all sites			**0.23**	**2.32**	**1.70**	**0.20**

Daily median values of glacial influx volume of best-fitting scenarios averaged by zones and seasons and average difference between the 75th and 25th percentiles of glacial influx estimates obtained from all sites on one measuring day.

between 0.01-0.17 m^3/s in winter, 0.00 to 0.11 m^3/s in spring, 1.06-1.30 m^3/s at its peak in summer, and 0.40-0.56 m^3/s in fall. Therefore, the volume of glacial water released from all the glaciers into AB is valued to be in the range 0.434-0.632 Gt/year (0.104-0.128 Gt/month in summer, 0.039-0.55 Gt/month in autumn, 0.001-0.016 Gt/month in winter, and 0.000-0.010 Gt/month in spring).

4 Discussion and conclusions

A novel method of estimating glacial influx volume has been implemented and evaluated. This methodology uses a comparison of hydrographic measurements and modeling results, utilizing an extensive dataset to affirm the validity of its findings. Other studies estimating glacial influx quantities frequently employed far fewer observational data than the 1830 measurements used in this study (Mortensen et al., 2013; Sutherland et al., 2014; Straneo and Cenedese, 2015).

The scale of the analysis is critical when examining ocean-cryosphere interactions. Straneo and Cenedese (2015) defined three glacial bay regions: the ice-ocean boundary zone, the glacial plume region, and the major fjord system. The current research focuses on AB hydrodynamics at this third scale. In this broad perspective, the vertical placement of glacial discharges and their initial velocity has no significant impact on the overall AB circulation. This conclusion could help investigate the hydrodynamics of other similar bays in the WAP region.

Based on all hydrographic measurements and model results the standard deviation of salinity was 0.22 and the standard deviation of water temperature was 0.90°C in AB (Figure 2 and Supplementary Figure 1). GMW has always been the most buoyant water mass, occurring at the surface of the water column, spreading in a distinctive pattern along the eastern boundary of AB, generated by the AB general circulation pattern. The freshwater content in the GMW outflow area is low throughout the year, the maximal FWT in the east AB zone was 0.27-0.35 m. The temperature of glacial water exhibits slight variations compared to AW, being either colder or warmer than AW at the moment of discharge. The GMW surface layer can undergo either warming or cooling as a consequence of atmospheric forcing, dependent on the air temperature.

By integrating the findings of glacial influx estimation from Section 4.2 with the analysis of the impact of different volumes of glacial discharge on water level shifts and circulation from Sections 4.1.1 and 4.1.2, it can be inferred that glacial influx does not alter the general hydrodynamics of AB. The double-celled horizontal circulation pattern, which regulates water exchange between AB and the ocean, has been observed to persist consistently throughout the year. Unlike the findings of Mortensen et al. (2013) and Straneo et al. (2011) in Greenland, no distinct modes of circulation specific to different seasons were identified in the whole AB. However, in the Ezcurra, MacKellar, and inner parts of Martel inlets, the presence of GMW can lead to the formation of buoyancy-driven vertical circulation. This circulation is expected to occur most of the time during the summer and beginning of the autumn (estimates of glacial input > 0.6 m^3/s) and to be particularly robust during short-term peak melt events (Figures 9, 11).

It is suspected that there exists a threshold volume of glacial influx, estimated to be within the range of 14 to 28 m^3/s ~ per 1 km of a glacial front. GMW is expected to significantly limit the interchange of water between the AB and the ocean above this threshold (Figures 9Z–CC), since the ocean induced general circulation in the AB is most intense at the surface, at the level in which GMW is transported outside AB. The estimated amounts of glacial influx did not reach this level at any given time of the analyzed period. The likelihood of such high glacial influx levels requires further inquiry, however it is outside of the scope of this investigation.

The current investigation uncovered key features of AB hydrodynamics (visualized in Figure 12), that set it apart from the better-studied fjords of the northern hemisphere. These differences are caused by the geomorphology of the region and different relative contributions of external forces acting upon the bay waters. Similar geomorphological, oceanographic and meteorological conditions can be found at other locations in South Shetlands, like the nearby Maxwell Bay, where the Mariana and Potter Coves may have a similar function to that of Admiralty Bay's inner inlets. Similarly to AB, no evidence of CDW incursions has been found in Maxwell Bay, and glacial water was only present in the top layers of the water column (Meredith et al., 2018; Jones et al., 2023).

To estimate the significance of the study's findings for the Antarctic Peninsula's bays, a more detailed comparison between them and AB must be given. In terms of scale, the AB (area = 150 km^2) is within the range of sizes found in WAP, e.g.: Andvord Bay has an area of 110 km^2, Barilari Bay 280 km^2, Flandres Bay 310 km^2, Charlotte Bay 110 km^2, Beascochea Bay 200 km^2. In addition, these bays are wide and have deeper sills than fjords in the northern hemisphere. This would suggest that rotational forces are important in all of them, just like in AB. Furthermore, its topography, with multiple inlets extending from the main bay, implies that there may be regions in which glacial inflow has the potential to alter local hydrodynamics and to create vertical circulation patterns.

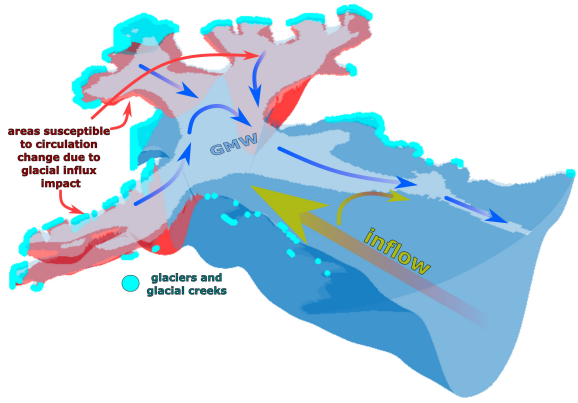

FIGURE 12
Key feature of Admiralty Bay hydrodynamics.

However, there are a few significant differences between AB and the bays along the WAP. The AB ice-water boundaries take up 25% of its overall coastline length, in WAP this percentage is usually higher. In addition, AB glaciers are shallower and smaller. For instance, grounding depths of four glaciers in Barilari Bay range from 168 to 367 m (Cape et al., 2019) compared to the maximal glacial grounding depth of 150 m in AB. Furthermore, CDW intrusions are more common further south along the Antarctic Peninsula. These intrusions might enhance faster melt rates of more deeply submerged glacial fronts, which can have a significant impact on local circulation (Meredith et al., 2010; Cape et al., 2019).

Katabatic wind events and precipitation—both of which are influenced by the high orography—play a more significant impact in the Antarctic Peninsula than in KGI (Cape et al., 2019; Lundesgaard et al., 2019). The entire region is susceptible to climate change (Bers et al., 2013) and extreme warm weather events have been reported, such as in February 2022 when temperatures above 10°C were recorded throughout WAP and South Shetlands (Gorodetskaya et al., 2023). These events are predicted to become more frequent in the future. Lastly, the sea ice presence is still a common occurrence along the WAP coast, so that freezing and melting influence local freshwater content variability.

It is important to thoroughly assess all of the aforementioned aspects before extending the techniques and conclusions from this study to other WAP locations. However, despite these differences, the glacial input estimates are in the same range in the whole region. The volume of glacial water released into AB during the summer is estimated to be in the range 0.104-0.128 Gt/month, in Andvord Bay, smaller than AB, it is 0.128 Gt/month, and 0.167 Gt/month in a larger Barilari Bay (Cape, et al. 2019; Hahn-Woernle et al., 2020).

All of these estimates are significantly lower than the glacial fluxes estimated for northern hemisphere fjords (Mernild et al., 2010; De Andrés et al., 2020). In Spitsbergen, the percentage share of glacial freshwater in the overall bay water budget was estimated to be around 1% (Cottier et al., 2010), in model-based study of Greenland fjords it was up to 0.25% (Cowton et al., 2015). In the summer, on average, the glacial freshwater contribution to the AB water budget is in the range of 0.19 to 0.23% (0.9–1.7 m3/s scenario results; see Supplementary Figure 5). Also, FWT in AB is lower than in, for example, Sermilik and Kangerdlugaauqq Greenlandic fjords, where in the summer it consistently exceeded 10 m (Sutherland et al., 2014), whereas in AB, even in the unrealistic maximum glacial influx scenarios, it seldom exceeded 3 m. This is due to relatively low glacial input volumes, as well as ocean-driven circulation that carries GMW out of AB in a thin surface layer, a phenomenon observed in other Antarctic bays by Hahn-Woernle et al. (2020) and Meredith et al. (2018).

Notably all of the previous estimates of glacial influx into the WAP bays concern summer months. Our study have provided first ever results showing its year-round variations. In AB the estimated glacial influx volumes rise more than ten times between spring/winter season and summer. These significant seasonal variations can be attributed to the absence of external warm water masses stimulating submarine melt during austral winter, a process demonstrated in studies conducted in Greenlandic fjords (Straneo et al., 2011; Mortensen et al., 2013) and in WAP region (Cook et al., 2016; Cape et al., 2019). This variability may also be exacerbated by the fact that the majority of the AB glaciers are shallowly grounded, causing melt to be primarily driven by external heat rather than hydrostatic pressure (Jenkins, 2011).

This study provides a comprehensive analysis of the hydrodynamic response of an Antarctic bay to changes in magnitude of glacial influx. Furthermore, with a large number of data points and high temporal resolution, this study offers, to the best of our knowledge, the most comprehensive assessment of seasonal variations in glacial discharge volumes to date. This enables the prediction of variations in circulation within a glacial bay over the course of a year.

Data availability statement

The datasets presented in this study can be found in online repositories. The names of the repository/repositories and accession number(s) can be found below: PANGAEA: https://doi.org/10.1594/PANGAEA.947909; Zenodo: 10.5281/zenodo.10277429; Zenodo 10.5281/zenodo.10277333.

Author contributions

MO: Conceptualization, Data curation, Formal analysis, Investigation, Methodology, Software, Validation, Visualization, Writing – original draft, Writing – review and editing. AH: Conceptualization, Funding acquisition, Methodology, Project administration, Resources, Supervision, Writing – review and editing.

Funding

The author(s) declare financial support was received for the research, authorship, and/or publication of this article. This work was supported by two grants from the National Science Centre, Poland: No. 2017/25/B/ST10/02092 ‘Quantitative assessment of sediment transport from glaciers of South Shetland Islands on the basis of selected remote sensing methods’ and No. 2018/31/B/ST10/00195 ‘Observations and modeling of sea ice interactions with the atmospheric and oceanic boundary layers’.

Acknowledgments

Special thanks are owed to Laboratory of Sedimentary and Environmental Processes - INCT-Criosfera Fluminense Federal

University - Geoscience Institute in Brazil for providing us with bathymetric data from Admiralty Bay, described in (Magrani et al., 2016). We are thankful to Deltares for making Delft3D Flow model available for calculations. Calculations were made possible thanks to computing power and software provided by CI TASK (Center of the Tri-City Academic Computer Network) in Gdańsk, Poland. We are grateful for the support of Arctowski Polish Antarctic Station's crew for all their help during measurement campaign.

Conflict of interest

The authors declare that the research was conducted in the absence of any commercial or financial relationships that could be construed as a potential conflict of interest.

Publisher's note

Supplementary material

The Supplementary Material for this article can be found online at: https://www.frontiersin.org/articles/10.3389/fmars.2024.1365157/full#supplementary-material

References

Bartholomaus, T. C., Larsen, C. F., and O'Neel, S. (2013). Does calving matter? Evidence for significant submarine melt. *Earth Planet Sci. Lett.* 380, 21–30. doi: 10.1016/j.epsl.2013.08.014

Battke, Z. (1990). Admiralty bay, king george island 1:50.000 map. *Insitute Ecol. PAS.*

Bers, A. V., Momo, F., Schloss, I. R., and Abele, D. (2013). Analysis of trends and sudden changes in long-term environmental data from King George Island (Antarctica): Relationships between global climatic oscillations and local system response. *Clim. Change* 116, 789–803. doi: 10.1007/s10584-012-0523-4

Cape, M. R., Vernet, M., Pettit, E. C., Wellner, J., Truffer, M., Akie, G., et al. (2019). Circumpolar deep water impacts glacial meltwater export and coastal biogeochemical cycling along the west Antarctic Peninsula. *Front. Mar. Sci.* 6. doi: 10.3389/fmars.2019.00144

Carbotte, S. M., Ryan, W. B. F., Hara, S. O., Arko, R., Goodwillie, A., Melkonian, A., et al. (2007). Antarctic multibeam bathymetry and geophysical data synthesis : An on-line digital data resource for marine geoscience research in the Southern Ocean. *10th Int. Symposium Antarctic Earth Sci.* 196. doi: 10.3133/ofr20071047SRP002

Carroll, D., Sutherland, D. A., Hudson, B., Moon, T., Catania, G. A., Shroyer, E. L., et al. (2016). The impact of glacier geometry on meltwater plume structure and submarine melt in Greenland fjords. *Geophys Res. Lett.* 43, 9739–9748. doi: 10.1002/2016GL070170

Chauché, N., Hubbard, A., Gascard, J. C., Box, J. E., Bates, R., Koppes, M., et al. (2014). Ice-ocean interaction and calving front morphology at two west Greenland tidewater outlet glaciers. *Cryosphere* 8, 1457–1468. doi: 10.5194/tc-8-1457-2014

Clarke, A., Meredith, M. P., Wallace, M. I., Brandon, M. A., and Thomas, D. N. (2008). Seasonal and interannual variability in temperature, chlorophyll and macronutrients in northern Marguerite Bay, Antarctica. *Deep Sea Res. 2 Top. Stud. Oceanogr.* 55 (18–19), 1988–2006. doi: 10.1016/j.dsr2.2008.04.035

Cook, A. J., Holland, P. R., Meredith, M. P., Murray, T., Luckman, A., and Vaughan, D. G. (2016). Ocean forcing of glacier retreat in the western Antarctic Peninsula. *Sci. (1979)* 353, 283–286. doi: 10.1126/science.aae0017

Cottier, F. R., Nilsen, F., Skogseth, R., Tverberg, V., Skarthhamar, J., and Svendsen, H. (2010). Arctic fjords: a review of the oceanographic environment and dominant physical processes. *Geological Society London Special Publications* 344, 35–50. doi: 10.1144/SP344.4

Cowton, T., Slater, D., Sole, A., Goldberg, D., and Nienow, P. (2015). Modeling the impact of glacial runoff on fjord circulation and submarine melt rate using a new subgrid-scale parameterization for glacial plumes. *J. Geophys Res. Oceans* 120 (2), 796–812. doi: 10.1002/2014JC010324

De Andrés, E., Slater, D. A., Straneo, F., Otero, J., Das, S., and Navarro, F. (2020). Surface emergence of glacial plumes determined by fjord stratification. *Cryosphere* 14, 1951–1969. doi: 10.5194/tc-14-1951-2020

Deltares, (2020). Delft3D 3D/2D modelling suite for integral water solutions Hydro-Morphodynamics. *User Manual*, 1–701.

Dotto, T. S., Mata, M. M., Kerr, R., and Garcia, C. A. E. (2021). A novel hydrographic gridded data set for the northern Antarctic Peninsula. *Earth Syst. Sci. Data* 13, 671–696. doi: 10.5194/essd-13-671-2021

Eayrs, C., Li, X., Raphael, M. N., and Holland, D. M. (2021). Rapid decline in Antarctic sea ice in recent years hints at future change. *Nat. Geosci.* 14 (7), 460–464. doi: 10.1038/s41561-021-00768-3

Forsch, K. O., Hahn-Woernle, L., Sherrell, R. M., Roccanova, V. J., Bu, K., Burdige, D., et al. (2021). Seasonal dispersal of fjord meltwaters as an important source of iron and manganese to coastal Antarctic phytoplankton. *Biogeosciences* 18, 6349–6375. doi: 10.5194/bg-18-6349-2021

Gerrish, L., Fretwell, P., and Cooper, P. (2021). *High resolution vector polylines of the Antarctic coastline (7.4) [Data set]*. (Cambridge, UK: British Antarctic Survey). doi: 10.5285/e46be5bc-ef8e-4fd5-967b-92863fbe2835

Gorodetskaya, I. V., Durán-Alarcón, C., González-Herrero, S., Clem, K. R., Zou, X., Rowe, P., et al. (2023). Record-high Antarctic Peninsula temperatures and surface melt in February 2022: a compound event with an intense atmospheric river. *NPJ Clim. Atmos. Sci.* 6. doi: 10.1038/s41612-023-00529-6

Gregory, J. M., White, N. J., Church, J. A., Bierkens, M. F. P., Box, J. E., Van Den Broeke, M. R., et al. (2013). Twentieth-century global-mean sea level rise: Is the whole greater than the sum of the parts? *J. Clim.* 26 (13), 4476–4499. doi: 10.1175/JCLI-D-12-00319.1

Hahn-Woernle, L., Powell, B., Lundesgaard, Ø., and van Wessem, M. (2020). Sensitivity of the summer upper ocean heat content in a Western Antarctic Peninsula fjord. *Prog. Oceanogr.* 183, 102287. doi: 10.1016/j.pocean.2020.102287

Hofmann, E. E., Klinck, J. M., Lascara, C. M., and Smith, D. A. (2011). *"Water mass distribution and circulation west of the Antarctic Peninsula and including Bransfield Strait.,"* (Washington DC, USA: American Geophysical Union). doi: 10.1029/ar070p0061

Holfort, J., Hansen, E., Østerhus, S., Dye, S., Jónsson, S., Meincke, J., et al. (2008). "Freshwater fluxes east of Greenland," in *Arctic–Subarctic Ocean Fluxes* (Springer Netherlands, Dordrecht), 263–287. doi: 10.1007/978-1-4020-6774-7_12

Inall, M. E., and Rippeth, T. P. (2002). Dissipation of tidal energy and associated mixing in a wide fjord. *Environ. Fluid Mechanics* 2 (3), 219–240. doi: 10.1023/A:1019846829875

IPCC (2022). "Sea level rise and implications for low-lying islands, coasts and communities," in *The Ocean and Cryosphere in a Changing Climate* (Cambridge UK: Cambridge University Press). doi: 10.1017/9781009157964.012

Jenkins, A. (1999). The impact of melting ice on ocean waters. *J. Phys. Oceanogr* 29 (9), 2370–2381. doi: 10.1175/1520-0485(1999)029<2370:TIOMIO>2.0.CO;2

Jenkins, A. (2011). Convection-driven melting near the grounding lines of ice shelves and tidewater glaciers. *J. Phys. Oceanogr.* 41, 2279–2294. doi: 10.1175/JPO-D-11-03.1

Jenkins, A., and Jacobs, S. (2008). Circulation and melting beneath George VI Ice Shelf, Antarctica. *J. Geophys. Res.* 113, C04013. doi: 10.1029/2007JC004449

Jones, R. L., Meredith, M. P., Lohan, M. C., Woodward, E. M. S., Van Landeghem, K., Retallick, K., et al. (2023). Continued glacial retreat linked to changing macronutrient supply along the West Antarctic Peninsula. *Mar. Chem.* 251, 104230. doi: 10.1016/j.marchem.2023.104230

Kimura, S., Holland, P. R., Jenkins, A., and Piggott, M.. (2014). The Effect of Meltwater Plumes on the Melting of a Vertical Glacier Face. *J. Phys. Oceanogr.* 44 (12), 3099–3117. doi: 10.1175/JPO-D-13-0219.1

Lundesgaard, Ø., Powell, B., Merrifield, M., Hahn-Woernle, L., and Winsor, P. (2019). Response of an antarctic peninsula fjord to summer katabatic wind events. *J. Phys. Oceanogr.* 49, 1485–1502. doi: 10.1175/JPO-D-18-0119.1

Lundesgaard, Ø., Winsor, P., Truffer, M., Merrifield, M., Powell, B., Statscewich, H., et al. (2020). Hydrography and energetics of a cold subpolar fjord: Andvord Bay, western Antarctic Peninsula. *Prog. Oceanogr.* 181, 102224. doi: 10.1016/j.pocean.2019.102224

Magrani, F., Neto, A. A., and Vieira, R. (2016). Glaciomarine sedimentation and submarine geomorphology in Admiralty Bay, South Shetland Islands, Antarctica. *2015 IEEE/OES Acoustics Underwater Geosciences Symposium Rio Acoustics* 2015. doi: 10.1109/RIOACOUSTICS.2015.7473614

Majdański, M., Środa, P., Malinowski, M., Czuba, W., Grad, M., Guterch, A., et al. (2008). 3D seismic model of the uppermost crust of the Admiralty Bay area, King George Island, West Antarctica. *Polar Res.* 29, 303–318.

Mankoff, K. D., Straneo, F., Cenedese, C., Das, S. B., Richards, C. G., and Singh, H. (2016). Structure and dynamics of a subglacial discharge plume in a Greenlandic fjord. *J. Geophys Res. Oceans* 121 (12), 8670–8688. doi: 10.1002/2016JC011764

Meredith, M. P., Falk, U., Bers, A. V., Mackensen, A., Schloss, I. R., Barlett, E. R., et al. (2018). Anatomy of a glacial meltwater discharge event in an Antarctic cove. *Philos. Trans. R. Soc. A: Mathematical Phys. Eng. Sci.* 376 (2122), 20170163. doi: 10.1098/rsta.2017.0163

Meredith, M. P., and King, J. C. (2005). Rapid climate change in the ocean west of the Antarctic Peninsula during the second half of the 20th century. *Geophys. Res. Lett.* 32, n/a–n/a. doi: 10.1029/2005GL024042

Meredith, M. P., Wallace, M. I., Stammerjohn, S. E., Renfrew, I. A., Clarke, A., Venables, H. J., et al. (2010). Changes in the freshwater composition of the upper ocean west of the Antarctic Peninsula during the first decade of the 21st century. *Prog. Oceanogr.* 87, 127–143. doi: 10.1016/j.pocean.2010.09.019

Mernild, S. H., Howat, I. M., Ahn, Y., Liston, G. E., Steffen, K., Jakobsen, B. H., et al. (2010). Freshwater flux to sermilik fjord, SE Greenland. *Cryosphere* 4 (4), 453–465. doi: 10.5194/tc-4-453-2010

Moffat, C., and Meredith, M. (2018). Shelf–ocean exchange and hydrography west of the Antarctic Peninsula: a review. *Philos. Trans. R. Soc. A: Mathematical Phys. Eng. Sci.* 376, 20170164. doi: 10.1098/rsta.2017.0164

Moffat, C., Owens, B., and Beardsley, R. C. (2009). On the characteristics of Circumpolar Deep Water intrusions to the west Antarctic Peninsula Continental Shelf. *J. Geophys. Res. Oceans* 114. doi: 10.1029/2008JC004955

Monien, D., Monien, P., Brünjes, R., Widmer, T., Kappenberg, A., Silva Busso, A. A., et al. (2017). Meltwater as a source of potentially bioavailable iron to Antarctica waters. *Antarct. Sci.* 29, 277–291. doi: 10.1017/S095410201600064X

Mortensen, J., Bendtsen, J., Lennert, K., and Rysgaard, S. (2014). Seasonal variability of the circulation system in a west Greenland tidewater outlet glacier fjord, Godthåbsfjord (64°N). *J. Geophys. Res.: Earth Surface* 119 (12), 2591–2603. doi: 10.1002/2014JF003267

Mortensen, J., Bendtsen, J., Motyka, R. J., Lennert, K., Truffer, M., Fahnestock, M., et al. (2013). On the seasonal freshwater stratification in the proximity of fast-flowing tidewater outlet glaciers in a sub-Arctic sill fjord. *J. Geophys Res. Oceans.* 118, 1382–1395. doi: 10.1002/jgrc.20134

Motyka, R. J., Hunter, L., Echelmeyer, K. A., and Connor, C. (2003). Submarine melting at the terminus of a temperate tidewater glacier, LeConte Glacier, Alaska, U.S.A. *Ann. Glaciol.* 36, 57–65. doi: 10.3189/172756403781816374

National Snow and Ice Data Center, C. (2023). *Sea Ice Index*. Available at: https://nsidc.org/data/seaice_index (Accessed June 7, 2023).

Naughten, K. A., Holland, P. R., and De Rydt, J. (2023). Unavoidable future increase in West Antarctic ice-shelf melting over the twenty-first century. *Nat. Clim. Change* 13 (11), 1222–1228. doi: 10.1038/s41558-023-01818-x

Osińska, M., Bialik, R. J., and Wójcik-Długoborska, K. A. (2021). Interrelation of quality parameters of surface waters in five tidewater glacier coves of King George Island, Antarctica. *Sci. Total Environ.* 771, 144780. doi: 10.1016/j.scitotenv.2020.144780

Osińska, M., Wójcik-Długoborska, K. A., and Bialik, R. J. (2022). Water conductivity, salinity, temperature, turbidity, pH, fluorescent dissolved organic matter (fDOM), optical dissolved oxygen (ODO), chlorophyll a and phycoerythrin measurements in Admiralty Bay, King George Island, from Dec 2018 to Jan 2022. *PANGAEA*. doi: 10.1594/PANGAEA.947909

Osińska, M., Wójcik-Długoborska, K. A., and Bialik, R. J. (2023). Annual hydrographic variability in Antarctic coastal waters infused with glacial inflow. *Earth Syst. Sci. Data* 15, 607–616. doi: 10.5194/essd-15-607-2023

Padman, L., Fricker, H. A., Coleman, R., Howard, S., and Erofeeva, L. (2002). A new tide model for the Antarctic ice shelves and seas. *Annals of Glaciology* 34, 247–254. doi: 10.3189/172756402781817752

Plenzler, J., Budzik, T., Puczko, D., and Bialik, R. J. (2019). Climatic conditions at Arctowski Station (King George Island, West Antarctica) in 2013-2017 against the background of regional changes. *Pol. Polar Res.* 40, 1–27. doi: 10.24425/ppr.2019.126345

Potapowicz, J., Szumińska, D., Szopińska, M., Bialik, R. J., Machowiak, K., Chmiel, S., et al. (2020). Seashore sediment and water chemistry at the Admiralty Bay (King George Island, Maritime Antarctica) – Geochemical analysis and correlations between the concentrations of chemical species. *Mar. pollut. Bull.* 152, 110888. doi: 10.1016/j.marpolbul.2020.110888

Poulin, F. J., Stegner, A., Hernández-Arencibia, M., Marrero-Díaz, A., and Sangrà, P. (2014). Steep shelf stabilization of the coastal bransfield current: Linear stability analysis. *J. Phys. Oceanogr.* 44 (2), 714–732. doi: 10.1175/JPO-D-13-0158.1

Powell, R., and Domack, G. W. (2002). Modern glaciomarine environments. *Modern Past Glacial Environments*, pp. 361–389. doi: 10.1016/B978-075064226-2/50015-5

Robakiewicz, M., and Rakusa-Suszczewski, S. (1999). Application of 3D circulation model to Admiralty Bay, King George Island, Antarctica. *Pol. Polar Res.* 20, 43–58.

Rückamp, M., Blindow, N., Suckro, S., Braun, M., and Humbert, A. (2010). Dynamics of the ice cap on King George Island, Antarctica: Field measurements and numerical simulations. *Ann. Glaciol.* 51, 80–90. doi: 10.3189/172756410791392817

Sangrà, P., Gordo, C., Hernández-Arencibia, M., Marrero-Díaz, A., Rodríguez-Santana, A., Stegner, A., et al. (2011). The Bransfield current system. *Deep Sea Res. 1 Oceanogr Res. Pap.* 58 (4), 390–402. doi: 10.1016/j.dsr.2011.01.011

Schloss, I. R., Abele, D., Moreau, S., Demers, S., Bers, A. V., González, O., et al. (2012). Response of phytoplankton dynamics to 19-year, (1991–2009) climate trends in Potter Cove (Antarctica). *J. Mar. Syst.* 92, 53–66. doi: 10.1016/j.jmarsys.2011.10.006

Sciascia, R., Straneo, F., Cenedese, C., and Heimbach, P. (2013). Seasonal variability of submarine melt rate and circulation in an East Greenland fjord. *J. Geophys. Res. Oceans* 118, 2492–2506. doi: 10.1002/jgrc.20142

Simões, J. C., Bremer, U. F., Aquino, F. E., and Ferron, F. A. (1999). Morphology and variations of glacial drainage basins in the King George Island ice field, Antarctica. *Ann. Glaciol.* 29, 220–224. doi: 10.3189/172756499781821085

Slater, D. A., Straneo, F., Das, S. B., Richards, C. G., Wagner, T. J. W., and Nienow, P. W. (2018). Localized plumes drive front-wide ocean melting of A Greenlandic tidewater glacier. *Geophys. Res. Lett.* 45, 12,350–12,358. doi: 10.1029/2018GL080763

Spall, M. A., Jackson, R. H., and Straneo, F. (2017). Katabatic wind-driven exchange in fjords. *J. Geophys Res. Oceans* 122, 8246–8262. doi: 10.1002/2017JC013026

Straneo, F., and Cenedese, C. (2015). The dynamics of Greenland's glacial fjords and their role in climate. *Ann. Rev. Mar. Sci.* 7, 89–112. doi: 10.1146/annurev-marine-010213-135133

Straneo, F., Curry, R., Sutherland, D., Hamilton, G., Cenedese, C., Vaage, K., et al. (2011). Impact of ocean stratification on submarine melting of a major Greenland outlet glacier. *Nat. Precedings*. doi: 10.1038/npre.2011.5670.1

Sutherland, D. A., Straneo, F., and Pickart, R. S. (2014). Characteristics and dynamics of two major Greenland glacial fjords. *J. Geophys. Res. Oceans* 119, 3767–3791. doi: 10.1002/2013JC009786

Thompson, A. F., Heywood, K. J., Thorpe, S. E., Renner, A. H. H., and Trasviña, A. (2009). Surface circulation at the tip of the antarctic peninsula from drifters. *J. Phys. Oceanogr.* 39, 3–26. doi: 10.1175/2008JPO3995.1

Trauth, M. H. (2010). *MATLAB® recipes for earth sciences*, *3rd ed* (Berlin, Germany: Springer). doi: 10.1007/978-3-642-12762-5

Valle-Levinson, A. (2010). Contemporary issues in estuarine physics. *Contemp. Issues Estuar. Phys*, 1–315. doi: 10.1017/CBO9780511676567

Valle-Levinson, A. (2022). *Introduction to estuarine hydrodynamics* (Cambridge University Press). Available at: https://books.google.com/books/about/Introduction_to_Estuarine_Hydrodynamics.html?hl=plandid=2PKazgEACAAJ (Accessed January 4, 2023).

Vaughan, D. G. (2006). Recent trends in melting conditions on the Antarctic Peninsula and their implications for ice-sheet mass balance and sea level. *Arct. Antarct. Alp. Res.* 38. doi: 10.1657/1523-0430(2006)038[0147:RTIMCO]2.0.CO;2

Wessem, J. M. V., and Laffin, M. K. (2020). *Regional Atmospheric Climate Model 2 (RACMO2), version 2.3p2 (2.3p2) [Data set]* Zenodo. doi: 10.5281/zenodo.3677641

Xu, Y., Rignot, E., Menemenlis, D., and Koppes, M. (2012). Numerical experiments on subaqueous melting of Greenland tidewater glaciers in response to ocean warming and enhanced subglacial discharge. *Ann. Glaciol.* 53, 229–234. doi: 10.3189/2012AoG60A139

Zhou, M., Niiler, P. P., and Hu, J. H. (2002). Surface currents in the bransfield and gerlache straits, Antarctica. *Deep Sea Res. Part I: Oceanographic. Res. Papers* 49, 267–280. doi: 10.1016/S0967-0637(01)00062-0

Zhou, M., Niiler, P. P., Zhu, Y., and Dorland, R. D. (2006). The western boundary current in the Bransfield Strait, Antarctica. *Deep Sea Res. 1 Oceanogr. Res. Pap* 53 (7), 1244–1252. doi: 10.1016/j.dsr.2006.04.003

Zhou, X., Zhu, G., and Hu, S. (2020). Influence of tides on mass transport in the Bransfield Strait and the adjacent areas, Antarctic. *Polar Sci.* 23, 100506. doi: 10.1016/j.polar.2020.100506

frontiers

Supplementary Material

Influence of glacial influx on the hydrodynamics of Admiralty Bay, Antarctica - study based on combined hydrographic measurements and numerical modeling

Maria Osińska[1]* and Agnieszka Herman[2]

[1] University of Gdańsk, Faculty of Oceanography and Geography, Gdańsk Poland

[2]Institute of Oceanology, Polish Academy of Sciences, Sopot, Poland.

*** Correspondence:**
Maria Osińska
maria.osinska@phdstud.ug.edu.pl

1 Supplementary Figures and Tables

Supplementary Fig. 1 displays the recorded salinity in in-depth measurements. It shows the freshest water always in the top layers of the water column. Supplementary Fig. 2 displays the data extracted from Dotto et al. (2021) and utilized for the determination of open boundary conditions in the model. As was noted in the main text, in the model, only data from the spring and summer seasons was utilized and subsequently interpolated across time in order to generate a continuous time series of water parameter values. However, the little variations seen in values across different seasons indicate that the model configuration effectively captures the AB water variability throughout the entire year. Supplementary Fig. 3 displays the absolute values of FWT, pycnocline depth, and depth-averaged velocities in test scenarios H0, H2, S0 and S2. It further demonstrates the limited significance of the initial velocity and vertical location of glacial discharges within the broader context of AB hydrodynamics. Supplementary Fig. 4 displays the standard deviations of FWT at each grid point of the model throughout the course of one lunar cycle in various glacial influx scenarios. As a result, it is a representation of the stability of glacial freshwater distribution in AB at various tidal phases. Its overall values increase as the glacial influx rises. However, in cases where glacial influx volumes are within reasonable limits (see Section 5), these values tend to be modest, particularly in the northeastern portion of AB where absolute FWT values are highest (Fig. 6). This is evidence of the relative stability of the pattern of freshwater transport in AB during the tidal cycle. Supplementary Fig. 5 presents data about the proportion of glacial freshwater within the overall water budget of AB in 14 model scenarios. It was calculated by taking the average of monthly mean FWT values divided by depth across all grid points.

Supplementary Table 1 shows energy dissipation and bed shear stress values distribution in model using 3D Chézy bottom roughness coefficients of 40 $m^{1/2}/s$, in both U and V directions. Its reasonable values proof that this coefficients is appropriate for modeling AB hydrodynamics. Additional model setup details used to configure the AB model are provided in Supplementary Table 2. The model variables that were not explicitly addressed in the main text or in Supplementary Table 2 were kept consistent with the configuration suggested by Deltares (2020).

1.1 Supplementary Figures

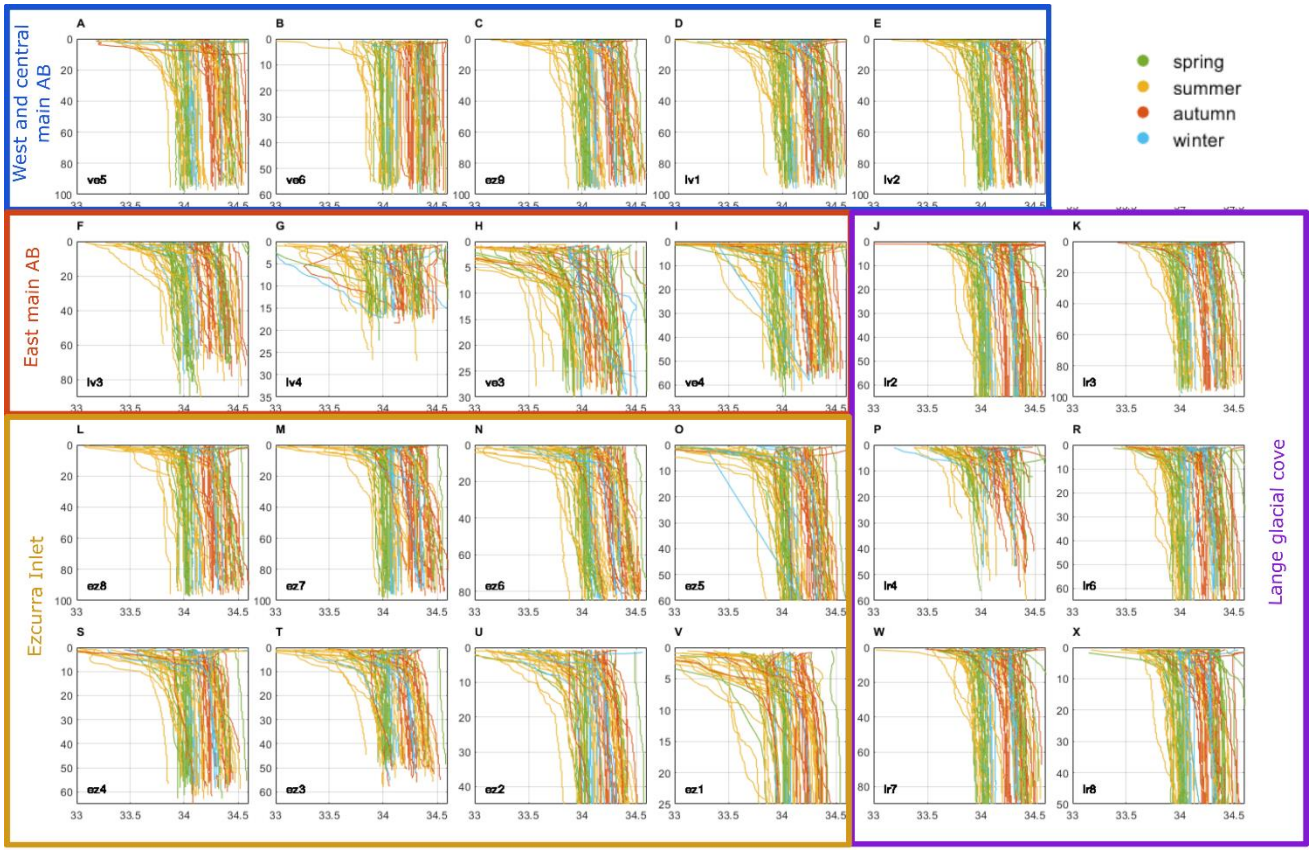

Supplementary Figure 1. Results of in-depth salinity measurements. In each plot results from a single sites are presented.

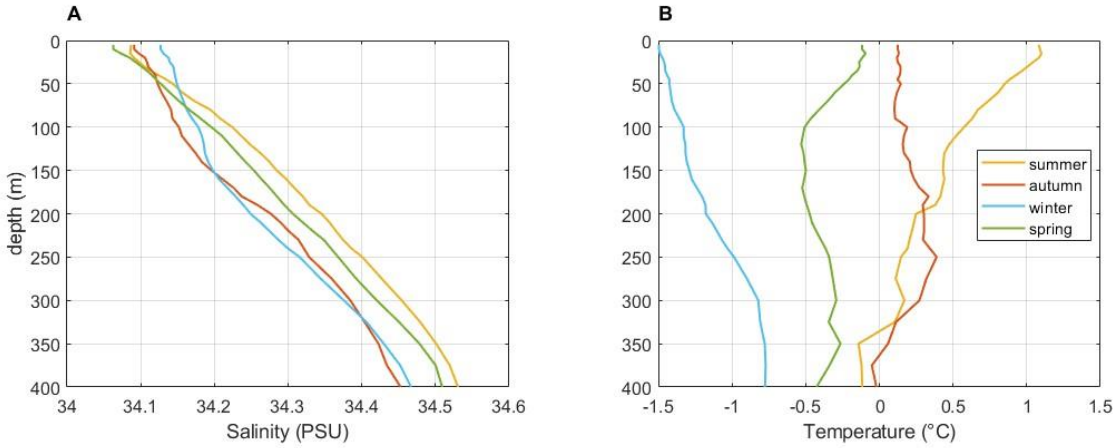

Supplementary Figure 2. (A) Seasonal salinity (PSU) and **(B)** temperature (˚C) reanalysis results from Dotto et al. (2021) used to establish open boundary conditions of AB model; site location -62.18, -58.40 (location in reanalysis grid – m=43 n=49).

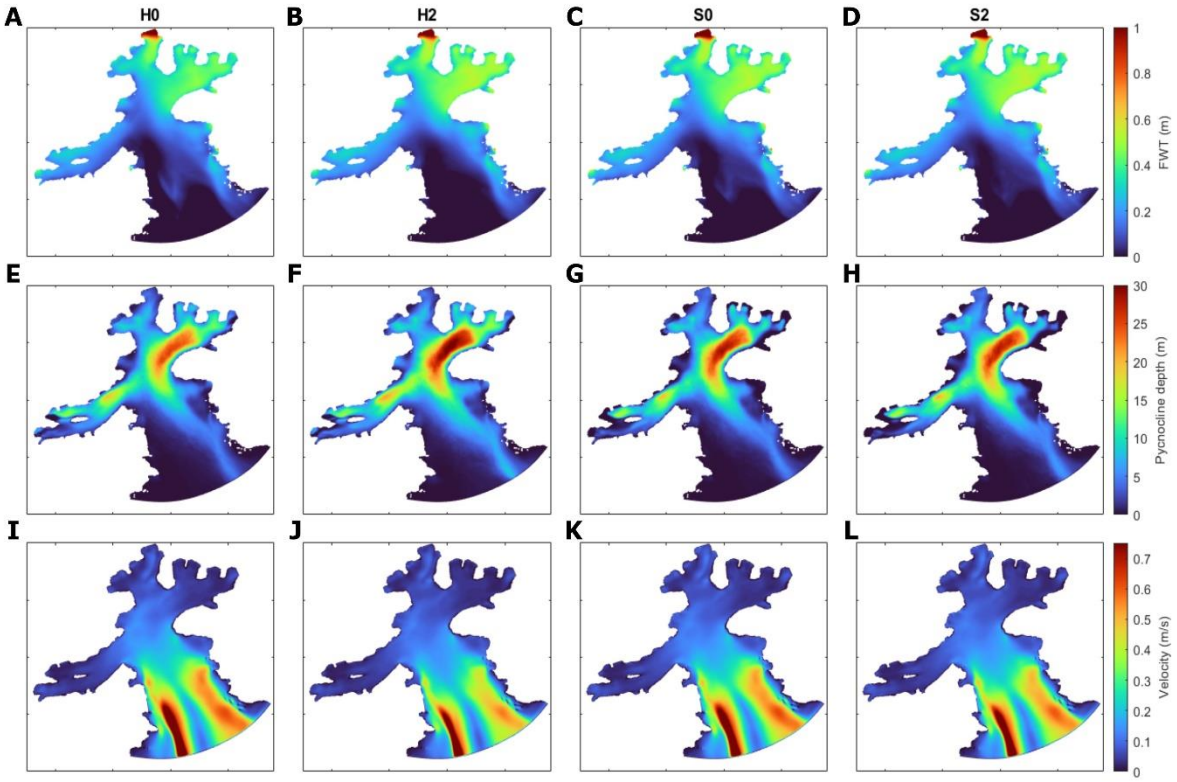

Supplementary Figure 3. Analogous to Fig.3 in the main text, only presented in absolute values: **(A-D)** FWT (m); **(E-H)** Pycnocline depth (m); **(I-L)** depth averaged velocities in m/s; **(A,E and I)** H0 scenario; **(B, F and J)** H2 scenario; **(C, G and K)** S0 scenario; **(D, H, and L)** S2 scenario. All figures depict mean values from period from 1.01.2022 to 28.01.2022.

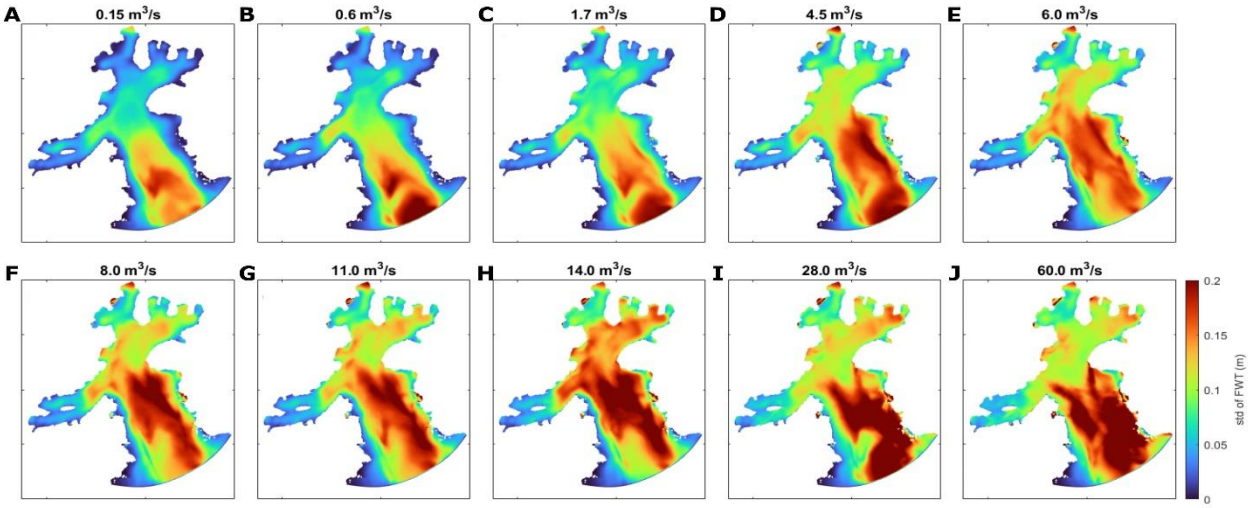

Supplementary Figure 4. Standard deviation of FWT values in AB during a period from 1.01.2022 to 28.01.2022.

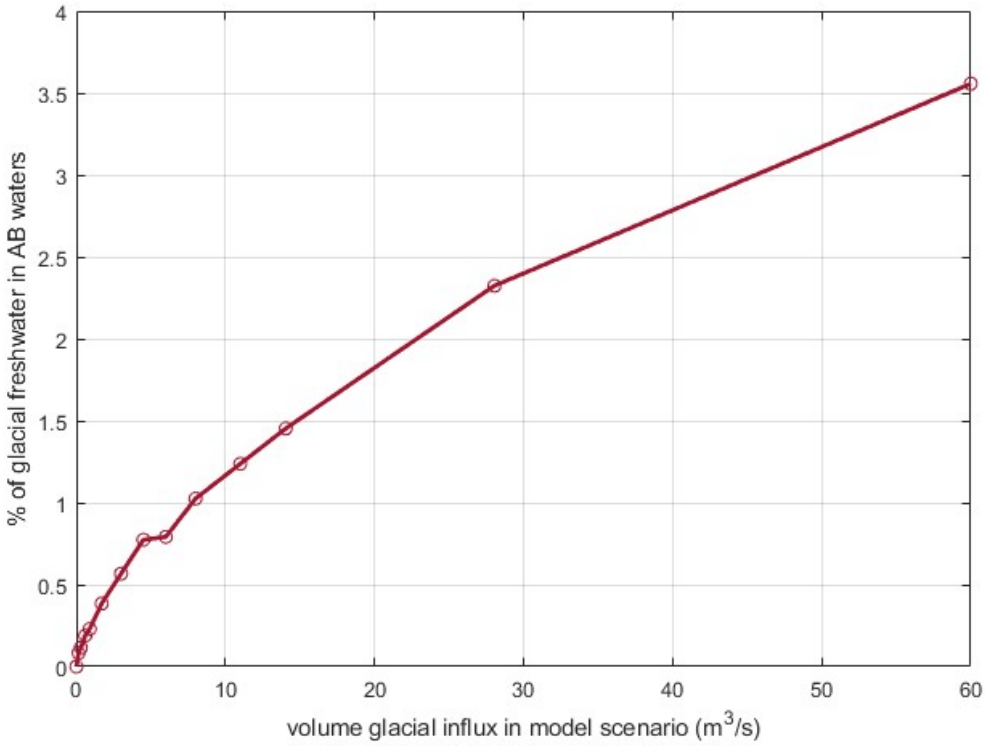

Supplementary Figure 5. Percentage of glacial freshwater in the total AB water budget over 14 model scenarios

1.2 Supplementary Tables

Supplementary Table 1. Statistics of the energy dissipation rates and bed shear stress. All values are based on model results from 0 m^3/s^{-1} model scenarios, averaged for the period 1.01.2022-28.01.2022.

	ENERGY DISSIPATION (M^2*S^{-3})		BED SHEAR STRESS ($N*M^{-2}$)	
	Whole domain	**Only bottom layer**		
MEAN	$8.69*10^{-5}$	$2.07*10^{-4}$	0.32	
MEDIAN	$9.14*10^{-8}$	$1.23*10^{-5}$	0.04	
25-75TH PRCTILE	$3.52*10^{-9}$ – $7.93*10^{-7}$	$2.00*10^{-6}$ – $5.77*10^{-5}$	0.01-0.11	
RANGE OF VALUES	Percentage	Percentage	**RANGE OF VALUES**	Percentage
0 -10^{-8}	31%	<1%	**0 – 0.05**	55%
10^{-8} -10^{-6}	46%	20%	**0.05-0.1**	18%
10^{-6} -10^{-4}	21%	59%	**0.1-0.2**	7%
10^{-4} -10^{-2}	1%	20%	**0.2 – 0.5**	5%
10^{-2} - 1	0%	0%	**0.5 - 1**	5%
1 - 10	0%	0%	**1-10**	8%

Supplementary Table 2. Additional details of AB model setup.

Number of grid cells	**31 619**
Number of layers	**50**
Duration of the modelling	**58 days**
Time step	**0.06 min (3.6 s)**
Initial conditions	**Salinity 34.1 ppt** **Temperature -0.2 ˚C**
Bottom roughness coefficients	**Used formula – 3D Chézy** **Uniform values U, V= 40 m1/2/s**
Model for 3D turbulence	**k-ε**

Hydrodynamic response of an Antarctic glacial bay to cross-bay winds and its potential impact on primary production

Maria Osińska[1,2,*] **and Agnieszka Herman**[2]

[1]University of Gdańsk, Faculty of Oceanography and Geography, Gdańsk, 80-309, Poland
[2]Institute of Oceanology of Polish Academy of Sciences, Sopot, 81-712, Poland
[*]corresponding.author: maria.osinska@phdstud.ug.edu.pl

ABSTRACT

Antarctic glacial bays are important, productive regions of the Southern Ocean. Certain glacial bays, including our research area, Admiralty Bay, are less favorable for phytoplankton growth due to wind-enhanced high energy levels, but they still host localized biological blooms. Westerly winds are predominant in Admiralty Bay; the strongest storms are from the east. These winds act perpendicular to the main axis of the bay. This study investigates the impact of cross-bay winds on the bay's hydrodynamics and its potential effects on primary production. A hydrodynamic model, coupled with a Lagrangian model tracking potential iron sources, was run under seven wind scenarios. Results indicate that all winds reduce water column stratification, but energy increase rate and circulation pattern shifts vary with wind direction. Westerly winds restrict outflow and promote the formation of submesoscale eddies near inner inlet openings, concentrating water masses that are expected to be iron-rich, potentially stimulating phytoplankton growth. Conversely, easterly winds enhance outflow, flushing bay waters and likely negatively impacting productivity. Limited observational and satellite-derived biological data provide supportive evidence for the model-based hypothesis that the direction of cross-bay winds, rather than just their magnitude, significantly influences local productivity.

Introduction

Due to their relatively high levels of primary production, Antarctic glacial bays of the West Antarctic Peninsula (WAP) region are essential for the Southern Ocean (SO) ecosystem. Phytoplankton blooms are prevalent in these areas, boosting the numbers of Antarctic krill, an important fish, bird, and marine mammal food source[1]. The high productivity observed in glacial bays can be attributed to the availability of iron, which is a limiting factor for primary production in the SO[2]. Iron is supplied to the SO through various mechanisms, the most significant for coastal waters being sediment resuspension through upwelling, sea-ice melt, dust deposition via precipitation, and glacial runoff[3–6].

The presence of iron sources alone is insufficient to establish a biological bloom, as many glacial bays are highly dynamic and are characterized by significant water exchange between the bay and the ocean, which flushes out nutrient-rich waters[7,8]. Therefore, in these bays, favorable hydrodynamic and geomorphological conditions are necessary for phytoplankton growth. Strong water column stratification has been found to be important for high levels of primary production[9]. If the nutrient source are the iron-rich bottom waters (BW), a mechanism must exist that elevates it to the euphotic layer. In an energetic environment, accumulation zones of nutrient-rich waters are required to give time for the phytoplankton bloom to emerge and for higher-level consumers to utilize it. Accumulation zones can develop when vorticity increases and eddies form, often shaped by the complexities of the seabed, such as mounts and basins[10,11]. Such submesoscale eddies are known to facilitate the development of localized hotspots of primary production[12].

Water column stratification, upwelling, elevated vorticity, and subsequent formation of water accumulation areas are influenced by the winds[9,10,13]. The impact of downfjord and upfjord winds on glacial bay circulation is well established, supported by numerous studies that investigated their effects on the hydrodynamics of elongated fjords where these winds prevail[13,14]. The Antarctic Peninsula coastline is highly intricate, comprising more than 100 bays adjacent to over 800 glaciers[15]. Numerous WAP bays are broad, allowing winds to affect them in the cross-bay axis; however, the impact of these winds on the bay hydrodynamics and its implications for the local environment remains unknown.

Admiralty Bay (AB), our research area, is located in the southwest of King George Island (KGI), South Shetland Islands, approximately 120 km northwest of the Antarctic Peninsula (Fig. 1 a). The main body of AB, measuring 18 km in length and 8 km in width, is characterized by weak water column stratification and a low Rossby radius of deformation (A), which averages 1.3 km throughout the year (estimate based on *in situ* measurements[7]). This classifies it as a 'broad bay' where rotational

dynamics play a significant role. Due to the absence of a pronounced sill (Fig. 1 b) AB's circulation is primarily driven by oceanic forcing, leading to a vigorous exchange of water between the ocean and the bay[7].

AB is known for its large and constant presence of penguins and marine mammals and, in fact, was named by British whalers and sealers who have been hunting them here since the 19th century[16]. Due to its rich animal populations, it is now designated both as an Antarctic Specially Managed Area and partially as an Antarctic Specially Protected Area. Primary production in AB is lower than in some other glacial bays due, among other factors, to its high dynamics stimulated by strong winds[8,17]. Despite this, the area has experienced significant temporary phytoplankton blooms[8,17]. Also, repeated localized feeding hotspots of whales and penguins have been observed by the staff of Arctowski Polish Antarctic Station in an area marked in yellow in Fig. 1 b (an example of such a feeding frenzy can be seen in Supplementary Video 1 online).

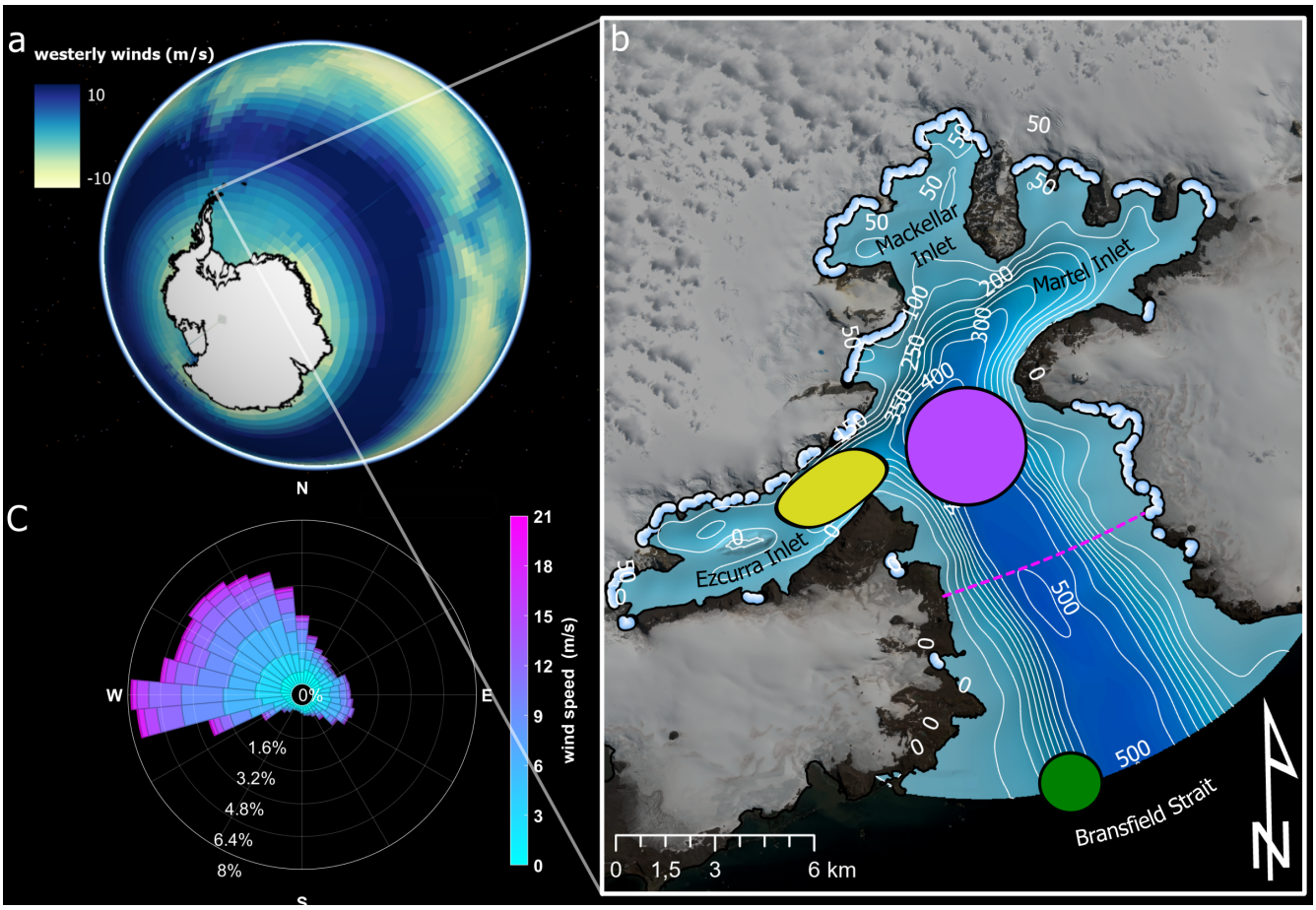

Figure 1. Admiralty Bay winds and bathymetry, **a.** westerly wind belt around Antarctica, the colormap shows the west wind component of long-term mean winds from 1991 to 2020[18], **b.** bathymetric map of Admiralty Bay[7]; thick light blue lines indicate glacial/water boundaries[19] and starting points of GMW particle tracking; pink circle—starting area of BW particle tracking; green circle—starting area of OB particle tracking; pink line—boundary of inner model domain; yellow field—known feeding hotspot; background—Sentinel imagery 29.12.2021, **c.** wind rose for Admiralty Bay from 15.12.2018 to 1.03.2023[20].

The bathymetry of AB, characteristic of bays in WAP, exhibits a deep fault exceeding 500 m at its center, with shallower inlets extending from the main body of the bay in various directions (Fig. 1 b). Twenty marine-terminating glaciers, seen in Fig. 1 b, are located along the AB coastline, releasing freshwater into the bay, primarily during austral summer and early autumn[7]. This freshwater mixes with the surrounding seawater, creating glacially modified waters (GMW). Previous research in AB confirms that GMW is a significant source of iron. Iron concentrations in sediments ranged from 2.40×10^2 to 5.15×10^3 µg/L measured in highly turbid glacial plume waters in close proximity to the ice front[21]. Dissolved iron concentrations in surface waters ranged from 8.49×10^{-4} to 1.74×10^{-3} µg/L, with peak levels observed closest to the glaciers[22]. These concentrations exceed typical levels found in the SO (previous studies have reported particulate iron concentrations in the coastal WAP and SO Atlantic sector ranging from 1.01×10^{-5} to 7.99×10^{-3} µg/L, and dissolved iron concentrations ranging from 5.58×10^{-6} to 4.41×10^{-4} µg/L[6,23]). Furthermore, although based on limited observations, Brandini and Rebello[24] demonstrated a positive

relationship between upwelling events and chlorophyll-a (*Chl-a*) concentrations in the AB, suggesting that upwelled BW also acts as a nutrient source for local phytoplankton communities. Based on this earlier research in AB and the recent findings by Annet et al.[4], as well as considering the region's low precipitation levels[25] and the decreasing sea ice extent[26], it seems reasonable to assume that BW and GMW are the primary sources of iron in AB.

Westerly and northwesterly winds are the prevailing wind directions in AB (Fig. 1 c). In recent years, due to the climate-change-related strengthening of circumpolar westerly winds (Fig. 1 a), AB has experienced an increase in the western wind component[27,28]. However, the analysis of data from 60 years of *in situ* observations has demonstrated that the 100 strongest wind events in this region were primarily caused by easterly and southeasterly winds[27]. Hence, the most frequent winds (westerly) and the strongest winds (easterly) are impacting AB waters perpendicularly to the main axis of the bay.

In short, AB is a broad glacial bay characterized by a weak water column stratification and an energetic water exchange with the open ocean. The capacity of this seemingly dynamic environment to sustain a vibrant ecosystem, as evidenced by frequently observed feeding hotspots, presents a conundrum that this study aims to address. We hypothesize that the apparent paradox can be explained by the additional forcing mechanism introduced to the system by cross-bay winds, which stimulate localized areas of biological productivity. Therefore, this study firstly seeks to understand the impact of cross-bay winds on the hydrodynamics of AB; further, it aims to explore the potential influence of these wind patterns on the development of localized biological blooms. Studying such processes requires a comprehensive approach combining observations and modelling. Empirical investigations in WAP glacial bays are inherently challenging. While extensive *in situ* datasets, such as that compiled by Osińska et al.[29], provide valuable insights into the variability of water properties, the logistical difficulties and safety concerns associated with conducting measurements, particularly under strong wind conditions, limit their scope. Furthermore, persistent cloud cover significantly restricts the utility of satellite data in visible bands (see Methods). Therefore, to isolate and examine the specific impact of cross-bay winds, we employ a high-resolution hydrodynamic model coupled with Lagrangian particle tracking model. This approach allows us to systematically analyze the effects of varying wind direction and magnitude on the bay's circulation, stratification, and particle transport. Finally, available *in situ* biological and satellite data are analyzed to assess if these wind-driven hydrodynamic changes in fact influence primary production levels in AB.

Results

Cross-bay wind effects on kinetic energy, stratification, and transport

Osińska and Herman[7] characterized the general circulation pattern within AB, revealing a system of two cyclonic cells that regulate water exchange between the Bransfield Strait and the bay, as depicted in Fig. 2 a. Ocean waters enter the bay primarily through a strong inflow current along its western boundary, while GMW is exported in the surface layer via a southerly outflow current in the east. To investigate the influence of cross-bay winds on this circulation pattern, the AB hydrodynamic model[7] was run in seven scenarios: a reference case without wind forcing (*no-wind* scenario) and three scenarios of increasing westerly and easterly winds each (Table 1). The used wind speeds of 7.5, 10, and 14 m/s correspond to the 50th, 75th, and 90th percentiles of all wind magnitudes recorded in AB.

	no-wind	*W-7.5*	*W-10*	*W-14*	*E-7.5*	*E-10*	*E-14*
wind direction (deg)	-	270	270	270	90	90	90
wind magnitude (m/s)	0	7.5	10	14	7.5	10	14
estimated Ekman layer depth D_E (m)	0	33	50	77	33	50	77

Table 1. Summary of the model runs.

Figure 2 a–c presents a comparison of kinetic energy content and depth-averaged horizontal velocities in *no-wind*, strong westerly wind (*W-14*), and strong easterly wind (*E-14*) scenarios (for maps in higher resolution for all scenarios see Supplementary Figs. S1–S7 online). The vertical profiles of the mean kinetic energy from all scenarios are given in Fig. 2 d. The results indicate that energy levels in AB waters increase with increased wind forcing; however, depending on the wind direction, distinct horizontal and vertical patterns are observed. Under westerly wind conditions (Fig. 2 b) energy increases in both the main body of the bay (in the whole domain increase of 25% in *W-7.5*, 61% in *W-10*, and 107% in *W-14* relative to the *no-wind* scenario) and most significantly in the inlets perpendicular to the bay's main axis: Ezcurra and Martel Inlets (EI and MI; Fig. 1 b). Since these inlets are shallower than the main body of AB, the increase in energy in spatially averaged vertical energy profiles is mostly seen within the upper 100 m (Fig. 2 d). Easterly winds (Fig. 2 c) result in a greater increase in energy (*E-7.5* 30% , *E-10* 127% , and *E-14* 352% increase). In contrast to westerly wind scenarios, this rise concentrates predominantly within the main body of AB, subsequently enhancing the velocities of the cyclonic circulation cell (for example, the inflow current in *E-14* is on average four times stronger than in the *no-wind* scenario). The rise in energy due to strengthening easterly winds is observed throughout the entire water column (Fig. 2 d).

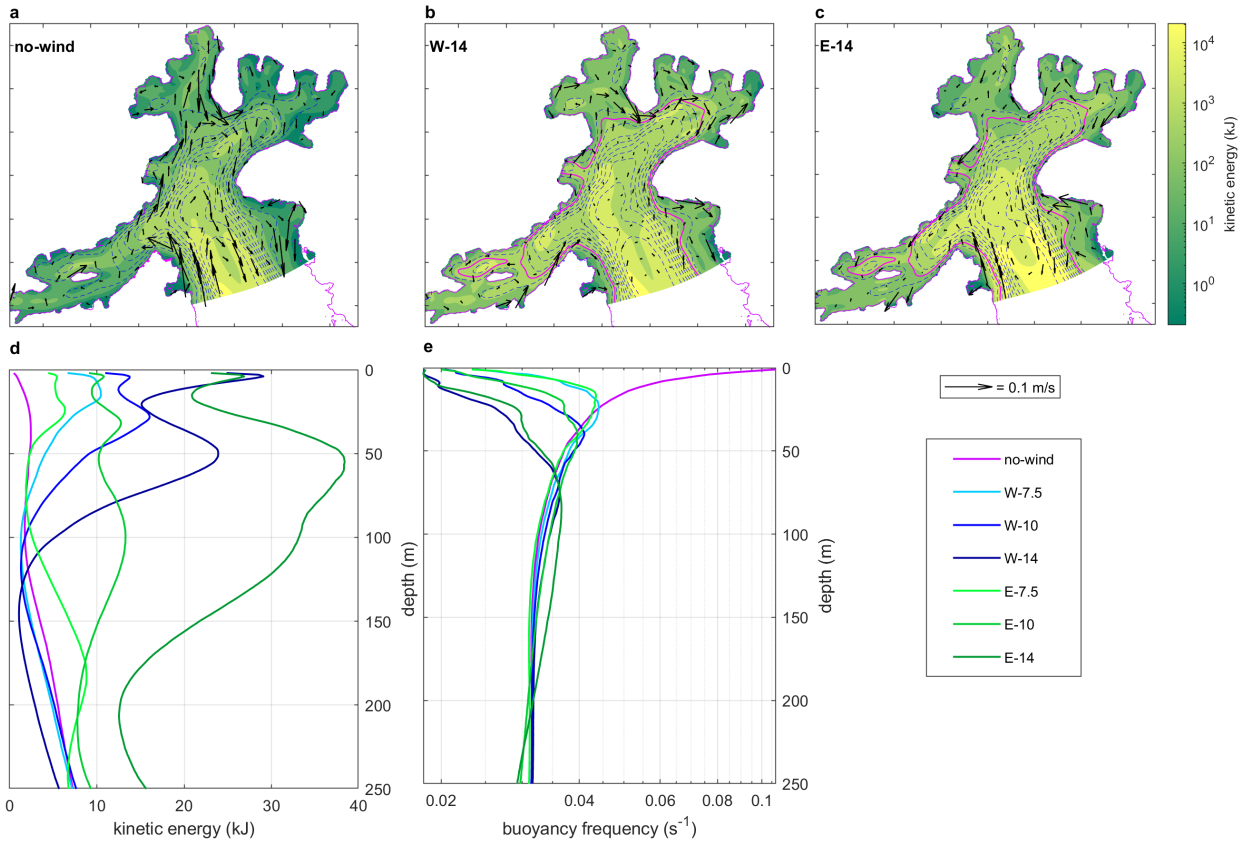

Figure 2. Shifts in AB hydrodynamics caused by wind forcing, **a-c.** spatial variations in *no-wind*, *W-14*, and *E-14* scenarios; colors represent kinetic energy integrated across the water column; arrows indicate depth-averaged horizontal velocity vectors; blue dashed lines show isobaths; magenta line shows the isobath equal to D_E, **d.** vertical profiles of the spatially mean kinetic energy, **e.** vertical profiles of the spatially mean buoyancy frequency (N). *Note*: all plots show mean values from Dec 7, 2021, to Jan 9, 2022 (33 days).

Since the intensification of easterly winds enhances circulation within the main body of AB, it leads to a significant increase in outflow from the model domain, with outflow of waters increasing by 38–108% as easterly winds strengthen. The volume of water exported from the AB boundary increases by only 3–15% with the strengthening of westerly winds (see Supplementary Fig. S8 online).

The stratification of the water column has been assessed through the buoyancy frequency (N)[30] (Methods). AB waters are well mixed even in the absence of wind forcing (Fig. 1 e). A maximum N of 0.11 s^{-1} is recorded in the upper layers in the *no-wind* scenario due to the presence of fresh GMW in the surface layer. N decreases with increasing wind magnitude regardless of wind direction. Low N corresponds to reduced A values: averaging 1.16 km in the absence of wind and approximately 0.6 km under all wind-induced scenarios, consistent with aforementioned A estimates derived from observations[7].

Particle tracks variability

To further investigate the water mass transport within AB, a Lagrangian particle tracking model was coupled to the hydrodynamic model. Three types of water masses were monitored: two expected sources of iron, GMW and BW, as well as open boundary waters (OB). OB refers to waters entering the AB from the Bransfield Strait, with their paths illustrating the influence of local winds on the penetration of ocean waters into the bay. In Fig. 1 b, the starting areas of these three particle groups are shown. Figure 3 a–c illustrates 25 randomly selected routes for each group under *no-wind*, *W-14*, and *E-14* wind conditions.

The statistics of OB particle tracks (green pathways in Fig. 3 a–c and their residence time across model scenarios shown in Fig. 3 d) indicate that easterly winds limit the oceanic influx into AB—in the *E-14* scenario: only 50% of the initially introduced particles remain in the domain for more than one day (the average residence time varies from 1.40 to 0.73 days with different magnitudes of easterly winds). This is illustrated in Fig. 3 c, where OB routes are nearly absent. In contrast, westerly winds have a comparable impact on the ocean penetration of AB waters as with no winds, with the average OB particle

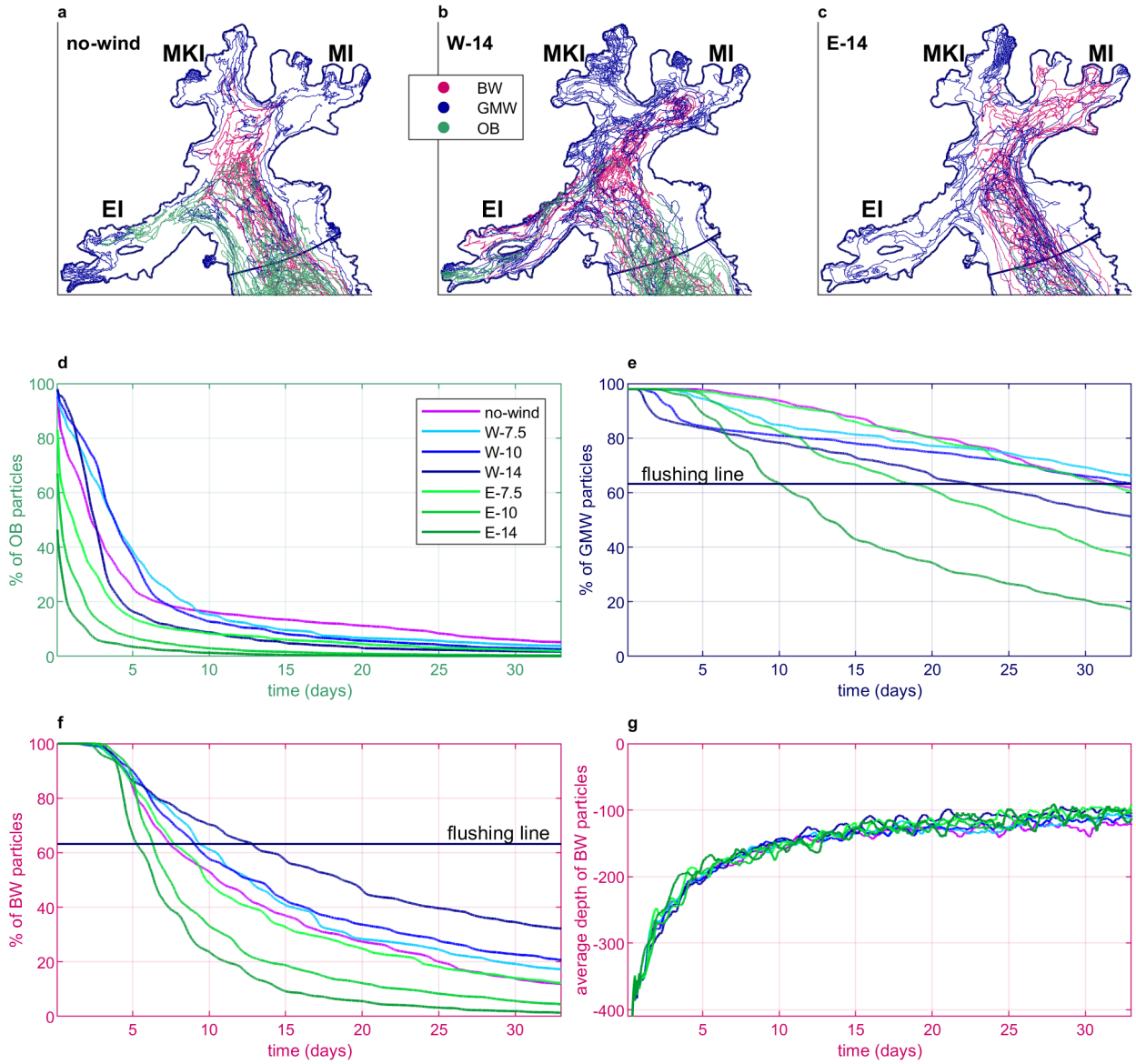

Figure 3. Pathways and residence time of tracked water particles in different wind scenarios, **a-c.** selected trajectories of BW, GMW, and OB particles in *no-wind*, *W-14*, and *E-14* wind conditions, respectively, **d.** residence time of OB particles in the model domain, **e.** residence time of GMW particles, **f.** residence time of BW particles, **g.** average depth of BW particles over time.

residence time in westerly wind scenarios varying from 3.75 to 5.69 days compared to 5.46 days in a *no-wind* scenario.

GMW (dark blue pathways in Fig. 3 a–c; residence time in Fig. 3 e) is exported from AB most rapidly during strong easterly winds. To assess this effect, we calculate the flushing time, which is defined as the duration needed to reduce the initial number of particles by a fraction of $1 - \exp^{-1} \approx 0.63$[31]. In *E-14*, GMW particles are flushed from AB within 10 days, which is twice as fast as in the *E-10* and *W-14*, and three times faster than in all other scenarios.

The residence time of BW particles in AB is also correlated with wind direction and magnitude (dark pink pathways in Fig. 3 a–c; residence time in Fig. 3 f). The stronger the westerly winds, the longer the BW particles stay in AB. The opposite effect arises from easterly winds. The BW particle flushing time between the *E-14* and *W-14* scenarios varies by 8 days (5 and 13 days, respectively). In *E-14,* after 33 days of modeling, less than 2% of BW particles remain in the AB, while in *W-14,* one-third remain inside. With westerly winds, similarly to GMW, BW pathways extend further into smaller AB inlets (Fig. 3 a-c). Across all simulated scenarios, BW particles were observed to rise from the seabed to an average depth of 100 m within

approximately 15 days (Fig. 3 g). This indicates that, regardless of wind conditions, the interaction between oceanic forcing and the shallowing bathymetry of AB consistently generates upwelling, effectively lifting BW into the higher ocean strata.

Formation of GMW and BW accumulation areas

To gain a more precise understanding of the factors that contribute to the observed disparities in residence time of GMW and BW particles in the modeled scenarios, it is necessary to examine vertical and horizontal flow pattern shifts caused by cross-bay winds (Fig. 4). During *no-wind* conditions, the main body of AB experiences downwelling along its eastern and western

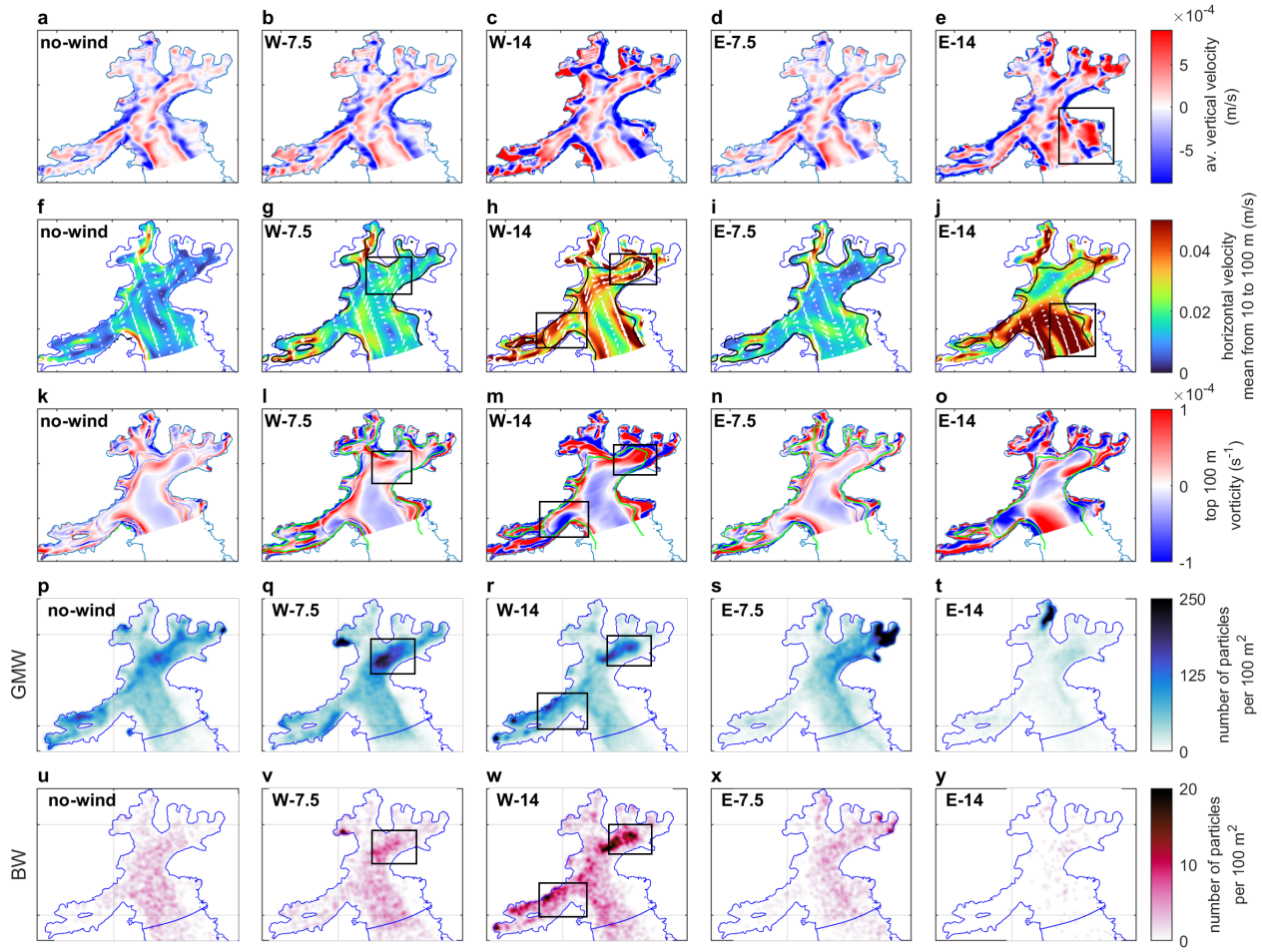

Figure 4. Changes in AB flow pattern in five wind scenarios, **a-e.** vertical velocities > |0.05| cm/s; positive values indicate movement upwards, **b-e.** anomalies in relation to *no-wind* scenario values, **f-j.** horizontal velocities averaged across 10-100 m depth; black line – the isobath corresponding to D_E, **k-o.** vorticity averaged across 10-100 m, with bathymetry; green line – D_E, **p-t.** GMW density maps after 33 days from release, **u-y.** BW density maps after 33 days from release. *Note*: Fig. 4 a-o. show mean values from Dec 7, 2021, to Jan 9, 2022 (33 days).

margins and upwelling in the center. This upwelling, seen in all scenarios, causes the aforementioned continuous lifting of BW particles. This pattern is enhanced by the increasing wind forcing seen in *W-7.5*, *W-14*, and *E-7.5* scenario results (Fig. 4 a–d; note that the values in panels b–e are anomalies with respect to those in panel a). A strong easterly wind of 14 m/s (*E-14*) generates a notable pressure gradient from east to west (difference of approximately 0.25 dbar between the west and east sides of AB), which induces upwelling along the eastern wall of the main body of AB (area indicated in the box in Fig. 4 e). This upwelling strengthens the easterly outflowing current (see the box in Fig. 4 j). The Ekman transport under easterly winds is directed southward toward the bay's mouth, thereby further increasing the outflowing current (Fig. 4 j). The enhancement of the outflow initiated by the upwelling explains why *E-14* exhibits qualitatively different behavior compared to other scenarios. This scenario is associated with the highest energy levels, the highest transport volumes out of the bay, and thus the fastest export of OB, GMW, and BW particles from the model domain (Figs. 2 d and 3).

The low A values (0.6 to 1.6 km in all scenarios) relative to the bay width ($\sim$ 8 km) result in a cyclonic circulation in AB, with the strongest currents flowing along the bay's coastline (Fig. 2 a). The shallower the waters, the more these currents can be influenced by the additional curl generated by the wind. Therefore, the larger the ratio of the Ekman layer depth (D_E) to the total water depth, the larger the increase in vorticity (see vorticity relation to D_E in Fig. 4 k–o, green lines show isobaths equal to D_E).

Despite the general cyclonic circulation in AB, an opposite, anticyclonic circulation cell exists in the surface waters of the main body of AB (Fig. 4 f). As the westerly winds increase, there is a rise in horizontal flow velocities, more significant within the inner waters of MI and EI compared to easterly wind scenarios (Fig. 4 f–j, and in high resolution in Supplementary Figs. S9–S15 online). At the inner inlets' openings, eddies are formed: in the *W-7.5* scenario, a cyclonic eddy forms between the Mackellar Inlet (MKI) and MI openings, while in the *W-14* scenario, much stronger but elongated eddies appear at the mouths of MI (cyclonic) and EI (anticyclonic; see the boxes in Fig. 4 g–h and l–m; vorticity for all scenarios is shown in Supplementary Figs. S16-S22 online). These eddies form when outflowing currents from MI and EI, moving along their southern edge, are affected by the wind curl, which redirects their flow northward, closing the circulation cells. Additionally, in the main body of AB, northerly Ekman transport enhances the surface anticyclonic cell, which reduces the net outflow from the bay (Fig. 4 h). This explains why the westerly wind speed does not increase the volume of transport out of the bay, even while the system's energy levels rise.

The entrapment of particles occurs in nonlinear eddies where rotational velocities exceed those of the surrounding fluid[32]. In *W-75*, *W-10*, and *W-14*, the horizontal velocities in the vortices at the mouths of EI and MI exceed those of the surrounding waters, and there is no significant increase in vertical mixing, providing favorable conditions for accumulation (Fig. 4 b, c, g, h, *W-10* in Supplementary Fig. S11 online). The eddies near the mouth of EI, MI, and within the large circulation cell in the main AB interchange waters, and trap particles between them for extended periods of time. Therefore, the eddies at the mouths of the inner inlets become accumulation areas of GMW and BW particles. This is confirmed by the density maps of GMW and BW particles after 33 days of modeling (boxes in Fig. 4 q, r, v, and w, corresponding to the same locations on the horizontal flow maps in panels g and h, and increased vorticity in panels l and m).

In the *no-wind* scenario, a surface eddy is formed at the same location as in the *W-7.5* scenario, corresponding to an area with increased amounts of GMW and BW particles. However, due to its lower velocity, its entrapment effect is weaker (Fig. 4 f, k, p, and u). As seen previously through residence-time analysis, the presence of easterly winds leads to a reduction in the amounts of GMW and BW particles within AB. Nonetheless, accumulation is observed in the *E-7.5* scenario in the east of MI (Fig. 4 s and x). Strong easterly winds (*E-14*) create an anticyclonic vortex at the entrance to EI. However, it is not categorized as a nonlinear eddy because its velocity is lower than that of the adjacent strong outflow current from the bay; thus, the waters within it are not accumulated but are rapidly flushed out (Fig. 4 j, o, t, and y).

Discussion

In both AB and Potter Cove (PC; a small but well-studied embayment of KGI, approximately 15 km west of AB, marked in Fig. 5 g), significant phytoplankton blooms were observed in 2010 and 2017, with *Chl-a* values exceeding 15 µg/L. These blooms have been attributed to particularly calm conditions that stabilized the water column, promoting phytoplankton presence in the euphotic zone[8,9,17]. Although vast blooms like those of 2010 and 2017, when they appear, are important for the local ecosystem, their occurrence frequency and thus significance is limited. Calm wind periods are rare in AB and throughout the WAP, and climate change is likely to further limit them[28] (Fig. 1 c). Therefore, it is crucial to understand how phytoplankton growth occurs under more typical, yet less favorable conditions.

We postulate that in these circumstances nonlinear submesoscale eddies play a significant role. This is supported by previous findings showing that both cyclonic and anticyclonic eddies can stimulate phytoplankton blooms by concentrating nutrient-rich particles[12], reducing vertical mixing and increasing light availability in the surface layers[33]. Our modeling results indicate that westerly winds are favorable for the formation of submesoscale eddies in AB, leading to the accumulation of BW and GMW particles. Consequently, we suggest that these eddies can serve as the foundation for biological hotspots, in which the concentration of iron-rich waters (BW and/or GMW) in the euphotic layer fuels phytoplankton growth. Crucially, our modeling indicates that this process is explicitly associated with westerly wind conditions, while easterly winds induce the opposite effect.

To investigate whether cross-bay winds indeed significantly influence phytoplankton growth in AB, we analyzed the relationship between *Chl-a* variability and concurrent wind conditions. While *Chl-a* reflects pigment levels rather than photosynthetic rates or biomass, its photosynthetic role makes it a proxy for primary production[34]. We used *Chl-a* data from Osińska et al.[29] (Fig. 5 b, c, e for locations; Fig. 5 a for dates) and the satellite-derived Copernicus GlobColour product[35] (GlobColour; Methods). Both datasets have limitations: the observational data lack records from high wind and easterly/southeasterly wind events and do not cover some key areas like the MI mouth. The GlobColour product has a coarse spatial resolution (4 km) and a 45.80% uncertainty. Nevertheless, Osińska et al.'s measurements are among the most

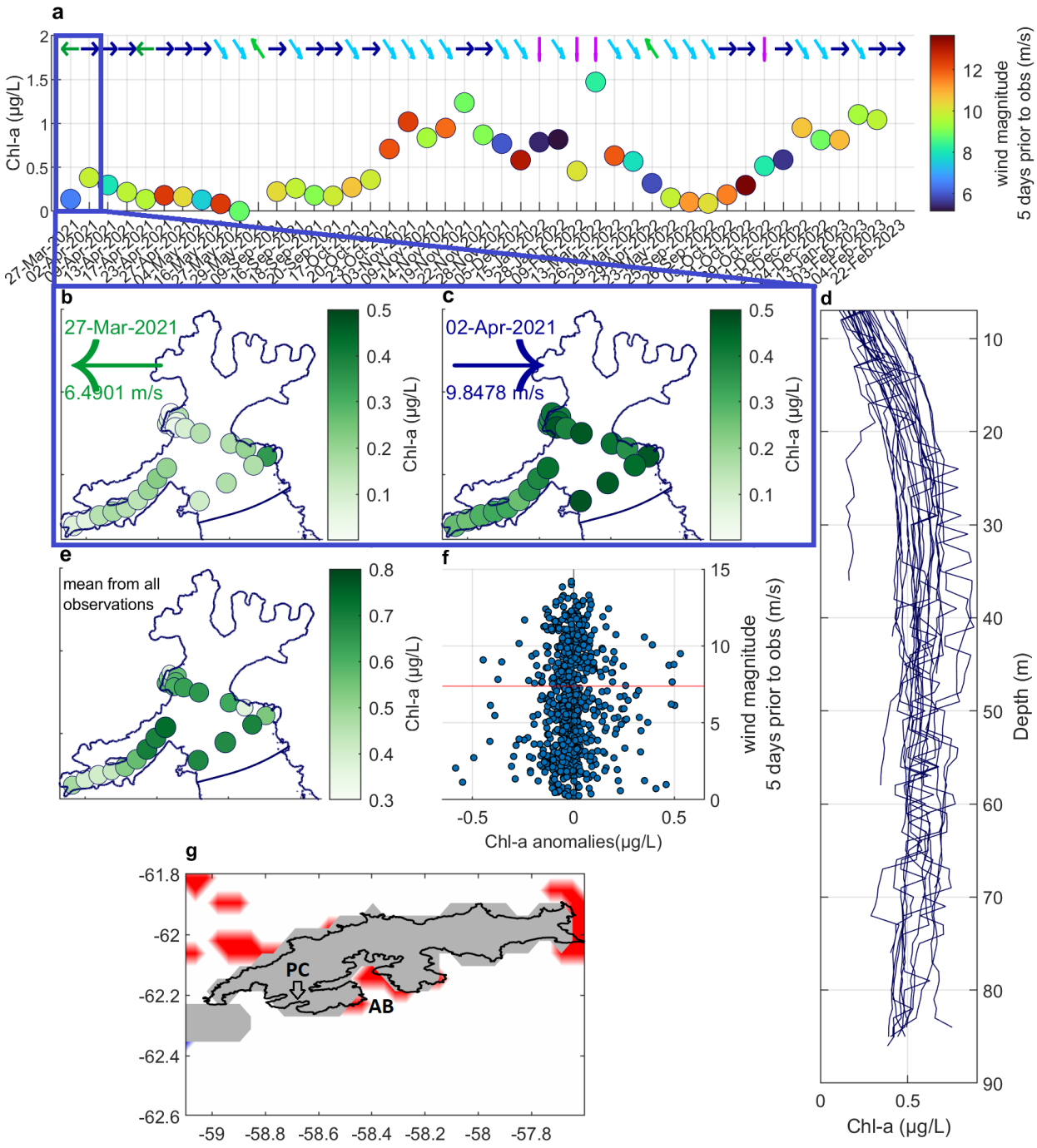

Figure 5. *Chl-a* content dependent on wind conditions; measured and from GlobColour, **a.** daily measured mean *Chl-a* values relationship with mean wind magnitude and predominant wind direction in 5 days prior to the measurement; the blue box highlights two days shown in detail in panels b and c, **b.** depth-avereged *Chl-a* values measured on 27th of Mar 2021, **c.** depth-averaged *Chl-a* values measured on 2nd of Apr 2021, **d.** *Chl-a* values from all measurements at each sampling site as function of depth, **e.** mean *Chl-A* from all measurements and depth-avereged at each site, **f.** mean daily GlobColour *Chl-a* anomalies relationship with wind magnitudes 5 days prior to the observation; red line – 7.5 m/s wind magnitude, **g.** areas around KGI in which U-test revealed a significant disparity between GlobColour *Chl-a* anomalies after westerly/easterly wind forcing; red areas – a significantly higher *Chl-a* values after westerly winds; white areas – no significant relation; grey areas – no data.

comprehensive datasets that describe water property variability in Antarctic glacial bays, and GlobColour provides the only high-temporal-resolution *Chl-a* estimates for this region. Therefore, although far from perfect, these datasets provide the most reliable *Chl-a* information available.

The variability of *Chl-a* levels from these two data sources, in relation to wind conditions, is illustrated in Fig. 5. Compared to other glacial bays in WAP, AB exhibits a comparatively low *Chl-a* values, with daily mean values rarely exceeding 1 μg/L, and maximum values recorded at approximately 40 m depth (Fig. 5 a and d; Supplementary Fig. S23 online for GlobColour data)[17,24,36,37]. Previous research attributed the reduced primary production in AB and PC to the strong wind-induced mixing and to the weak stratification in these bays[8,9]. If this hypothesis were true, a negative correlation would be expected between wind speed and *Chl-a* anomalies. However, we found no statistically significant correlation between the GlobColour *Chl-a* anomalies and wind speed (correlation coefficient $r = -0.10$; Fig. 5 f). Furthermore, several instances of positive *Chl-a* anomalies were observed after periods of strong winds, indicating that phytoplankton can reach relatively high concentrations even after wind-driven reduction of water-column stratification (Fig. 5 a and f; note the line in Fig. 5 f at 7.5 m/s wind magnitude, above which reduced N values are observed, as shown in Fig. 2 e). These observations suggest that strong vertical mixing is not a prerequisite to high primary productivity in AB, and that alternative mechanisms that stimulate productivity must be considered.

Spatial patterns further reinforce our hypothesis regarding the role of submesoscale eddies: areas of simulated GMW and BW accumulation correspond to regions of increased observed productivity. The highest mean *Chl-a* values were measured near the mouth of EI, with slightly lower values observed in central AB (Fig. 5 e). A significant proportion (82%) of these measurements were preceded by westerly or northwesterly winds, indicating that these locations are particularly conducive to phytoplankton growth under typical westerly wind conditions. The area of increased *Chl-a* in central AB aligns with an enhanced surface anticyclonic circulation cell predicted by the model (Fig. 4 g and h). The EI mouth is of particular interest due to its consistently high *Chl-a* values and frequent observations of feeding whales and penguins. This supports our modeling-based conclusions on the importance of areas at the mouths of inner inlets, where wind forcing influences a large portion of the water column and promotes the formation of eddies.

Unfortunately, among the four instances of *in situ* observations conducted on days after periods of easterly or southeasterly winds (Fig. 5 a), only one had a sufficiently brief interval from a consecutive measurement day to allow a direct estimate of the impact of a wind direction shift from easterly to westerly on *Chl-a* levels. Specifically, on March 27, 2021 (Fig. 5 b), after a period of easterly winds averaging 6.5 m/s, *Chl-a* concentrations were markedly low, with a mean value of 0.1 μg/L. During the subsequent five days, the average westerly wind magnitude reached 9.85 m/s. During this period the mean *Chl-a* value increased to 0.4 μg/L by April 2 (Fig. 5 c), with particularly elevated levels observed in the central region of AB and at the mouth of EI. Although this observation fits our hypothesis, it is based on a single case and thus, obviously, has no statistical significance. However, the satellite data provide a further support for the proposed *Chl-a*–wind relationshp. A Mann–Whitney U-test reveals that GlobColour *Chl-a* anomalies in AB are significantly higher after periods of westerly winds compared to easterly winds (average p = 0.046 for grid points in AB; see Methods). This effect appears to be specific to AB, with significant differences observed at 7 of 9 points within the bay (red areas in Fig. 5 g). In the broader KGI region, no significant differences were found (p = 0.459 across the area mapped in Fig. 5 g), indicating that bay-scale dynamics, rather than larger-scale regional processes, drive the *Chl-a*–wind relationship.

In conclusion, the available observational data, while limited, support our model-derived conjecture regarding the role of cross-bay winds in modulating productivity within Antarctic glacial bays. Our findings suggest that water column stratification alone does not account for the variability in *Chl-a* levels in AB. Regions prone to eddy formation under typical wind conditions exhibit increased productivity, and *Chl-a* values are statistically higher after periods of westerly winds compared to easterly winds. Modeling results show how these disparities can be convincingly explained by changes in AB flow patterns caused by different directions of cross-bay winds. Therefore, the predicted strengthening of westerly winds is expected to enhance AB productivity, while easterly wind events are expected to limit it. We anticipate similar effects in other glacial bays of the WAP, with phytoplankton growth influenced positively or negatively depending on the bay's orientation relative to the cross-bay wind direction.

Conclusions

Our research highlights the crucial role of cross-bay winds in shaping circulation patterns within Antarctic glacial bays. In AB westerly winds impede water exchange between the bay and the open ocean and foster formation of submesoscale eddies. The location of these eddies is linked to local geomorphology and is most common near the mouths of the inner inlets, where the Ekman depth D_E approaches the water depth. These eddies can serve as accumulation zones for water masses, including GMW and BW, which are presumed to be key sources of iron in AB. This accumulation is expected to positively influence primary production, potentially leading to the creation of localized biological blooms. In contrast, easterly winds enhance the flushing of AB waters by strengthening the circulation cell in the main body of the bay and significantly increasing the strength

of the outflow current. Consequently, easterly winds are presumed to reduce primary production by advecting nutrients and phytoplankton out of the bay.

Using hydrodynamical modeling as its primary tool, this study investigates the significance of a single, previously understudied factor shaping glacial bay circulation: cross-bay winds. It provides critical insights into the potential impacts of strong wind forcing, which would be unattainable through observational methods alone. This is particularly valuable, as wind intensification is projected to increase in the WAP region. The results suggest that wind direction, rather than just wind magnitude, can have significant and far-reaching effects. This study also proposes a possible explanation for how primary production can be maintained in the high-energy coastal waters of the WAP. Future research, integrating coupled hydrodynamical, iron, and biological modeling, could build on this foundation to provide a more comprehensive understanding of glacial bay bloom dynamics and a quantitative assessment of the significance of this mechanism.

The glacial bays of Antarctica are undergoing significant transformation due to climate change. The circumpolar westerly winds are intensifying, the influx of glacial water is increasing, and the extent of sea ice is decreasing. All of these factors influence glacial bay hydrodynamics and primary production. This study represents the first investigation of the direct effects of common cross-bay winds on the hydrodynamics of an Antarctic glacial bay and their potential implications for local primary productivity. We suggest that analogous mechanisms may operate in other similarly shaped bays of WAP where cross-bay winds frequently occur. In a broader context, this study contributes to understanding the impact of ongoing regional transformations on primary production in the coastal regions of the WAP, which is crucial for the food chain and carbon cycle of the entire SO.

Methods

Wind data were obtained from the Antarctic Mesoscale Prediction Model[20] (AMPS). The hourly wind direction and magnitude values from seventeen AMPS model grid points from the period December 15, 2018, to March 1, 2023, were collected and spatially averaged. This time range corresponds to the period of the *in situ* measurement campaign conducted in AB, as detailed by Osińska et al.[29]. The *Chl-a* measurements conducted during this campaign used an optical sensor calibrated with deionized water, without laboratory validation of its absolute values. Consequently, all documented *Chl-a* levels are biased by the same value. Both the mean and median *Chl-a* value recorded during winter (from June, July, and August), a season known to have the lowest phytoplankton presence, is −0.44 µg/L with a standard deviation of 0.07 µg/L. Consequently, −0.44 µg/L was taken as an accurate representation of 0 µg/L, and all measured values were adjusted accordingly. Days during the winter months (June, July, and August) and days with measurements taken from fewer than 10 sites were excluded from the analyzed dataset (Fig. 5). In the analysis of the relationship between wind forcing and *Chl-a* levels (Fig. 5), AMPS wind data averaged over five days prior to each *Chl-a* measurement day was used. The five-day period was chosen because modeling has shown it to be the maximum time required for the AB circulation pattern to adjust and reach a new equilibrium after a change in wind conditions.

Due to limited availability of high-resolution satellite color imagery for the AB region resulting from persistent cloud cover (for instance, during the over four-year-long sampling campaign, only 16 Sentinel-2 L2A images with less than 15% cloud cover were available from AB) an alternative approach was necessary to assess daily variability in *Chl-a* concentrations. Therefore, daily *Chl-a* estimates from the GlobColour[35] product were utilized. Data were extracted from a region surrounding KGI (within the spatial limits 63.10–61.73°S, 59.34–57.48°W, $n = 1466$) for the period December 15, 2018, to March 1, 2023. To investigate the potential influence of wind forcing on *Chl-a* levels, a comparative analysis was conducted between days following westerly and easterly wind events (defined as the predominant wind direction during the five days prior to each observation, consistent with the approach used in the measured *Chl-a* data analysis). Initially, *Chl-a* anomalies were calculated to account for seasonal variability. This involved generating a 30-day moving average of *Chl-a* concentrations for each grid point. Subsequently, daily *Chl-a* anomalies were derived by subtracting the smoothed 30-day average from the corresponding daily *Chl-a* value. The *Chl-a* anomaly data were then categorized into three groups: (1) anomalies following easterly wind forcing (predominant wind direction between 45° and 135°), (2) anomalies following westerly wind forcing (predominant wind direction between 225° and 315°), and (3) all remaining data. This classification resulted in 845 *Chl-a* daily values associated with westerly wind events and 167 daily values associated with easterly wind events. A two-sample Mann-Whitney U test was then performed to test the null hypothesis of no significant difference between the *Chl-a* anomaly distributions for the westerly and easterly wind categories. The U-test was chosen since the Shapiro-Wilk test indicated a statistically significant departure from normality for both the easterly and westerly wind condition datasets. This test was applied to each grid point within the GlobColour dataset.

Hydrodynamical modelling was performed using the Delft3D Flow model[38], following the detailed setup outlined by Osińska et al.[7,38]. Two modifications were made: the resolution of the open boundary condition was improved from three to five data points, and a uniform 3D Chézy bottom roughness coefficient of 50 $m^{1/2}/s$ was applied. The analysis of results in this paper is limited to the region outlined by the pink line in Fig. 1 b, approximately 5 km from the model's open boundary. Glacial water influx was introduced uniformly across all glacial fronts, with a volume of 0.64 m^3/s per approximately 1 km of

glacial front. This corresponds to a total of 19 m^3/s, representing the average value of glacial influx to AB during the months of December and January, as estimated by Osińska et al.[7].

The D-WAQ Part particle tracking model[39] has been coupled with the hydrodynamical model. The Delft3D Flow model ran with a timestep of 0.06 minutes, and results were recorded every 12 minutes. Based on its results, the particle tracking model was calculated with a 3-minute timestep. The vertical resolution of the D-WAQ Part model was established at 25 layers within the σ-coordinate system.

The vertical dispersion values fed to D-WAQ Part were calculated by the Delft3D Flow using a $k-\varepsilon$ turbulence model. Horizontal dispersion values were also calculated using Delft3D Flow; however, in the Delft3D framework, additional horizontal dispersion may be added into Lagrangian model calculations. The additional horizontal dispersion is expressed as $D = at^b$, where t denotes particle age. The coefficient a represents a constant addition of dispersion, while b is the dispersion growth factor. As the goal of this study is to monitor individual tracers rather than collective clouds of particles, we set $b = 0$, thus making a a total added horizontal dispersion coefficient. Given that horizontal dispersion values are recorded in the results of dynamic turbulence models and utilized in pathway tracking calculations, it is recommended that the supplementary dispersion values remain low, approximately 1 m^2/s[39]. There are no direct measurements of dispersion in this area; therefore, we tested three scenarios of additional horizontal dispersion: 0.03 m^2/s (estimation based on[40]), 0.07 m^2/s (suggested value by the model developer in the example case[39]), and 1 m^2/s (the default a value). The testing indicated that, statistically, this value did not significantly influence the results, demonstrating that the hydrodynamical turbulence values and model resolution are sufficient and that this additional coefficient is of lesser importance. The middle value of 0.07 m^2/s was used in all subsequent calculations.

Three water masses were monitored in the D-WAQ Part model: GMW, BW, and OB. Tracked particles were released in four groups at distinct moments of the tidal cycle: at maximum high water, during the middle of the ebb tide, at minimum low water, and in the middle of the flood tide. The presented results are averaged across these four groups, thereby reducing the potential impact of the tidal cycle on the model results. For each release point and moment, 150 particles were tracked. GMW water particles were observed from 52 points along the ocean/glacier interface (Fig. 1 b), at the bottom, middle, and top of the water column, resulting in a total of 86,400 GMW particles being tracked. BW tracking started from 20 evenly distributed points in the innermost section of the deep trench located in the center of AB, as indicated in Fig. 1 b by a purple circle, totaling 12,000 BW water tracers. OB particles were released from the center of the robust inflowing western current in the western section of the open boundary (green dot in Fig. 1 b), from 25 depths, contributing to a total of 15,000 tracked OB water pathways. Modeling continued for a duration of 39 days (Dec 1st, 2021–Jan 9th, 2022), which included a 5-day spin-up period. Particle tracking and wind forcing began during day 6.

Calculations of buoyancy frequency N were performed using the Gibbs Oceanographic Toolbox function `gsw_N^2`, divided by 2π and square-rooted[41].

The first baroclinic Rossby radius of deformation (A) was calculated using the formula[42]:

$$A = \frac{c}{|f|} \tag{1}$$

where f is the Coriolis parameter and c is the internal wave speed:

$$c = \frac{1}{\pi}\int_{-H}^{0} N(z)dz \tag{2}$$

Ekman layer depth (D_E) was estimated using a simplifying assumption of constant vertical viscosity A_{Vi} which was estimated taking the maximum vertical eddy viscosity at a given model grid point. Subsequently D_E was calculated using a simple formula[43]:

$$D_E = \frac{1}{n}\sum_{i=1}^{n} \pi\sqrt{\frac{2A_{Vi}}{|f|}} \tag{3}$$

The vorticity was calculated as the curl of the horizontal velocity field, averaged through 33 days of modeling.

Data availability statement

The modelling setup files and results are available from the corresponding author on reasonable request.

The observational data analyzed during the current study can be found in online repositories:
PANGAEA - https://doi.org/10.1594/PANGAEA.947909;
Zenodo - 10.5281/zenodo.10277429; Zenodo 10.5281/zenodo.10277333.

References

1. Ducklow, H. W. *et al.* Marine pelagic ecosystems: The West Antarctic Peninsula. *Philos. Transactions Royal Soc. B: Biol. Sci.* **362**, 67–94, DOI: 10.1098/rstb.2006.1955 (2007).

2. de Baar, H. J., Bathmannt, U., Smetacek, V., Löscher, B. M. & Veth, C. Importance of iron for plankton blooms and carbon dioxide drawdown in the Southern Ocean. *Nature* **373**, DOI: 10.1038/373412a0 (1995).

3. Boyd, P. W., Arrigo, K. R., Strzepek, R. & van Dijken, G. L. Mapping phytoplankton iron utilization: Insights into Southern Ocean supply mechanisms. *J. Geophys. Res. Ocean.* **117**, DOI: 10.1029/2011JC007726 (2012).

4. Annett, A. L. *et al.* Comparative roles of upwelling and glacial iron sources in Ryder Bay, coastal western Antarctic Peninsula. *Mar. Chem.* **176**, DOI: 10.1016/j.marchem.2015.06.017 (2015).

5. De Jong, J. *et al.* Natural iron fertilization of the Atlantic sector of the Southern Ocean by continental shelf sources of the Antarctic Peninsula. *J. Geophys. Res. Biogeosciences* **117**, DOI: 10.1029/2011JG001679 (2012).

6. Jones, R. L. *et al.* Antarctic glaciers export carbon-stabilised iron(II)-rich particles to the surface Southern Ocean. *Nat. Commun. 2025 16:1* **16**, 1–10, DOI: 10.1038/s41467-025-59981-y (2025).

7. Osińska, M. & Herman, A. Influence of glacial influx on the hydrodynamics of Admiralty Bay, Antarctica - study based on combined hydrographic measurements and numerical modeling. *Front. Mar. Sci.* **11**, 1365157, DOI: 10.3389/FMARS.2024.1365157 (2024).

8. Schloss, I. R. *et al.* On the phytoplankton bloom in coastal waters of southern King George Island (Antarctica) in January 2010: An exceptional feature? *Limnol. Oceanogr.* **59**, 195–210, DOI: 10.4319/lo.2014.59.1.0195 (2014).

9. Höfer, J. *et al.* The role of water column stability and wind mixing in the production/export dynamics of two bays in the Western Antarctic Peninsula. *Prog. Oceanogr.* **174**, DOI: 10.1016/j.pocean.2019.01.005 (2019).

10. Zhao, K. X., Stewart, A. L., McWilliams, J. C., Fenty, I. G. & Rignot, E. J. Standing Eddies in Glacial Fjords and Their Role in Fjord Circulation and Melt. *J. Phys. Oceanogr.* **53**, 821–840, DOI: 10.1175/JPO-D-22-0085.1 (2023).

11. Neder, C. *et al.* Modelling suspended particulate matter dynamics at an Antarctic fjord impacted by glacier melt. *J. Mar. Syst.* **231**, 103734, DOI: 10.1016/J.JMARSYS.2022.103734 (2022).

12. Sandulescu, M., López, C., Hernández-García, E. & Feudel, U. Plankton blooms in vortices: The role of biological and hydrodynamic timescales. *Nonlinear Process. Geophys.* **14**, DOI: 10.5194/npg-14-443-2007 (2007).

13. Cushman-Roisin, B., Asplin, L. & Svendsen, H. Upwelling in broad fjords. *Cont. Shelf Res.* **14**, DOI: 10.1016/0278-4343(94)90044-2 (1994).

14. Lundesgaard, Ø., Powell, B., Merrifield, M., Hahn-Woernle, L. & Winsor, P. Response of an Antarctic Peninsula Fjord to Summer Katabatic Wind Events. *J. Phys. Oceanogr.* **49**, 1485–1502, DOI: 10.1175/JPO-D-18-0119.1 (2019).

15. Davison, B. J., Hogg, A. E., Moffat, C., Meredith, M. P. & Wallis, B. J. Widespread increase in discharge from west Antarctic Peninsula glaciers since 2018. *The Cryosphere* **18**, 3237–3251, DOI: 10.5194/tc-18-3237-2024 (2024).

16. Rakusa-Suszczewski, S. The past and present of King George Island (South Shetland Islands, Antarctica). *Pol. Polar Res.* **19**, 249–252 (1998).

17. Wasiłowska, A., Tatur, A. & Rzepecki, M. Massive diatom bloom initiated by high winter sea ice in Admiralty Bay (King George Island, South Shetlands) in relation to nutrient concentrations in the water column during the 2009/2010 summer. *J. Mar. Syst.* **226**, 103667, DOI: 10.1016/j.jmarsys.2021.103667 (2022).

18. Kanamitsu, M. *et al.* NCEP-DOE AMIP-II reanalysis (R-2). *Bull. Am. Meteorol. Soc.* **83**, DOI: 10.1175/bams-83-11-1631 (2002).

19. Gerrish, L., Fretwell, P. & Cooper, P. High resolution vector polylines of the Antarctic coastline (7.4) [Data set]. Tech. Rep., UK Polar Data Centre, Natural Environment Research Council, UK Research & Innovation (2021). DOI: https://doi.org/10.5285/e46be5bc-ef8e-4fd5-967b-92863fbe2835.

20. Powers, J. G. *et al.* Real-time mesoscale modeling over Antarctica: The Antarctic mesoscale prediction system. *Bull. Am. Meteorol. Soc.* **84**, DOI: 10.1175/BAMS-84-11-1533 (2003).

21. Wójcik-Długoborska, K. A., Osińska, M. & Bialik, R. J. The impact of glacial suspension color on the relationship between its properties and marine water spectral reflectance. *IEEE J. Sel. Top. Appl. Earth Obs. Remote. Sens.* DOI: 10.1109/JSTARS.2022.3166398 (2022).

22. Sierpinski, S., Baquer, L. M., Martins, C. C. & Grassi, M. T. Exploratory evaluation of iron and its speciation in surface waters of Admiralty Bay, King George Island, Antarctica. *Anais da Acad. Brasileira de Ciencias* **95**, DOI: 10.1590/0001-3765202320211520 (2023).

23. Klunder, M. B., Laan, P., Middag, R., Baar, H. J. D. & van Ooijen, J. C. Dissolved iron in the Southern Ocean (Atlantic sector). *Deep. Sea Res. Part II: Top. Stud. Oceanogr.* **58**, 2678–2694, DOI: 10.1016/J.DSR2.2010.10.042 (2011).

24. Brandini, F. P. & Rebello, J. Wind field effect on hydrography and chlorophyll dynamics in the coastal pelagial of Admiralty Bay, King George Island, Antarctica. *Antarctic Sci.* **6**, DOI: 10.1017/s0954102094000672 (1994).

25. Plenzler, J., Budzik, T., Puczko, D. & Bialik, R. J. Climatic conditions at Arctowski Station (King George Island, West Antarctica) in 2013-2017 against the background of regional changes. *Pol. Polar Res.* **40**, 1–27, DOI: 10.24425/PPR.2019.126345 (2019).

26. National Snow and Ice Data Center & CIRES. Sea Ice Index (2023).

27. Turner, J. *et al.* Strong wind events in the Antarctic. *J. Geophys. Res. Atmospheres* **114**, DOI: 10.1029/2008JD011642 (2009).

28. Swart, N. C. & Fyfe, J. C. Observed and simulated changes in the Southern Hemisphere surface westerly wind-stress. *Geophys. Res. Lett.* **39**, DOI: 10.1029/2012GL052810 (2012).

29. Osińska, M., Wójcik-Długoborska, K. A. & Bialik, R. J. Annual hydrographic variability in Antarctic coastal waters infused with glacial inflow. *Earth Syst. Sci. Data* **15**, 607–616, DOI: 10.5194/essd-15-607-2023 (2023).

30. IOC, SCOR & IAPSO. The international thermodynamic equation of seawater – 2010: Calculation and use of thermodynamic properties. *Intergov. Oceanogr. Comm. Manuals Guid. No. 56* (2010).

31. Monsen, N. E., Cloern, J. E., Lucas, L. V. & Monismith, S. G. A comment on the use of flushing time, residence time, and age as transport time scales. *Limnol. Oceanogr.* **47**, DOI: 10.4319/lo.2002.47.5.1545 (2002).

32. Castelao, R. M., Dinniman, M. S., Amos, C. M., Klinck, J. M. & Medeiros, P. M. Eddy-Driven Transport of Particulate Organic Carbon-Rich Coastal Water Off the West Antarctic Peninsula. *J. Geophys. Res. Ocean.* **126**, DOI: 10.1029/2020JC016791 (2021).

33. Kahru, M., Mitchell, B. G., Gille, S. T., Hewes, C. D. & Holm-Hansen, O. Eddies enhance biological production in the Weddell-Scotia Confluence of the Southern Ocean. *Geophys. Res. Lett.* **34**, DOI: 10.1029/2007GL030430 (2007).

34. Huot, Y. *et al.* Does chlorophyll a provide the best index of phytoplankton biomass for primary productivity studies? *Biogeosciences Discuss.* (2007).

35. (CMEMS), E. C. M. S. I. Global ocean colour (copernicus-globcolour), bio-geo-chemical, l4 (monthly and interpolated) from satellite observations (1997-ongoing), DOI: https://doi.org/10.48670/moi-00281.

36. Lipski, M. Variations of physical conditions, nutrients and chlorophyll a contents in Admiralty Bay (King George Island, South Shetland islands, 1979). *Pol. Polar Res.* **8**, 307–332 (1987).

37. Schloss, I. R. *et al.* Response of phytoplankton dynamics to 19-year (1991–2009) climate trends in Potter Cove (Antarctica). *J. Mar. Syst.* **92**, 53–66, DOI: 10.1016/j.jmarsys.2011.10.006 (2012).

38. Deltares. Delft3D 3D/2D modelling suite for integral water solutions Hydro-Morphodynamics (2020).

39. Deltares. D-WAQ PART - User Manual (2024).

40. Neumann, D., Callies, U. & Matthies, M. Marine litter ensemble transport simulations in the southern North Sea. *Mar. Pollut. Bull.* **86**, 219–228, DOI: 10.1016/J.MARPOLBUL.2014.07.016 (2014).

41. McDougall, P., Trevor J. ; Barker. Getting started with TEOS-10 and the Gibbs Seawater (GSW) Oceanographic Toolbox. *Scor/Iapso Wg127* (2011).

42. Chelton, D. B., Deszoeke, R. A., Schlax, M. G., El Naggar, K. & Siwertz, N. Geographical variability of the first baroclinic Rossby radius of deformation. *J. Phys. Oceanogr.* **28**, DOI: 10.1175/1520-0485(1998)028<0433:GVOTFB>2.0.CO;2 (1998).

43. Olbers, D., Willebrand, J. & Eden, C. *Ocean dynamics*, vol. 9783642234507 (Springer, 2012).

44. Padman, L., Fricker, H. A., Coleman, R., Howard, S. & Erofeeva, L. A new tide model for the Antarctic ice shelves and seas. *Annals Glaciol.* **34**, 247–254, DOI: 10.3189/172756402781817752 (2002).

45. Dotto, T. S., Mata, M. M., Kerr, R. & Garcia, C. A. A novel hydrographic gridded data set for the northern Antarctic Peninsula. *Earth Syst. Sci. Data* **13**, 671–696, DOI: 10.5194/ESSD-13-671-2021 (2021).

Funding declaration

This research was funded by two grants from the National Science Centre in Poland: No. 2017/25/B/ST10/02092 'Quantitative assessment of sediment transport from glaciers of South Shetland Islands on the basis of selected remote sensing methods' and No. 2018/31/B/ST10/00195 'Observations and modeling of sea ice interactions with the atmospheric and oceanic boundary layers'.

Acknowledgements

Special thanks are owed to Laboratory of Sedimentary and Environmental Processes - INCT-Criosfera Fluminense Federal University - Geoscience Institute in Brazil for providing us with bathymetric data from Admiralty Bay. We thank the publishers of all open-source data used in the setup of this model: the National Center for Atmospheric Research and the Byrd Polar Research Center of The Ohio State University for providing AMPS modelled wind data, and NOAA for compiling observational wind data for validation; Earth and Space Research for producing the CATS2008 tides model[44]; and[45] for sharing grided temperature and salinity reanalysis data. We thank Deltares for making the Delft3D Flow model available for calculations. CI TASK (Center of the Tri-City Academic Computer Network) in Gdańsk, Poland, offered computing power and software to enable calculations. We thank Daniel Pereira for creating the Wind-Rose MATLAB add-on utilized in this paper. Finally, we would like to express our heartfelt gratitude to the various members of the Arctowski Polish Antarctic Station crew for their assistance with observations and measurements.

Author contributions statement

M.O. Conceptualization, Data curation, Formal analysis, Investigation, Methodology, Software, Validation, Visualization, Writing – original draft; AH: Conceptualization, Funding acquisition, Methodology, Project administration, Resources, Supervision, Writing – review and editing

Additional information

The authors declare no competing interests.

Supplementary Information

Hydrodynamic response to cross-bay winds in an Antarctic glacial bay and its potential impact on primary production

Maria Osińska[1,2],* and Agnieszka Herman[2]

[1]University of Gdańsk, Faculty of Oceanography and Geography, Gdańsk, 80-309, Poland

[2]Institute of Oceanology of Polish Academy of Sciences, Sopot, 81-712, Poland

*corresponding.author: maria.osinska@phdstud.ug.edu.pl

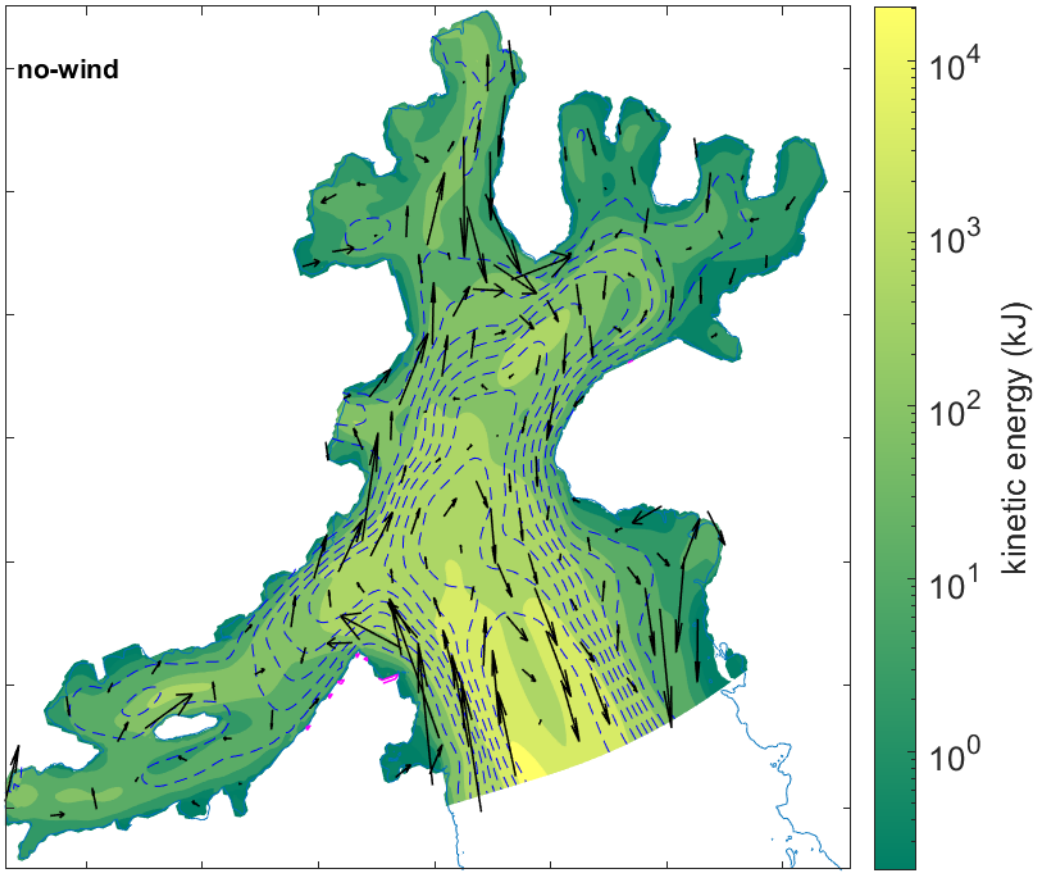

Figure S1. *No-wind scenario kinetic energy and depth averaged velocities; colors represent kinetic energy integrated across the water column; arrows indicate depth-averaged horizontal velocity vectors; blue spaced lines show isobaths, with a magenta line highlighting the isobath = D_E. {Note}: showing mean values from Dec 7, 2021, to Jan 9, 2022 (33 days).*

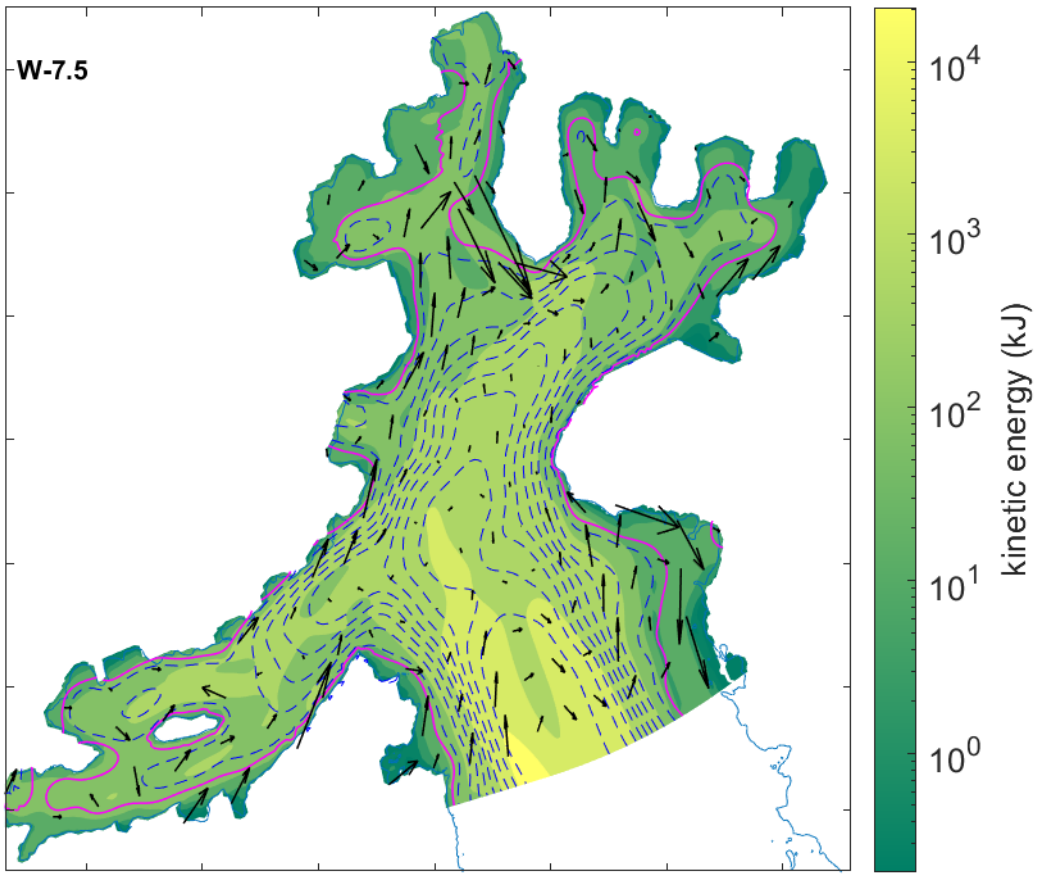

***Figure S2**. As in Fig. S1, but for W-7.5 scenario.*

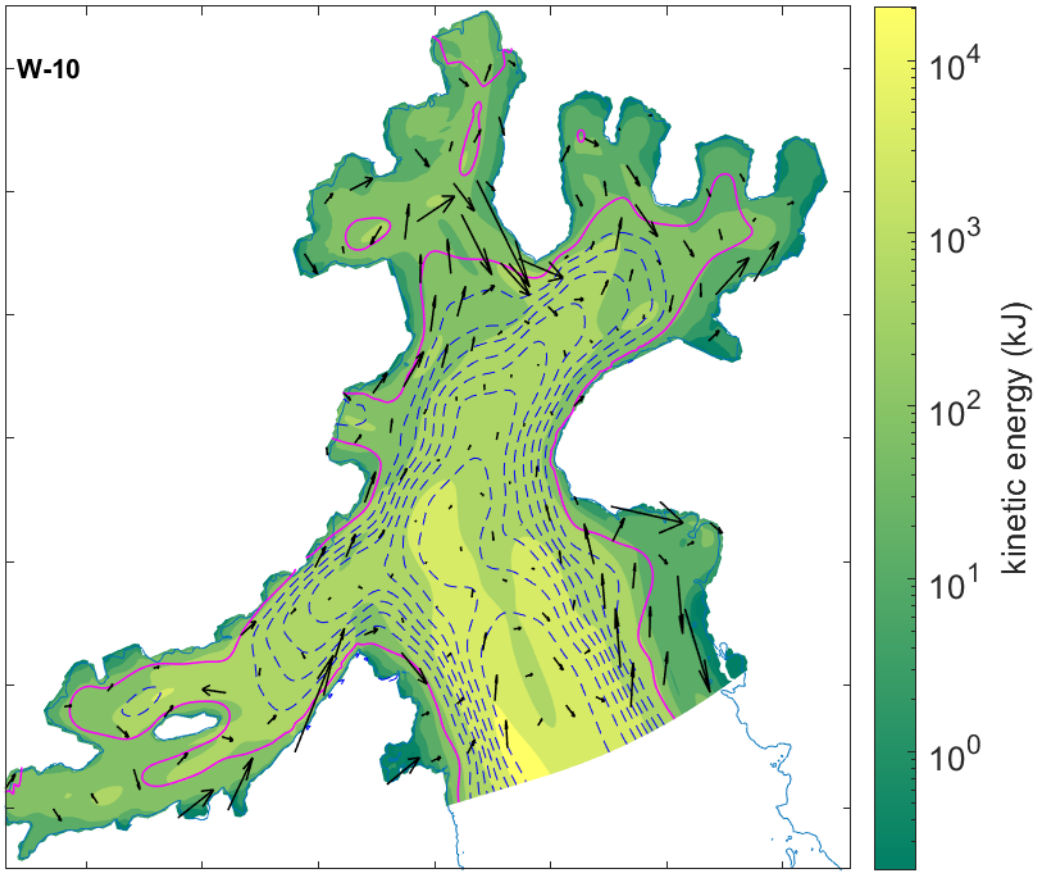

Figure S3. *As in Fig. S1, but for W-10 scenario.*

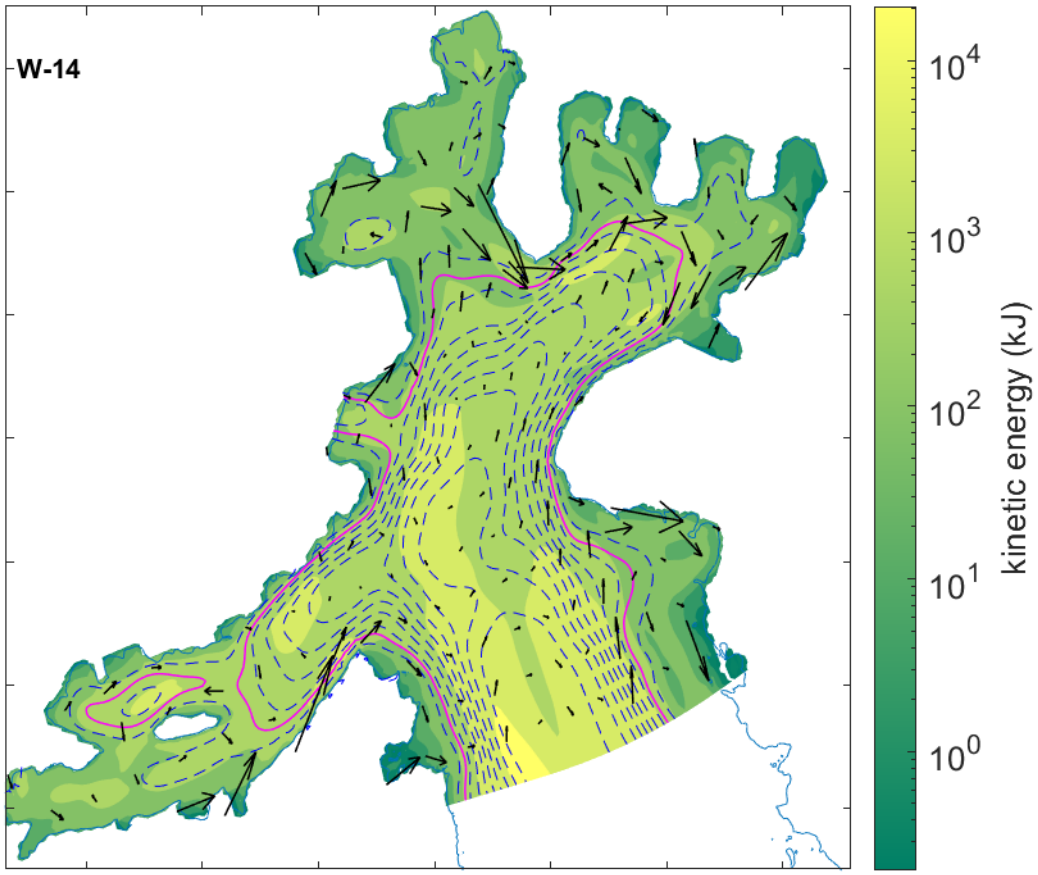

Figure S4. *As in Fig. S1, but for W-14 scenario.*

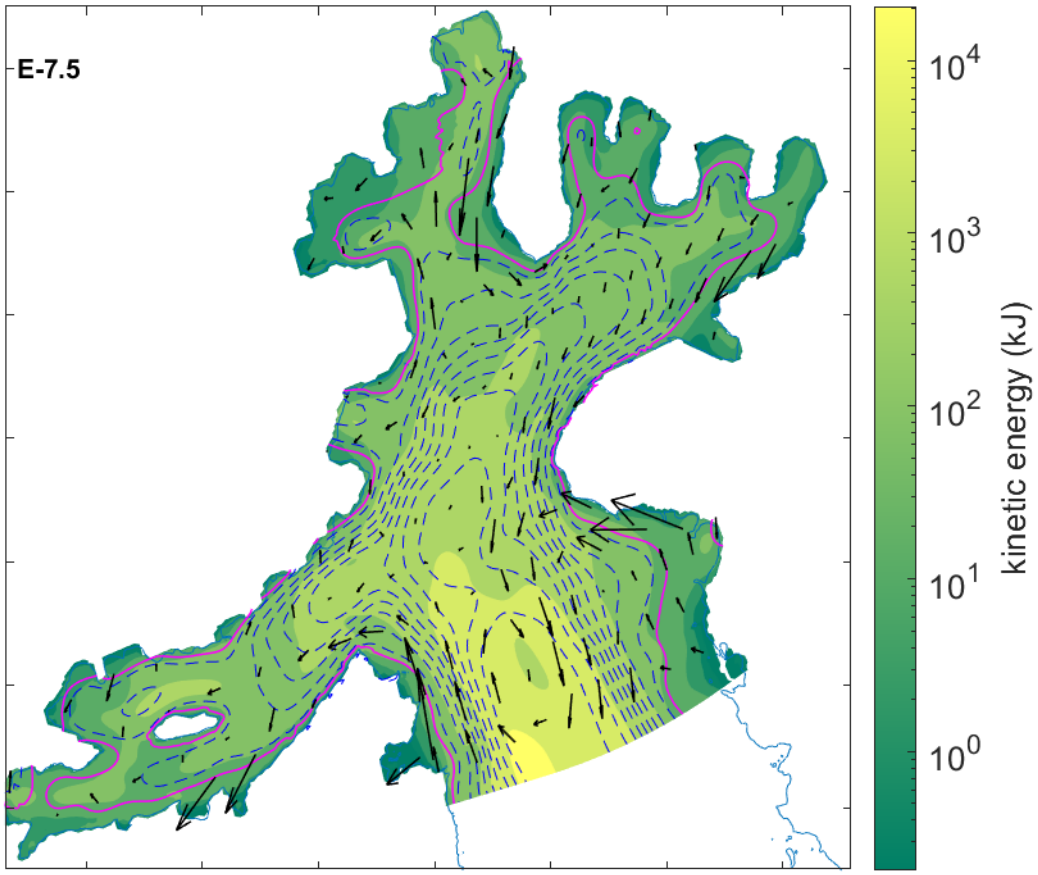

Figure S5. *As in Fig. S1, but for E-7.5 scenario.*

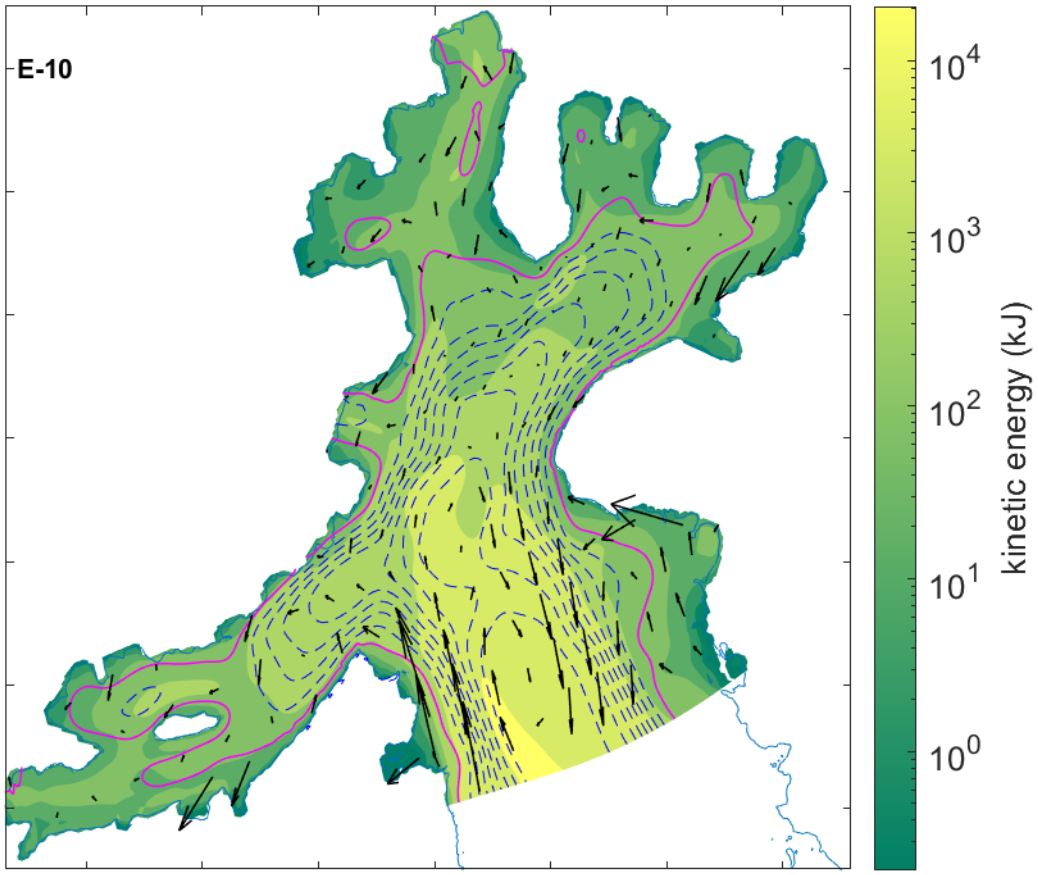

Figure S6. *As in Fig. S1, but for E-10 scenario.*

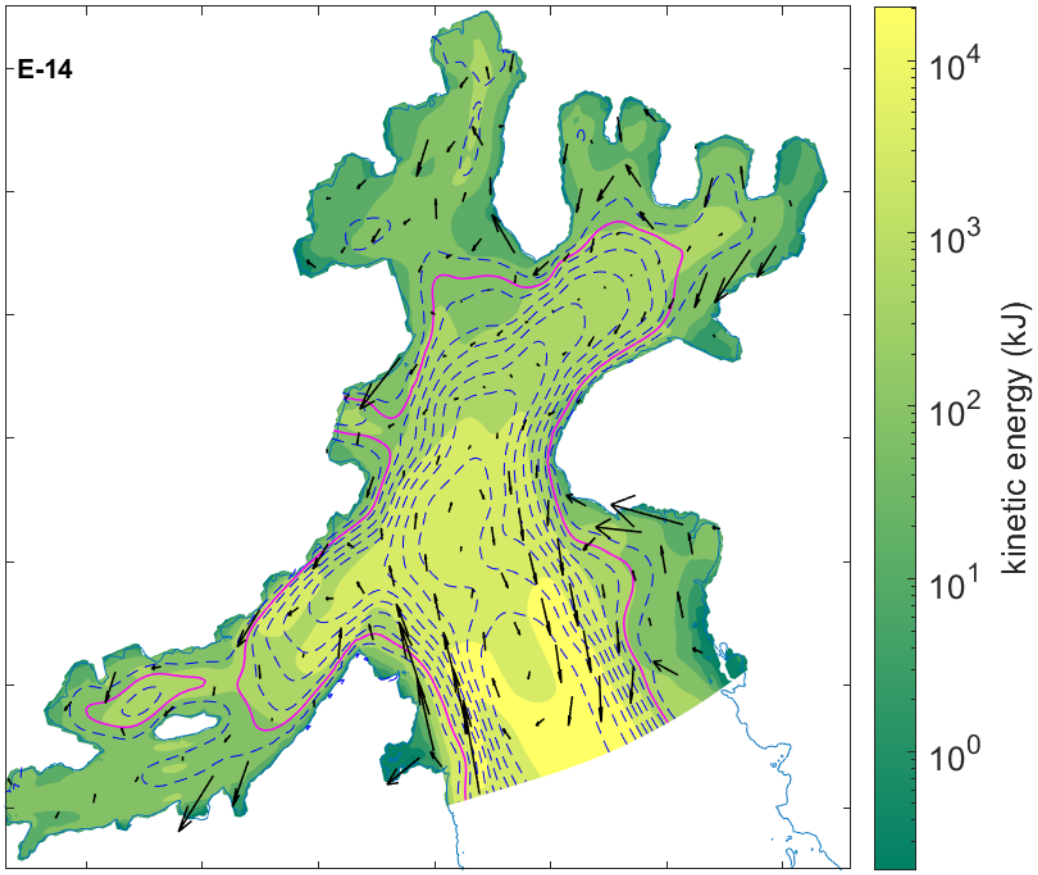

Figure S7. *As in Fig. S1, but for E-14 scenario.*

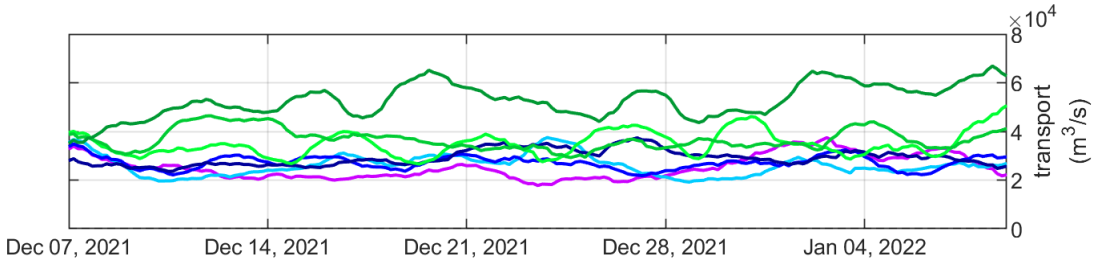

Figure S8*. Volume of transport through the cross-section in the main AB (pink line in Fig. 1 b) in seven model scenarios.*

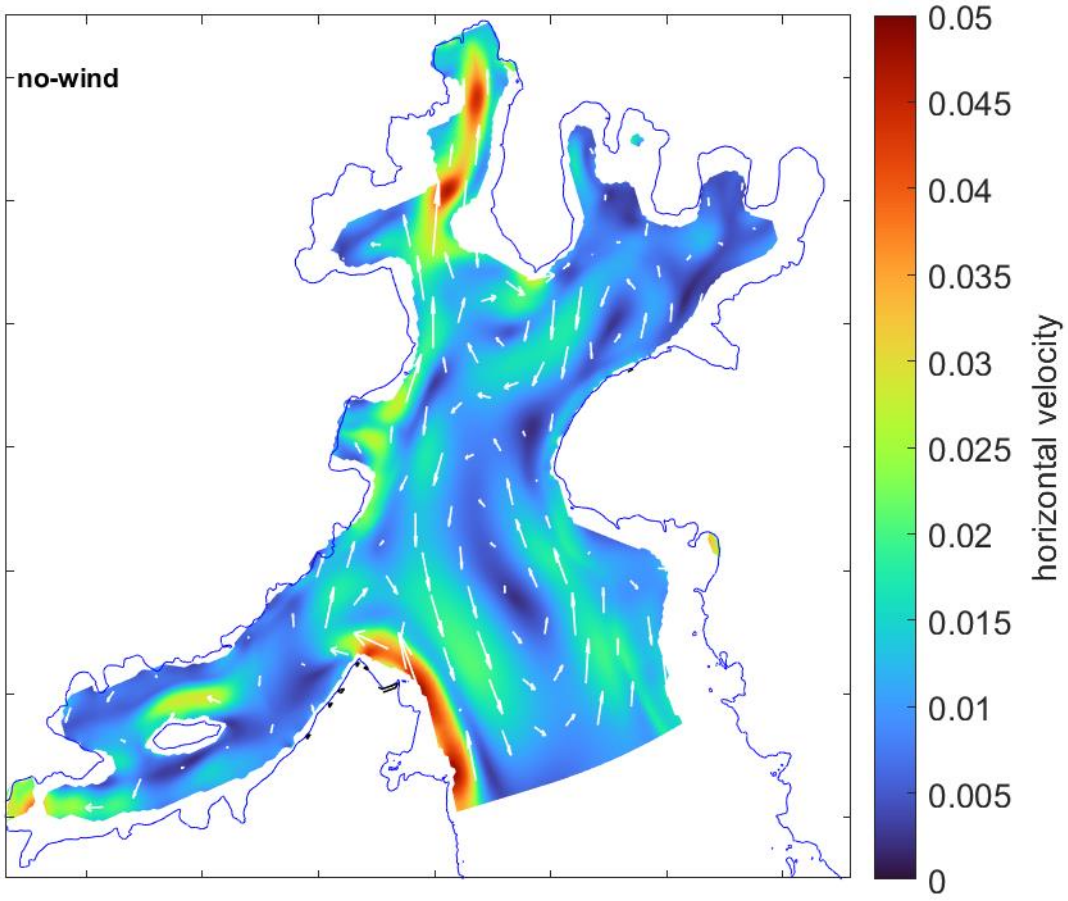

Figure S9. *No-wind scenario horizontal velocities averaged across 10-100 m depth, with a black line highlighting the isobath = D_E. {Note}: showing mean values from Dec 7, 2021, to Jan 9, 2022 (33 days).*

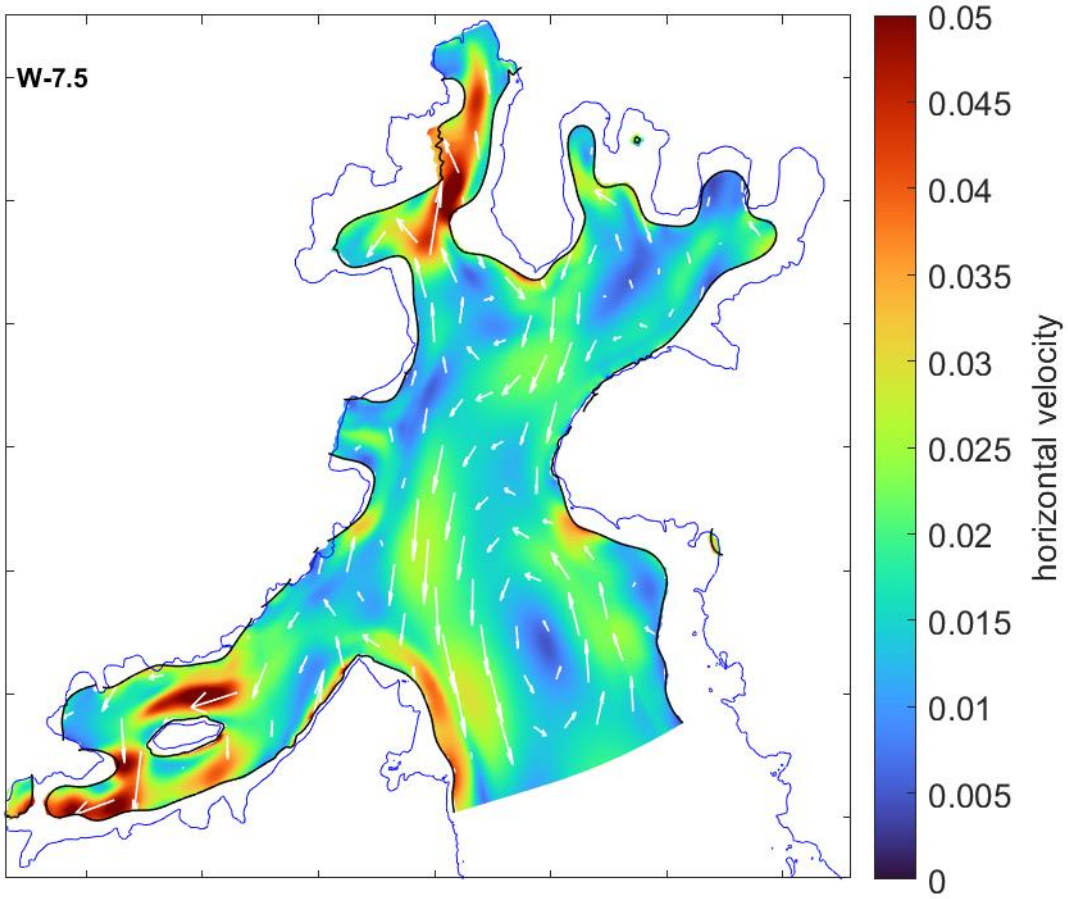

Figure S10. *As in Fig. S9, but for W-7.5 scenario.*

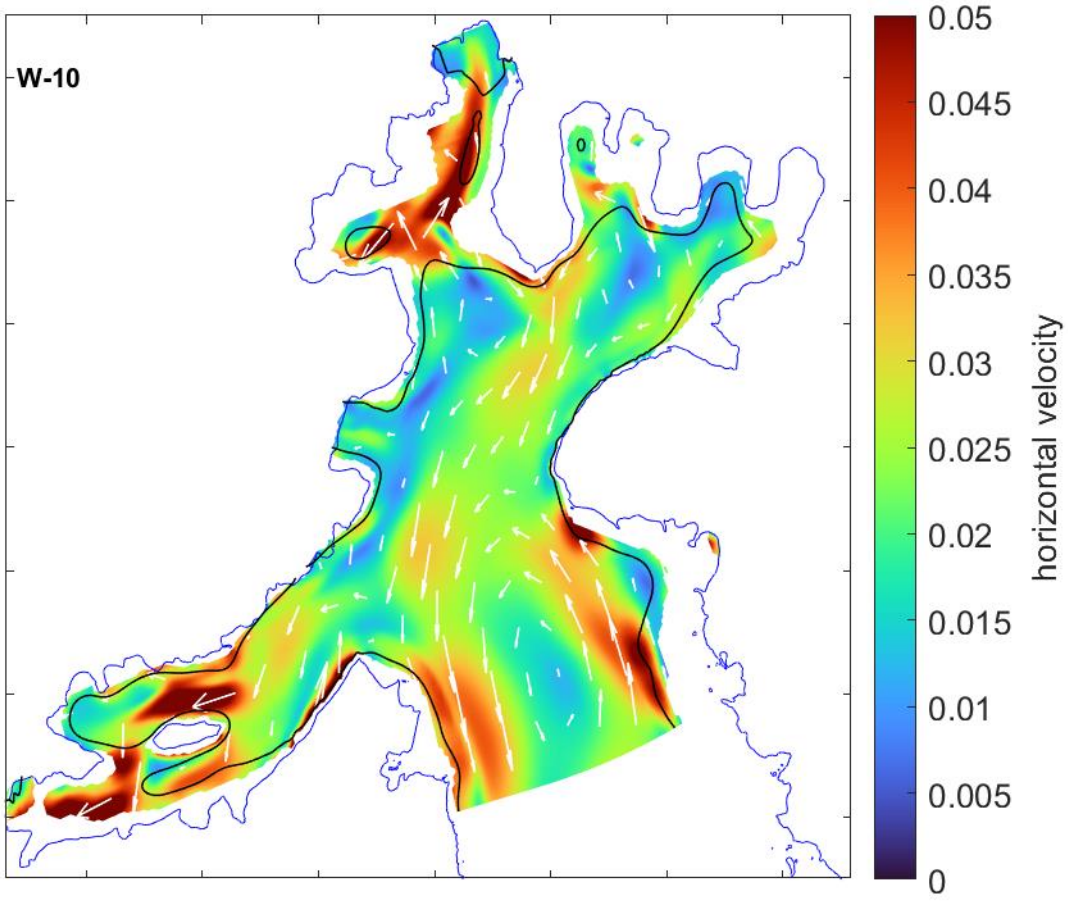

Figure S11. *As in Fig. S9, but for W-10 scenario.*

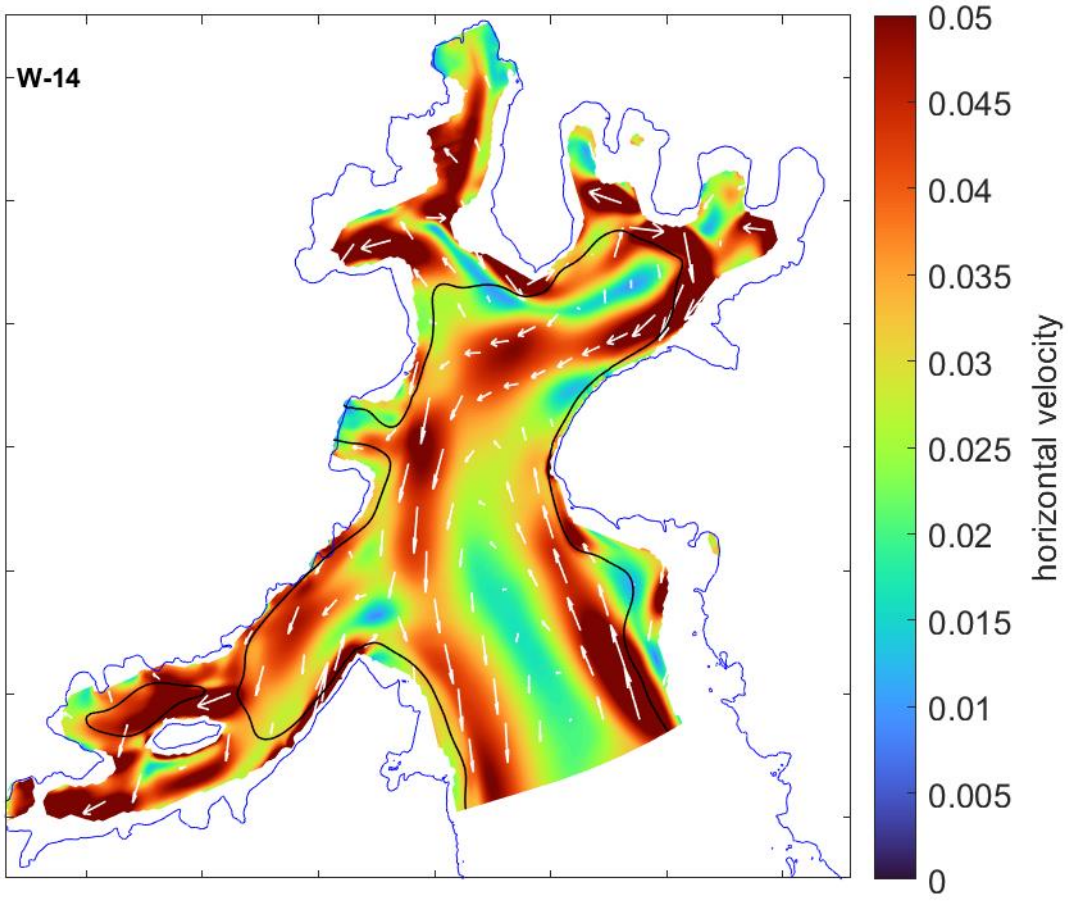

Figure S12. *As in Fig. S9, but for W-14 scenario.*

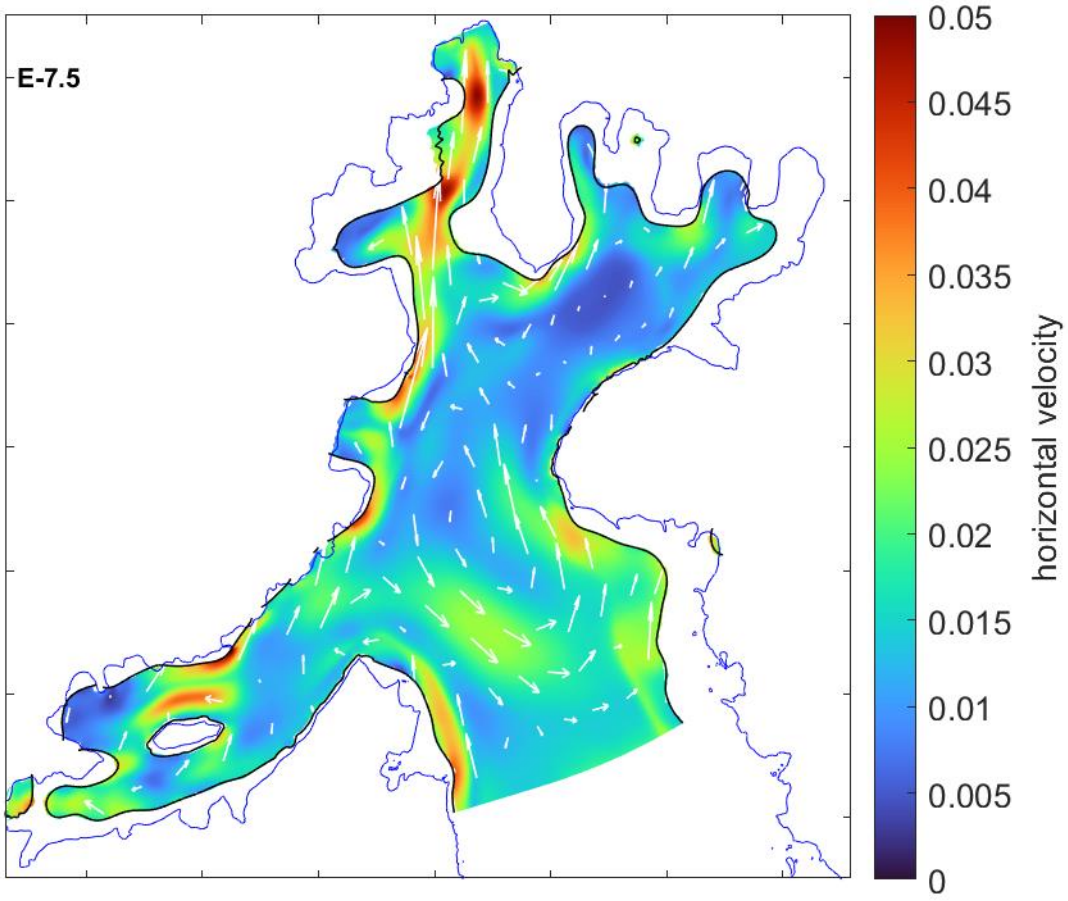

Figure S13. *As in Fig. S9, but for E-7.5 scenario.*

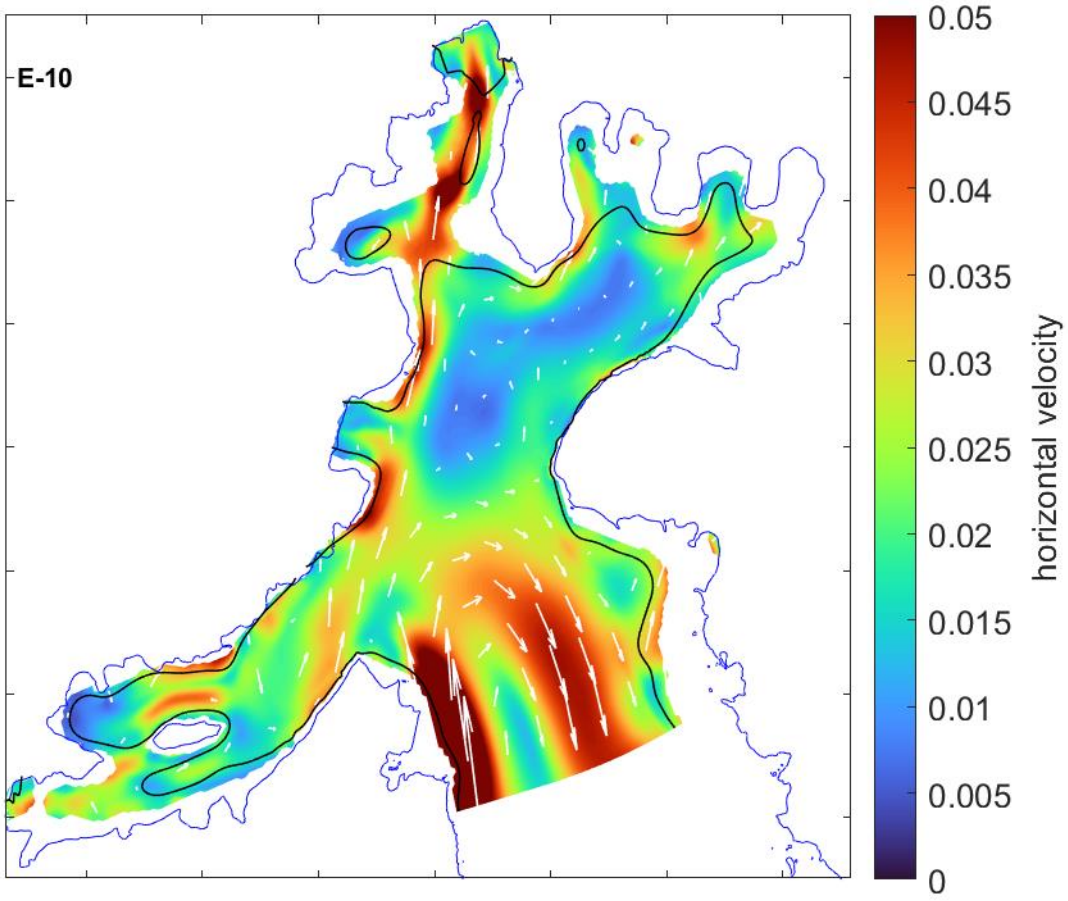

Figure S14. *As in Fig. S9, but for E-10 scenario.*

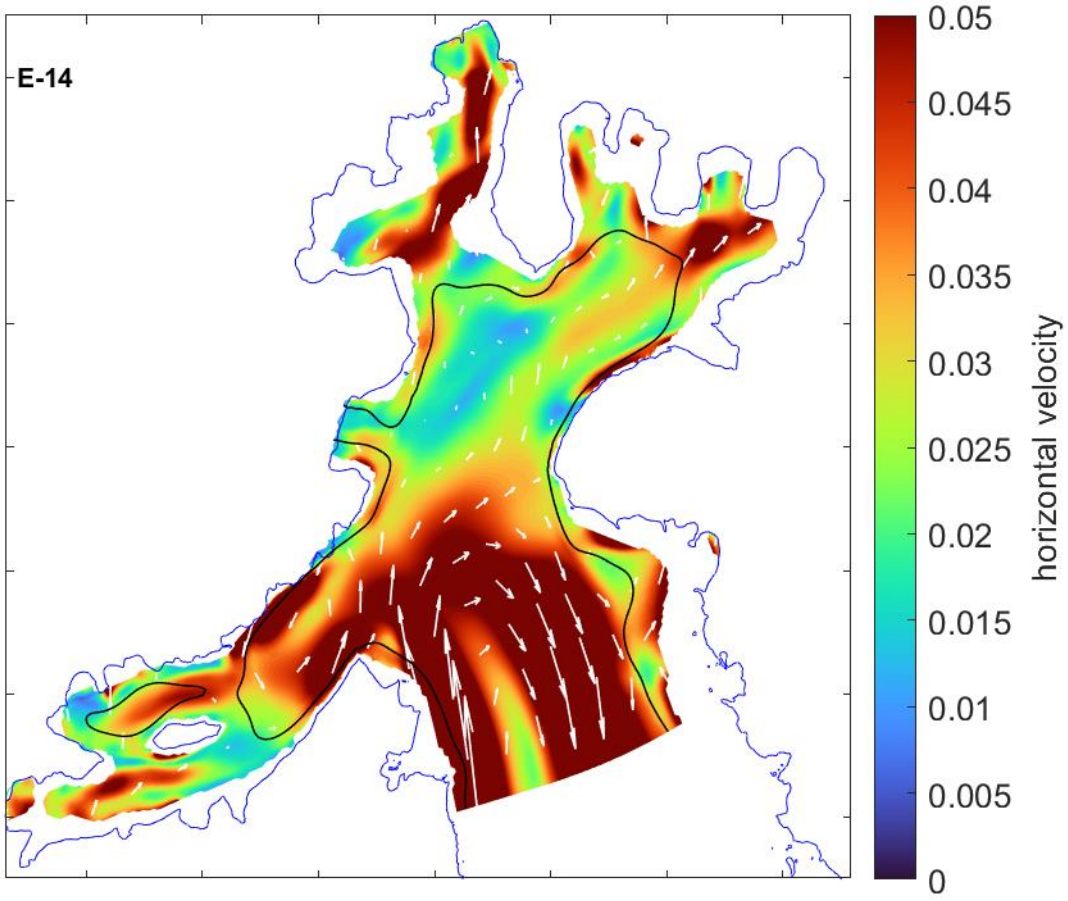

Figure S15. *As in Fig. S9, but for E-14 scenario.*

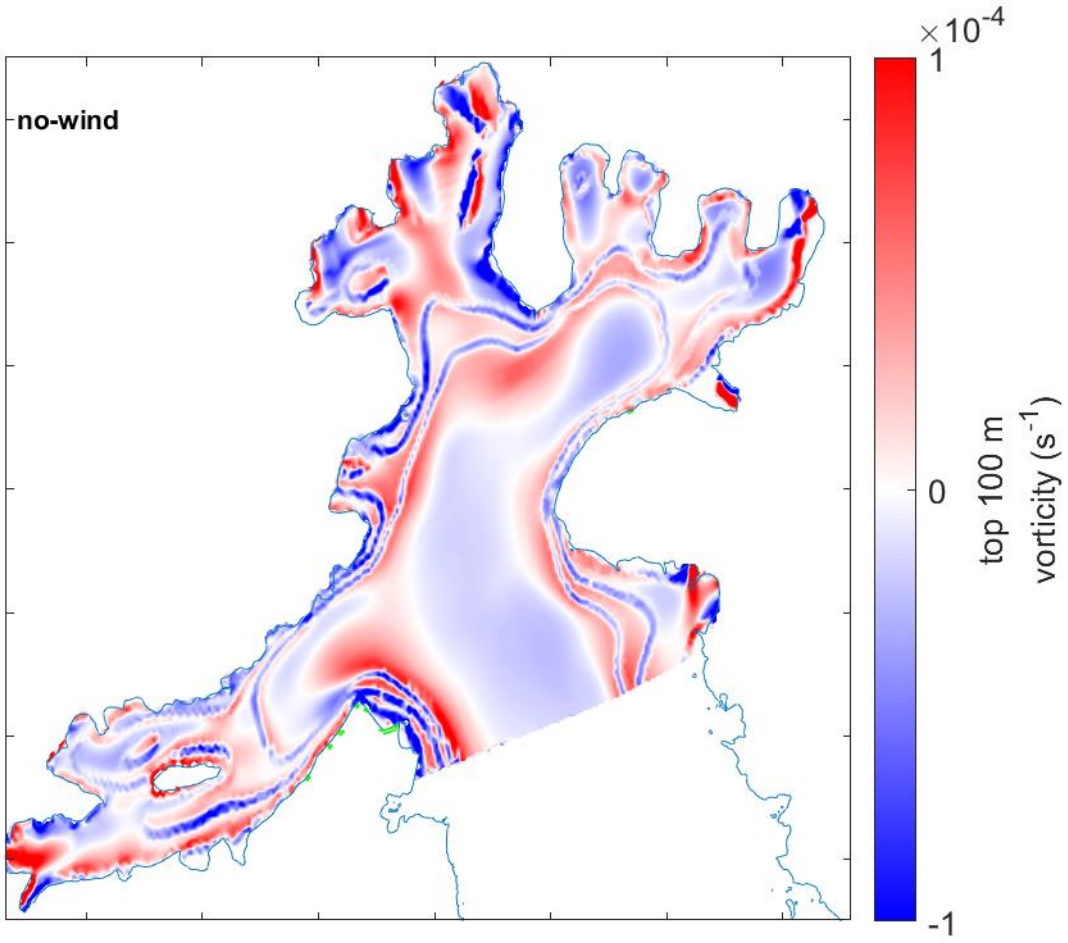

Figure S16. *No-wind vorticity across 10-100 m depth. {Note}: showing mean values from Dec 7, 2021, to Jan 9, 2022 (33 days).*

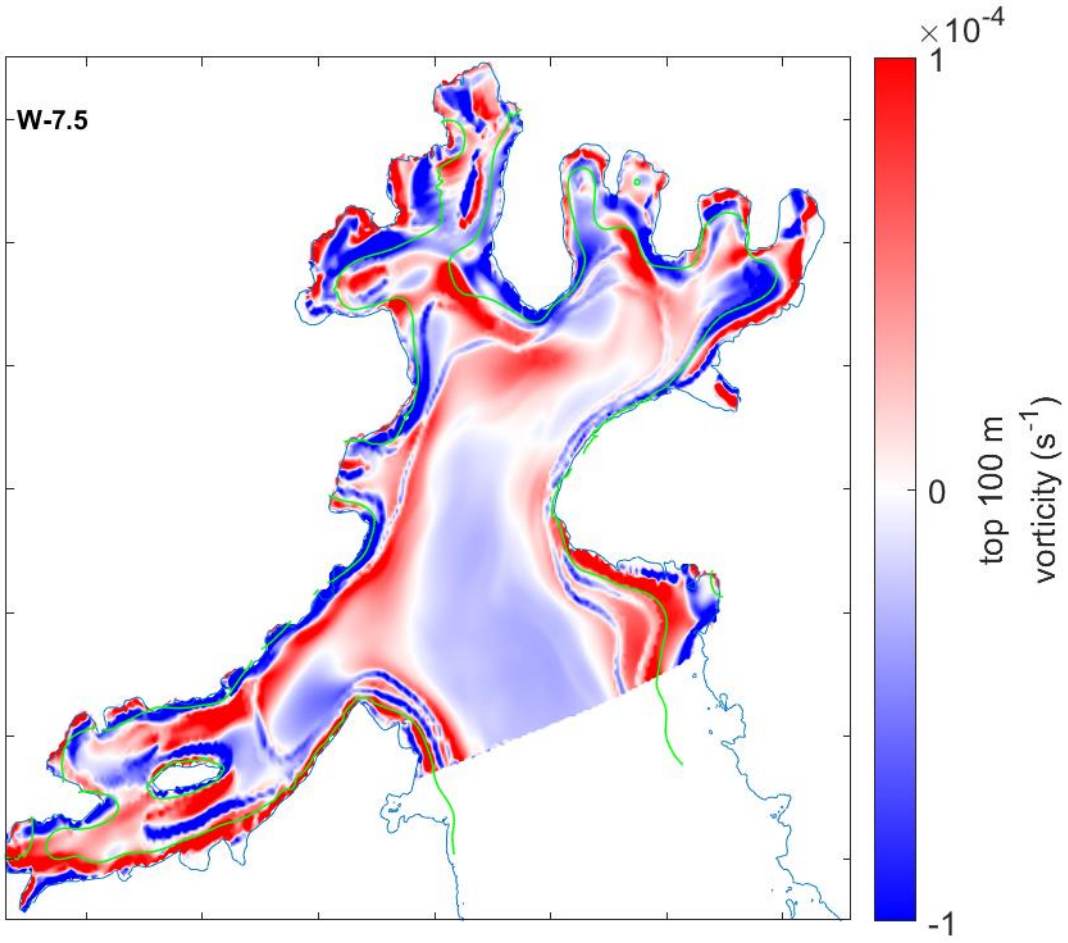

Figure S17. *As in Fig. S16, but for W-7.5 scenario.*

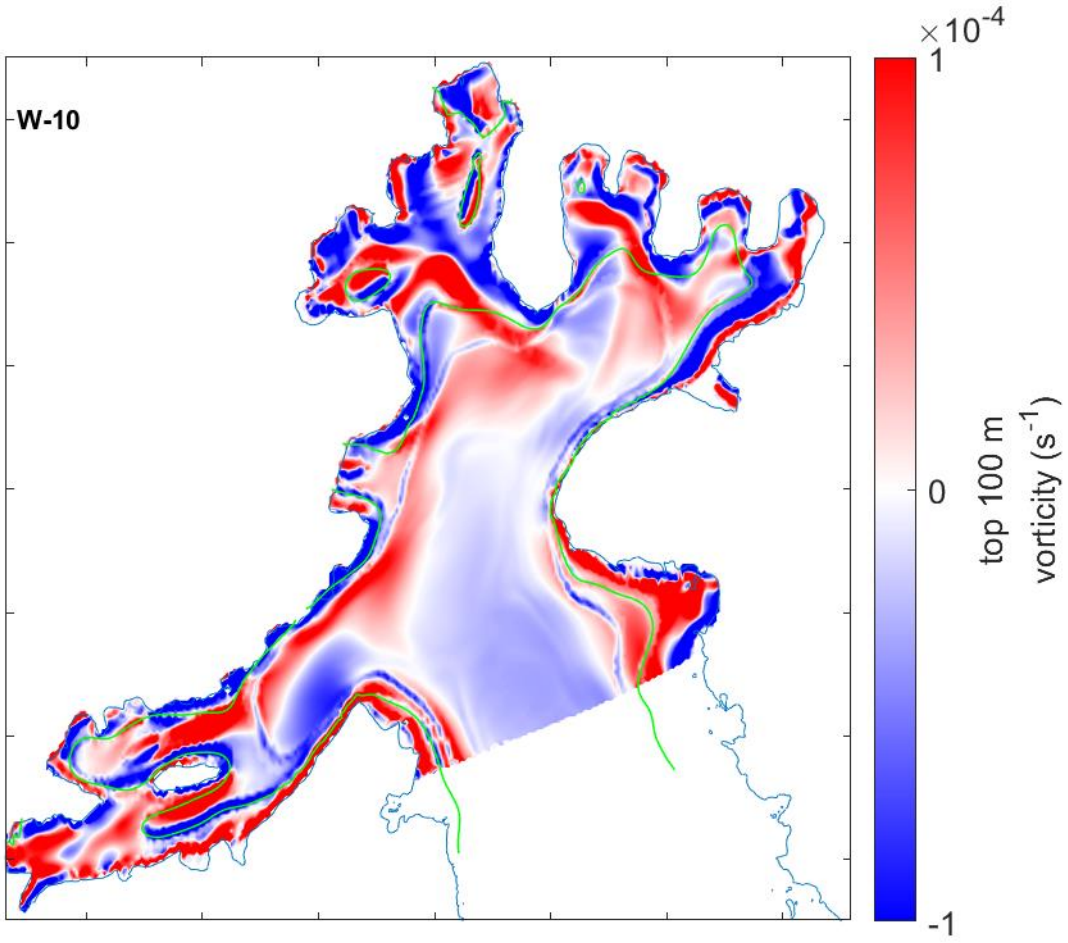

Figure S18. *As in Fig. S16, but for W-10 scenario.*

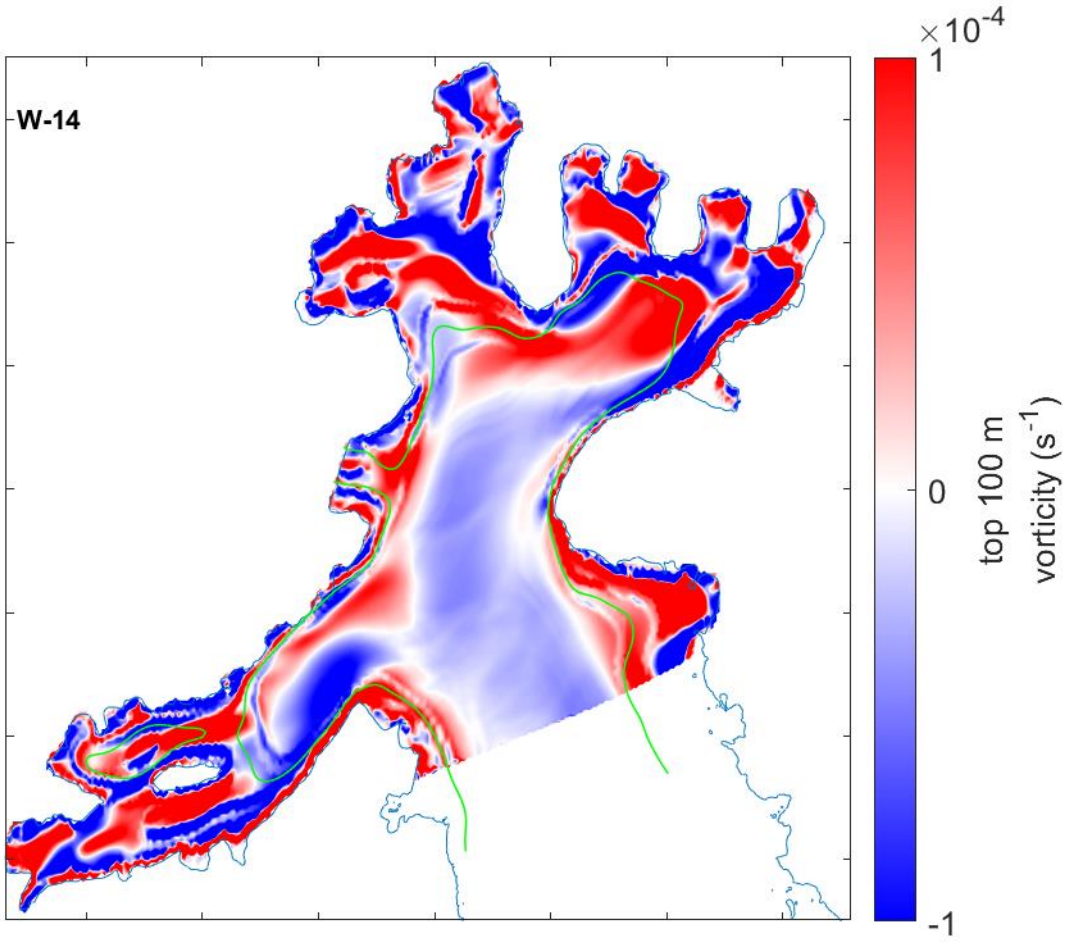

Figure S19. *As in Fig. S16, but for W-14 scenario.*

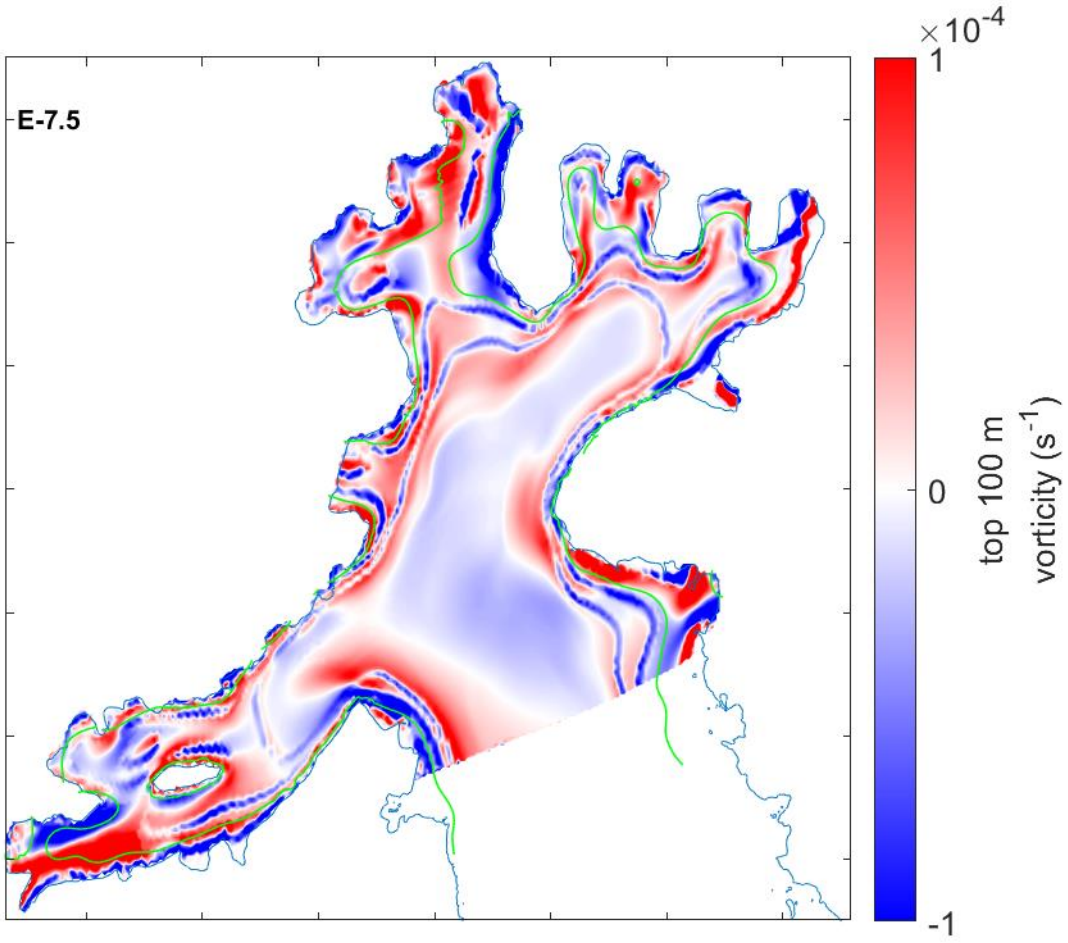

Figure S20. *As in Fig. S16, but for E-7.5 scenario.*

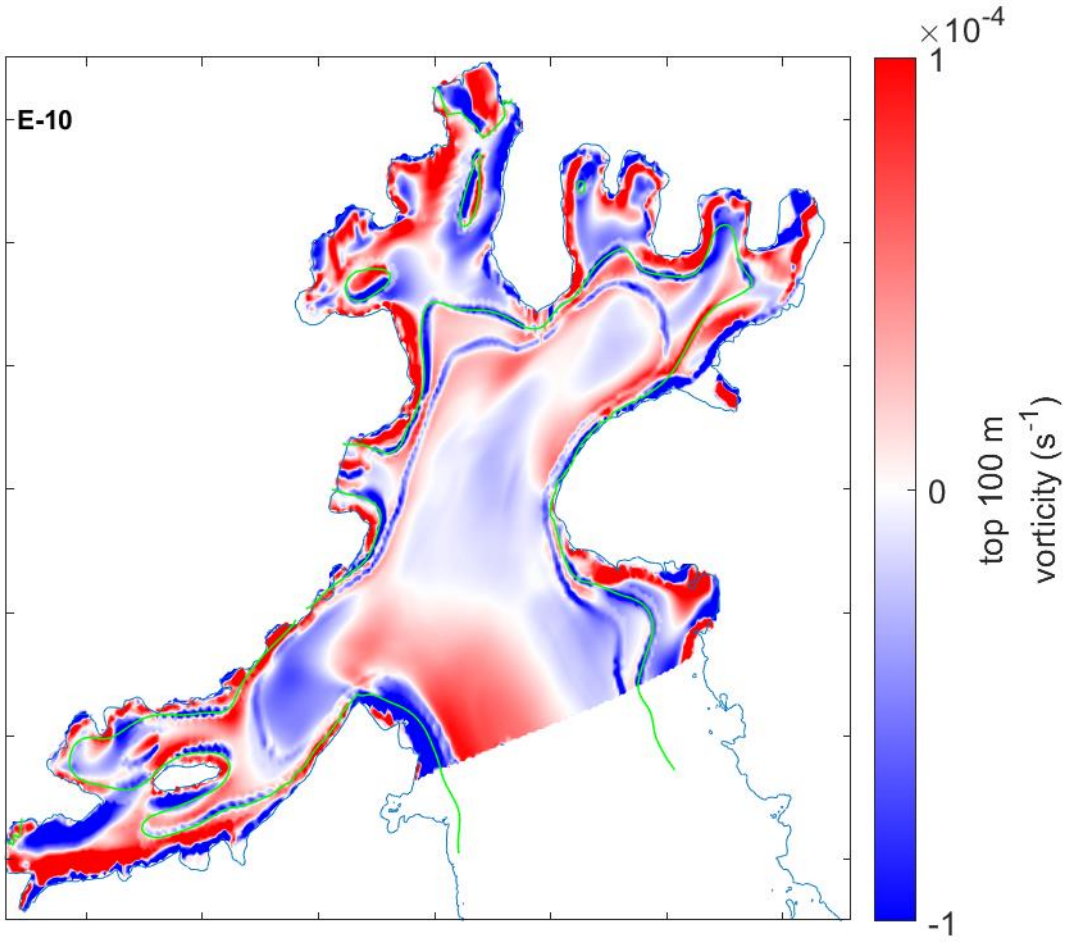

Figure S21. *As in Fig. S16, but for E-10 scenario.*

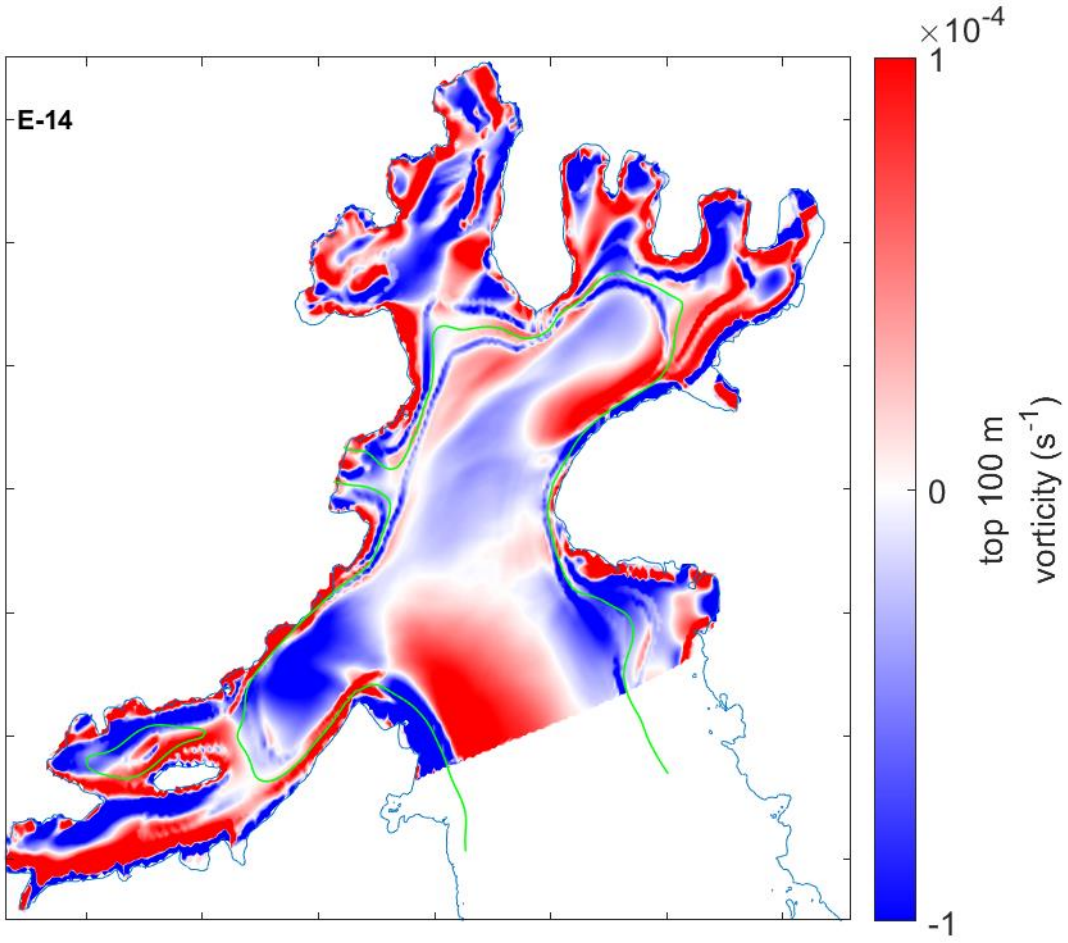

Figure S22. *As in Fig. S16, but for E-14 scenario.*

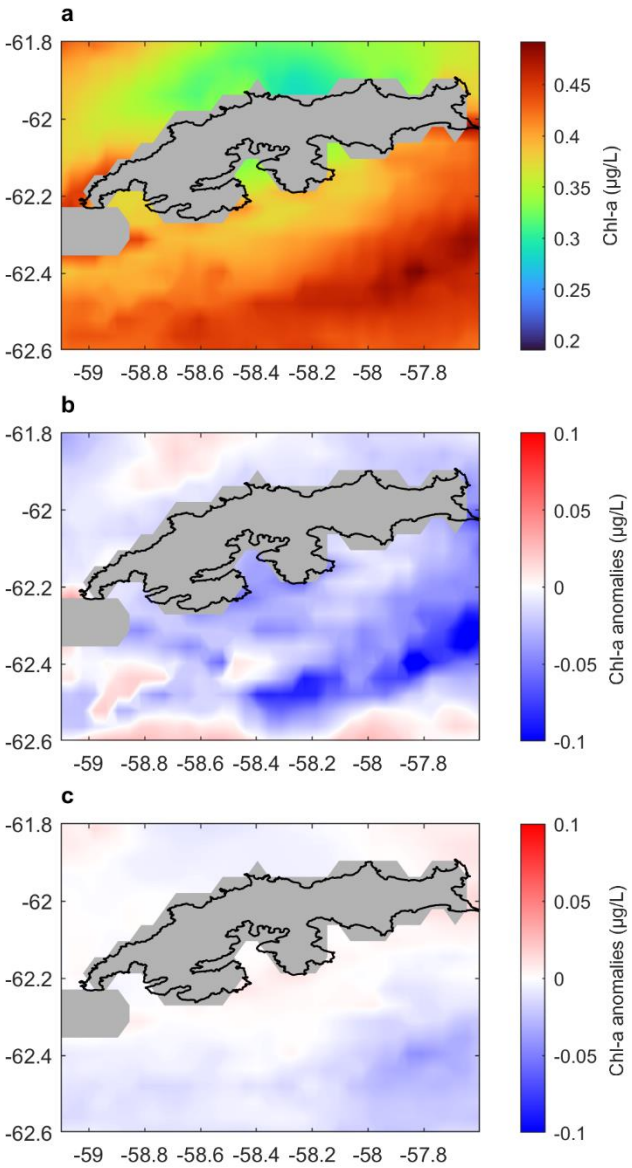

Figure S 23. *Chl-a estimates from the Copernicus-GlobColour dataset;* ***a.*** *mean values from December 15, 2018, to March 1, 2023;* ***b***. *mean anomalies pertaining to* ***a.,*** *on days following days of predominant easterly wind impact;* ***c.*** *identical to b., but following days of westerly wind influence.*